creative commons
COMMONS DEED

저작자표시-비영리-변경금지 2.0 대한민국

이용자는 아래의 조건을 따르는 경우에 한하여 자유롭게

- 이 저작물을 복제, 배포, 전송, 전시, 공연 및 방송할 수 있습니다.

다음과 같은 조건을 따라야 합니다:

저작자표시. 귀하는 원저작자를 표시하여야 합니다.

비영리. 귀하는 이 저작물을 영리 목적으로 이용할 수 없습니다.

변경금지. 귀하는 이 저작물을 개작, 변형 또는 가공할 수 없습니다.

- 귀하는, 이 저작물의 재이용이나 배포의 경우, 이 저작물에 적용된 이용허락조건을 명확하게 나타내어야 합니다.
- 저작권자로부터 별도의 허가를 받으면 이러한 조건들은 적용되지 않습니다.

저작권법에 따른 이용자의 권리는 위의 내용에 의하여 영향을 받지 않습니다.

이것은 이용허락규약(Legal Code)을 이해하기 쉽게 요약한 것입니다.

Disclaimer

dCollection

이학박사 학위논문

Intrinsic Neural Streams for Perception and Action: Cortical Orchestra Conducted by Purpose and Function

지각과 행동에 대한 내재적 신경 정보처리: 목적과 기능에 대한 대뇌 지각 네트워크

2020년 2월

서울대학교 대학원

협동과정 뇌과학 전공

윤 석 윤

Intrinsic Neural Streams for Perception and Action: Cortical Orchestra Conducted by Purpose and Function

지도교수 정 천 기

이 논문을 이학박사 학위논문으로 제출함.
2019년 12월

서울대학교 대학원
협동과정 뇌과학 전공
윤 석 윤

윤석윤의 이학박사 학위논문을 인준함.
2019년 12월

위 원 장 _____ 이 인 아 (인)

부위원장 _____ 정 천 기 (인)

위 원 _____ 박 혜 윤 (인)

위 원 _____ 김 성 필 (인)

위 원 _____ 이 준 열 (인)

Intrinsic Neural Streams for Perception and Action: Cortical Orchestra Conducted by Purpose and Function

Seokyun Ryun

Interdisciplinary Program in Neuroscience
The Graduate School

A Thesis Submitted to the Faculty of Interdisciplinary Program in Brain Science, in Partial Fulfillment of the Requirements for the Degree of Doctor of Philosophy in Science at the Seoul National University, Seoul, Korea

Dec 2019

Approved by thesis committee:

Chairman	**Inah Lee**
Vice-Chairman	**Chun Kee Chung**
Member	**Hye Yoon Park**
Member	**Sung-Phil Kim**
Member	**Joonyeol Lee**

ABSTRACT

Intrinsic Neural Streams for Perception and Action: Cortical Orchestra Conducted by Purpose and Function

Seokyun Ryun
Interdisciplinary Program in Neuroscience
The Graduate School
Seoul National University

Tactile and proprioceptive perceptions are crucial for our daily life as well as survival. At the peripheral level, the transduction mechanisms and characteristics of mechanoreceptive afferents containing information required for these functions, have been well identified. However, our knowledge about the cortical processing mechanism for them in human is limited. The present series of studies addressed the macroscopic neural mechanism for perceptual processing of tactile and proprioceptive perception in human cortex.

In the first study, I investigated the macroscopic neural characteristics for various vibrotactile and texture stimuli including artificial and naturalistic

ones in human primary and secondary somatosensory cortices (S1 and S2, respectively) using electrocorticography (ECoG). I found robust tactile frequency-specific high-gamma (HG, 50–140 Hz) activities in both S1 and S2 with different temporal dynamics depending on the stimulus frequency. Furthermore, similar HG patterns of S1 and S2 were found in naturalistic stimulus conditions such as coarse/fine textures. These results suggest that human vibrotactile sensation involves macroscopic multi-regional hierarchical processing in the somatosensory system, even during the simplified stimulation.

In the second study, I tested whether the movement-related HG activities in parietal region mainly represent somatosensory feedback such as proprioception from periphery or primarily indicate cortico-cortical neural processing for movement preparation and control. I found that sensorimotor HG activities are more dominant in S1 than in M1 during voluntary movement. Furthermore, the results showed that movement-related HG activities in S1 mainly represent proprioceptive and tactile feedback from periphery.

Given the results of previous two studies, the final study aimed to identify the large-scale cortical networks for perceptual processing in human. To do this, I combined direct cortical stimulation (DCS) data for eliciting somatosensation and ECoG HG band (50 to 150 Hz) mapping data during tactile stimulation and movement tasks, from 51 (for DCS mapping) and 46 patients (for HG mapping) with intractable epilepsy. The results showed that somatosensory perceptual processing involves neural activation of widespread somatosensory-related network in the cortex. In addition, the spatial distributions of DCS and HG functional maps showed considerable similarity

in spatial distribution between high-gamma and DCS functional maps. Interestingly, the DCS-HG combined maps showed distinct spatial distributions depending on the somatosensory functions, and each area was sequentially activated with distinct temporal dynamics. These results suggest that macroscopic neural processing for somatosensation has distinct hierarchical networks depending on the perceptual functions. In addition, the results of the present study provide evidence for the "perception and action" related neural streams of somatosensory system.

Throughout this series of studies, I suggest that macroscopic somatosensory network and structures of our brain are intrinsically organized by perceptual function and its purpose, not by somatosensory modality or submodality itself. Just as there is a purpose for human behavior, so is our brain.

Key words: Somatosensory, Tactile, Electrocorticography, Direct cortical stimulation, High gamma, Proprioception

Student Number: 2013-20398

CONTENTS

Abstract i

Contents iv

List of Tables ix

List of Figures x

List of Abbreviations xiv

PART I. INTRODUCTION

CHAPTER 1: Somatosensory System 1

1.1. Mechanoreceptors in the Periphery 2

1.2. Somatosensory Afferent Pathways 4

1.3. Cortico-cortical Connections among Somatosensory-related Areas 7

1.4. Somatosensory-related Cortical Regions 8

CHAPTER 2: Electrocorticography 14

2.1. Intracranial Electroencephalography 14

2.2. High-Gamma Band Activity 18

CHAPTER 3: Purpose of This Study 24

PART II. EXPERIMENTAL STUDY

CHAPTER 4: Apparatus Design 26

4.1. Piezoelectric Vibrotactile Stimulator 26

4.2. Magnetic Vibrotactile Stimulator 29

4.3. Disc-type Texture Stimulator 33

4.4. Drum-type Texture Stimulator 36

CHAPTER 5: Vibrotactile and Texture Study 41

5.1. Introduction 42

5.2. Materials and Methods 46

5.2.1. Patients 46

5.2.2. Apparatus 47

5.2.3. Experimental Design 49

5.2.4. Data Acquisition and Preprocessing 50

5.2.5. Analysis 51

5.3. Results 54

5.3.1. Frequency-specific S1/S2 HG Activities 54

5.3.2. S1 HG Attenuation during Flutter and Vibration 62

5.3.3. Single-trial Vibration Frequency Classification 64

5.3.4. S1/S2 HG Activities during Texture Stimuli 65

5.4. Discussion....69
5.4.1. Comparison with Previous Findings....69
5.4.2. Tactile Frequency-dependent Neural Adaptation....70
5.4.3. Serial vs. Parallel Processing between S1 and S2....72
5.4.4. Conclusion of Chapter 5....73

CHAPTER 6: Somatosensory Feedback during Movement....74
6.1. Introduction....75
6.2. Materials and Methods....79
6.2.1. Subjects....79
6.2.2. Tasks....80
6.2.3. Data Acquisition and Preprocessing....82
6.2.4. S1-M1 HG Power Difference....85
6.2.5. Classification....86
6.2.6. Timing of S1 HG Activity....86
6.2.7. Correlation between HG and EMG signals....87
6.3. Results....89
6.3.1. HG Activities Are More Dominant in S1 than in M1....89
6.3.2. HG Activities in S1 Mainly Represent Somatosensory

Feedback....94
6.4. Discussion....100
6.4.1. S1 HG Activity Mainly Represents Somatosensory Feedback 100
6.4.2. Further Discussion and Future Direction in BMI....102
6.4.3. Conclusion of Chapter 6....103

CHAPTER 7: Cortical Maps of Somatosensory Function....104
7.1. Introduction....106
7.2. Materials and Methods....110
7.2.1. Participants....110
7.2.2. Direct Cortical Stimulation....114
7.2.3. Classification of Verbal Feedbacks....115
7.2.4. Localization of Electrodes....115
7.2.5. Apparatus....116
7.2.6. Tasks....117
7.2.7. Data Recording and Processing....119
7.2.8. Mapping on the Brain....120
7.2.9. ROI-based Analysis....122
7.3. Results....123
7.3.1. DCS Mapping....123
7.3.2. Three and Four-dimensional HG Mapping....131

7.3.3. Neural Characteristics among Somatosensory-related Areas...144
7.4. Discussion....146
7.4.1. DCS on the Non-Primary Areas....146
7.4.2. Two Streams of Somatosensory System....148
7.4.3. Functional Role of ventral PM....151
7.4.4. Limitation and Perspective....152
7.4.5. Conclusion of Chapter 7....155

PART III. CONCLUSION

CHAPTER 8: Conclusion and Perspective....156
8.1. Perspective and Future Work....157

References....160
Abstract in Korean....173

LIST OF TABLES

CHAPTER 5: Vibrotactile and Texture Study

Table 5-1 Demographics of all subjects.....47

Table 5-2 Results of significance testing among various stimulus frequencies 57

CHAPTER 6: Somatosensory Feedback during Movement

Table 6-1 Clinical profiles 80

Table 6-2 Behavior information 84

CHAPTER 7: Cortical Maps of Somatosensory Function

Table 7-1 Demographics of the subjects 111

LIST OF FIGURES

CHAPTER 2: Electrocorticography

Figure 2-1 Difference in spectral resolution between ECoG and MEG.....16

Figure 2-2 Conventional ECoG monitoring procedure in Seoul National University Hospital 17

Figure 2-3 Time-frequency representations of HG activity from various techniques.....21

CHAPTER 4: Apparatus Design

Figure 4-1 Piezoelectric actuator and result of noise test. 28

Figure 4-2 Magnetic vibrotactile stimulator and the diagram of vibrotactile stimulation system.....30

Figure 4-3 Initially calibrated raw signal and diagram of calibration procedure 32

Figure 4-4 Hardware and system diagram of texture stimulator 35

Figure 4-5 Drum-type texture stimulator 38

Figure 4-6 System diagram of drum-type texture stimulator 40

CHAPTER 5: Vibrotactile and Texture Study

Figure 5-1 Stimulator design and surface of texture 48

Figure 5-2 Representative time-frequency plots for flutter and vibration conditions in S1 and S2.....55

Figure 5-3 HG time-frequency plots from other subjects.....56

Figure 5-4 Frequency-specific HG activity in intracerebral electrode.....59

Figure 5-5 HG and ERP time series in S2.....60

Figure 5-6 Topographical maps of the HG power differences between the flutter and vibration stimulus conditions.....61

Figure 5-7 S1 HG power time series under the flutter and vibration stimulus conditions.....63

Figure 5-8 Classification results.....65

Figure 5-9 Representative time-frequency plots for coarse and fine textures in S1 and S2.....67

Figure 5-10 Topographical maps of HG power level differences between the coarse and fine texture conditions.....68

CHAPTER 6: Somatosensory Feedback during Movement

Figure 6-1 Topographical maps of HG activities during hand grasping and elbow flexion.....90

Figure 6-2 Topographical maps of functional mapping results by direct cortical stimulation.....91

Figure 6-3 Spatiotemporal dynamics of HG activities during two

conditions 92

Figure 6-4 Mean HG power differences and movement classification accuracy.....93

Figure 6-5 Representative time-frequency plots during hand grasping and reaching tasks in the M1 and S1.....94

Figure 6-6 HG power time traces during cued movements.....96

Figure 6-7 HG onset timing.....97

Figure 6-8 Relationship between HG and EMG fluctuations during the pre-movement period.....99

CHAPTER 7: Cortical Maps of Somatosensory Function

Figure 7-1 Brain atlas used in this study 124

Figure 7-2 3-D DCS functional maps.....126

Figure 7-3 3-D DCS functional maps of each body part.....127

Figure 7-4 Differences in spatial distributions of electrodes between left and right hemispheres 128

Figure 7-5 3-D DCS functional maps based on the quality of sensation 129

Figure 7-6 3-D DCS functional maps for qualities of sensations elicited felt in the hand/finger/arm 130

Figure 7-7 Individual sensation report and time-frequency plots for tactile stimulation.....132

Figure 7-8 Locations of all electrodes and sampling densities of electrodes.....133

Figure 7-9 Three-dimensional HG Significance maps 136

Figure 7-10 HG maps for vibrotactile stimuli 137

Figure 7-11 Differences in HG activities at the individual level 138

Figure 7-12 Difference in the number of responsive electrodes between movement-related and tactile conditions.....139

Figure 7-13 Beta and theta band maps of coarse texture and hand grasping conditions 140

Figure 7-14 Cortical maps of the HG differences between the coarse and fine texture conditions in somatosensory-related areas 141

Figure 7-15 Four-dimensional HG maps for movement and texture conditions 143

Figure 7-16 HG temporal dynamics of each area.....145

Figure 7-17 HG temporal dynamics of each area during coarse texture stimulation.....145

LIST OF ABBREVIATIONS

A1, primary auditory cortex

AAL, automated anatomical labeling

ADC, analog-digital converter

AIP, anterior intraparietal area

ANG or AG, angular gyrus

BA, Brodmann's area

BMI, brain-machine interface

BNC, baby Neill constant

BOLD, blood-oxygen level dependent (signal)

CAR, common average reference

CIP, caudal intraparietal area

CT, computerized tomography

DCS, direct cortical stimulation

ECoG, electrocorticography

DAC, digital-analog converter

DAQ, data acquisition system and analog/digital output

DRG, dorsal root ganglia

DCN, dorsal column nuclei

EEG, electroencephalography

EMG, electromyography

ERD, event-related desynchronization

ERS, event-related synchronization

FIR, finite impulse response

FLE, frontal lobe epilepsy

fMRI, functional magnetic resonance imaging

FOp, frontal operculum

GTO, Golgi tendon organ

HHT, Hilbert-Huang transform

HG, high-gamma

ICMS, intracortical microstimulation

iEEG, intracranial electroencephalography

IIR, infinite impulse response

IPG, inferior parietal gyrus

IPL, inferior parietal lobule

IPS, intraparietal sulcus

ITG, inferior temporal gyrus

LDV, Laser-Doppler vibrometer

LIP, lateral intraparietal area

M1, primary motor cortex

MEG, magnetoencephalography

MFG, middle frontal gyrus

MIP, medial intraparietal area

MNI, Montreal Neurological Institute

MP, matching pursuit

MR, magnetic resonance

MTG, middle temporal gyrus

OLE, occipital lobe epilepsy

OP, opercular region

PA, power amplifier

PC, Pacinian corpuscle

PIP, posterior parietal area

PLE, parietal lobe epilepsy

PM, premotor cortex

PoCG, postcentral gyrus

PPR, posterior parietal reach region

PreCG, precentral gyrus

PTr, pars triangularis

PV, parietal ventral area

RA1, rapidly adapting type 1

RA2, rapidly adapting type 2

ROI, region of interest

ROp, Rolandic operculum

S1, primary somatosensory cortex

S2, secondary somatosensory cortex

SA1, slowly adapting type 1

SA2, slowly adapting type 2

SD, standard deviation

SE, standard error

SFG, superior frontal gyrus

SMA, supplementary motor area

SMG, supramarginal gyrus

SPL, superior parietal lobule

STFT, short-time Fourier transform

STG, superior temporal gyrus

SVM, support vector machine

TLE, temporal lobe epilepsy

TTL, transistor-transistor logic

UART, universal asynchronous receiver/transmitter

US, ultrasonic, or ultrasound

V1, primary visual cortex

VIP, ventral intraparietal area

VP, ventro-posterior nucleus

VPI, ventro-posterior inferior nucleus

VPL, the lateral part of ventro-posterior nucleus

VPM, the medial part of ventro-posterior nucleus

VPS, ventro-posterior superior nucleus

WT, wavelet transform

PART I. INTRODUCTION

Chapter 1: Somatosensory System

Our ability to detect external environment outside our body is fundamentally based on the faithful biological sensors of our whole body – the receptors. Information from these receptors is transmitted to our brain via numerous insulated fibers, and is represented to our internal window for perception, recognition, and internal calculation preparing our behaviors. Somatosensory system is one of the most basic, essential systems to perform these functions above. Unlike other sensory systems, especially vision and audition, it controls direct mechanical interactions between external environment and our body, and even physical state inside our body. Although it is extremely difficult to imagine the situation with no functioning of entire somatosensory system because it is unconsciously activated during our whole lives, loss of all somatosensory functions causes the most devastating scenario than other sensory systems. In this chapter, I will discuss the fundamental structures and characteristics of somatosensory system. Especially, I mainly focus on the tactile and proprioception of somatosensory system, which are directly related to this study.

1.1. Mechanoreceptors in the Periphery

At the somatosensory periphery, the information about mechanical deformations of our body is converted to electrical signals by numerous mechanoreceptors. Various types of mechanoreceptors are involved in this conversion, however, in terms of their functionalities and areal characteristics, these mechanoreceptors can be classified into cutaneous and proprioceptive mechanoreceptors.

Cutaneous mechanoreceptors, located in the skin, respond to the deformation of skin with different physical sensitivity depending on the type. Rapidly adapting type 1 (RA1) receptor, or Meissner corpuscle, is densely distributed (43 % of all tactile afferents in the skin of hand) near the epidermal site, and is very sensitive to transient deformations in the frequency range of 5 to 50 Hz (flutter) (Johansson and Flanagan, 2008). Rapidly adapting type 2 (RA2) receptor, or Pacinian corpuscle, is located in the deep inside the skin, and its distribution is relatively sparse compared to that of the RA1 receptor (13 %). It responds faster than RA1, in the sensitive frequency range of 40 to 500 Hz (vibration) (Bell et al., 1994). Additionally, both RA1 and RA2 receptors are less sensitive to the static deformation of skin, such as pressure (Knibestol, 1973). Since these two receptors are exclusively sensitive to vibratory stimuli, they are conventionally considered as key submodalities for vibrotaction (Delmas et al., 2011). There also exist receptors specialized for

static skin deformations, slowly adapting type 1 (SA1; 25 % of all tactile afferents in the skin of hand) and 2 (SA2; 19 %) receptors, or Merkel disc and Ruffini ending, respectively. Although these receptors respond slightly to transient stimuli (~5 Hz), they are robustly sensitive to the sustained stimuli such as pressure, tension and stretch (Knibestol, 1975). Thus, it has been considered that SA1 and SA2 receptors play critical roles in tactile pattern and shape recognition, respectively (Delmas et al., 2011).

Proprioceptive receptors transduce the mechanical deformations of tendons, muscles, and ligaments, into neuronal signals which contain information about body position, applied force, and movement of body. These receptors may be divided into three categories: muscle spindle afferents, Golgi tendon organs (GTOs), and joint mechanoreceptors. Muscle spindle afferents can further be divided into the primary and secondary spindle afferents (also known as type 1a and type 2 fibers, respectively) (Delhaye et al., 2018). Generally, primary spindle afferents are more sensitive to the mechanical dynamics of muscles than secondary spindle afferents (Cheney and Preston, 1976). Since the response patterns of these afferents are very complicated during active movement, the exact response characteristics are largely unknown (Delhaye et al., 2018; Dimitriou and Edin, 2008). GTOs, or type 1b fibers, show extreme sensitivity to the tension of tendon and isometric contraction of muscles (Edin and Vallbo, 1990). Joint mechanoreceptors, located in the joint

capsules, are exclusively sensitive to the applied force on the joint and its movement. In contrast, they are less sensitive to the deformation of skin or muscle (Grigg and Greenspan, 1977). However, unlike their expected roles in proprioception, these mechanoreceptors robustly respond during hyperextension and hyperflexion, but are not sensitive to moderate joint movements (Burke et al., 1988).

1.2. Somatosensory Afferent Pathways

Transduced somatosensory information is then transmitted to the central nervous system via peripheral fiber tracts in our body. There are three afferent pathways to the central nervous system: the dorsal column-medial lemniscus, the anterolateral system, and the somatosensory pathways to the cerebellum (Gallace and Spence, 2014). Among them, the dorsal column-medial lemniscus pathway mainly relays tactile and proprioceptive information. At the periphery, neuronal signals from cutaneous mechanoreceptors are mainly transmitted through type Aβ sensory fibers with a conduction velocity of 30 to 80 m/s (Delhaye et al., 2018). In contrast, those from proprioceptive ones are mainly conveyed via type Aα fibers with that of 80 to 120 m/s (Siegel and Sapru, 2005). These types of fibers enter the dorsal root ganglia (DRG) in the spinal cord, and most of them ascend toward the second order neurons in the dorsal column nuclei (DCN) of the brainstem. The distribution of afferent neurons in the DCN

exhibits not only the somatotopical organization, but also the modality-specific organization (Niu et al., 2013; Smith and Deacon, 1984). At this level, the second order neurons decussate and their axons ascend toward the contralateral side of the ventro-posterior complex of thalamus, through the medial lemniscus. The anterolateral system, another ascending pathway, mainly conveys information of thermal and noxious stimuli, but also transmit some information of crude touch including pressure to the ventro-posterior complex (Gallace and Spence, 2014).

Synapses between the second (from DCN to thalamus) and third order neurons (from thalamus to cortex) occur in the ventro-posterior complex of thalamus. This region can be divided into following: the ventro-posterior superior nucleus (VPS), the ventro-posterior nucleus (VP) including the lateral part (VPL) and the medial part (VPM), and the ventro-posterior inferior nucleus (VPI). Cutaneous and proprioceptive fibers mainly project their axons to the VPL and VPS, respectively. Additionally, the VPM receives input from the trigeminal nucleus, and the major input of VPI is the thermal and nociceptive fibers (Apkarian and Shi, 1994; Kim et al., 2007).

Generally, the third order neurons from the ventro-posterior complex directly project their signals to the cerebral cortex. Unlike spinothalamic tract, the cortical area projected from the third order neurons of the ventro-posterior complex of thalamus is relatively wide-spread, but most of them ascend toward

the primary somatosensory cortex (S1) (Jones and Powell, 1970; Whitsel et al., 1978). The S1 consists of four subdivisions: Brodmann's areas (BA) 3a, 3b, 1, and 2. In primates including human, the BA 3b is considered the primary somatosensory area in non-primates (Kaas, 1983). The VPL mainly sends the signals to BA 3b, but also projects output to the BA 3a, 1, 2, the secondary somatosensory cortex (S2), the posterior parietal cortex (PPC), and the insular cortex (Dijkerman and de Haan, 2007; Friedman and Murray, 1986; Jones et al., 1979). The VPL also sends a small portion of outputs to the motor-related areas such as the primary motor cortex (M1) (Jeannerod et al., 1984). Additionally, there exist projections from the VPS, which mainly contains the proprioceptive information, to BA 3a and 2 (Cusick et al., 1985). Consequently, the neuronal signals containing proprioceptive information are projected dominantly to the BA 3a, although the hand/finger area of BA 3a also receives input from cutaneous afferents (Phillips et al., 1971; Tanji and Wise, 1981). In contrast, the BA 3b and BA 1 mainly receive the cutaneous information (Whitsel et al., 1971).

However, proprioceptive and cutaneous afferents cannot be simplified in a subdivision-specific manner within the S1. Neurons in BA 1 mainly respond to cutaneous stimuli, but also respond during movement detection tasks (Gardner, 1988). Lesion in BA 3a causes severe impairment on the tactile discrimination performances (Randolph and Semmes, 1974).

1.3. Cortico-cortical Connections among Somatosensory-related Areas

The S1 is the main entrance of somatosensory information, and performs the early-processing for abstraction or feature extraction. Further somatosensory processing occurs in multiple cortical areas via various cortico-cortical fiber tracts. Although the anatomical connections do not always guarantee the functional connections, I mainly introduce the anatomical ones in this chapter. The S1 has reciprocal connections with the S2 (Friedman et al., 1980; Pons and Kaas, 1986). Although the S2 also receives inputs from the thalamus, there is strong evidence that neurons in S2 almost exclusively respond to the somatosensory stimulation via cortico-cortical pathways such as the S1-S2 serial connection, but the reverse (from S2 to S1) is not true (Pons et al., 1987). The S1 also projects outputs to the parietal ventral area (PV), located near the S2. The posterior parietal cortex (PPC) receives inputs directly from the S1. For example, the BA 1 sends signals to the inferior parietal lobule (IPL; BA 7b in monkeys), and both BA 1 and 2 project signals to the BA 5 (part of superior parietal lobule, SPL) (Pearson and Powell, 1985; Pons and Kaas, 1986). The S2 in both hemispheres are densely interconnected, and thus, these areas respond bilaterally to the external stimuli. The S2 is reciprocally connected to the insula (Friedman et al., 1986), and this pathway may be closely related to the higher-

order tactile processing (Preusser et al., 2015). The S2 also projects output to the bilateral PPC and the premotor cortex (PM) of the same hemisphere (Disbrow et al., 2003; Friedman et al., 1986). The PPC sends its output to the S2, so the PPC and S2 are interconnected, but it does not imply that these areas simultaneously process neural information for the specific sensory stimulus. The PPC also projects output to various cortical areas including the PM, superior temporal sulcus, and limbic area (Dijkerman and de Haan, 2007).

Overall, the somatosensory pathway from the S1 may be divided into two streams. One is from the S1 to lateral parietal and insular regions including the S2, PV and adjacent parietal areas. Another one projects to the dorsal parietal regions including BA 5, SPL, and IPS. It has been assumed that the former one is related to the higher-order tactile processing such as tactile object recognition, whereas the latter one is closely linked to the movement-related neural processing (Delhaye et al., 2018; Dijkerman and de Haan, 2007).

1.4. Somatosensory-related Cortical Regions

In this section, I briefly describe the functional characteristics of the somatosensory-related cortical areas. Although the feed-forward and feed-back mechanisms via the thalamocortical pathway are also important for modulation of somatosensory information; however, it is beyond the scope of this study, and thus, I mainly focus on the cortex.

Primary somatosensory cortex (S1). The S1 is well-known and extensively studied somatosensory area. Until now, however, its exact encoding mechanism for the somatosensory afferent signals has not been fully understood. The most distinct feature of S1 is its somatotopical organization. Each area of S1 represent corresponding each body part, but this organization is not completely compartmentalized (Flesher et al., 2016; Kurth et al., 2000; Overduin and Servos, 2004). Like the primary visual cortex (V1) and auditory cortex (A1), S1 plays critical roles in the early processing of somatosensory signals. In BA 3b, submodality-specific (i.e., flutter, vibration and pressure) neuronal firing activities are found, but most neurons respond to the afferent signals of multiple submodalities (Pei et al., 2009). It is generally considered that feature abstraction is processed further and receptive field (RF) become larger, as the somatosensory information stream proceeds from BA 3b to 1 and 2. Since the S1 directly processes the somatosensory information from peripheral afferents, lesions in this area cause various sensorimotor deficits. Lesions in BA 3b lead to the most severe deficits such as almost complete abolition of somatosensory function. The neuronal activities in BA 1 are predominantly affected by inputs from BA 3b, thus, lesions in this region show selective impairment of somatosensory functions (Carlson, 1981). Neurons in BA 2 receive inputs from both joint/muscle and cutaneous receptors (Merzenich et al., 1978), and lesions

of this area result in deficits of both proprioceptive and tactile functions (Delhaye et al., 2018; Randolph and Semmes, 1974).

Secondary somatosensory cortex (S2) and neighboring areas.

In human, the boundary and subdivisions of S2 area have not yet been completely defined, although there exist several studies to assess this (Eickhoff et al., 2006; Eickhoff et al., 2007). It is quite clear that this region involves in both the low and high order tactile processing such as shape recognition, tactile discrimination and decision making (Lin and Forss, 2002; Romo et al., 2002). S2 neurons show higher tactile stimulus selectivity, more blurred RF, and more complex response pattern than S1 neurons (Ruben et al., 2001; Sinclair and Burton, 1993). In addition, it is well-known that lesions of S2 and neighboring structures such as supramarginal gyrus (SMG) cause tactile agnosia (Caselli, 1991; Reed et al., 1996). However, the relevance of S2 to proprioceptive processing is controversial (Disbrow et al., 2003). I will deal with this topic deeply in Chapter 7.

BA 5 and 7. In human, the BA 5 and 7 are considered two subdivisions of the SPL. Actually, SPL cannot be classified only into somatosensory area, because this area processes multiple sensory modalities and is regarded as the center of multisensory integration. In addition, the SPL is involved in maintaining

internal representations of body state for sensorimotor integration (Wolpert et al., 1998), and in the dorsal pathway in vision. In somatosensory processing, this area is closely related to the movement control and spatial processing for objects. The SPL is also linked to the movement intention, so the intended movement can be decoded by neural activities in this area (Aflalo et al., 2015). Neurons in SPL are activated by both proprioceptive and cutaneous stimuli. However, lesions of SPL cause mild deficits in tactile perception and discrimination, but significant abnormalities in the reach-and-grasp tasks (Delhaye et al., 2018; Padberg et al., 2010; Pause et al., 1989).

Intraparietal sulcus (IPS). The IPS is located on the lateral sulcus between the SPL and inferior parietal lobule (IPL) in primates. The IPS is highly involved in motor intention and planning of specific movements (Andersen and Buneo, 2002). This area has been divided into several subregions based on their functional characteristics: the anterior intraparietal area (AIP), the lateral intraparietal area (LIP), the caudal intraparietal area (CIP), ventral intraparietal area (VIP), the posterior parietal reach region (PPR). The AIP plays an important role in planning of hand movement such as grasping. The LIP is critically involved in planning of eye movements (Andersen and Buneo, 2002). The VIP seems to be related to the multisensory integration for spatial representation (Duhamel et al., 1998; Schlack et al., 2005). The CIP is not

involved in somatosensory processing, but in higher-level visual processing (Kaas, 2012). The PPR includes medial intraparietal area (MIP) and the posterior parietal area (PIP). This area is closely related to the planning of reaching movements (Andersen and Buneo, 2002).

Inferior parietal lobule (IPL). The IPL is a multimodal association area, and is involved in various perceptual and cognitive functions including somatosensory, language, emotion, body image representation, and movement intention (Desmurget et al., 2009; Sanai et al., 2008). In addition, this area is considered a part of mirror neuron system. This area can be divided into two areas: the SMG and angular gyrus (ANG). In monkey, neurons in these areas respond during not only somatosensory stimulation, but also during movement, and visual stimulation (Rozzi et al., 2008). Lesions in IPL cause several perceptual deficits such as tactile agnosia, sensory aphasia and spatial neglect (Gazzaniga, 2009; Reed and Caselli, 1994). Little is known about the involvement and perceptual relevance of IPL in somatosensory processing.

Premotor cortex (PM). The PM has traditionally been considered a crucial area for movement preparation. However, neurons in the ventral PM (vPM) respond to the somatosensory stimulation both in monkey and human (Avanzini et al., 2016; Rizzolatti et al., 1981). Specifically, converging evidence has suggested

that vPM is involved in the transformation of sensory information from parietal area into action, and in the tactile perceptual decision (Romo et al., 2004). The vPM is also related to the modulation of S1 during voluntary movement without somatosensory feedback (Christensen et al., 2007).

Insula. The insula is located deep inside the sylvian fissure. Generally, this area is believed to be involved in the high-order perceptual and cognitive functions. In somatosensory processing, the insula may play critical roles in perceptual recognition (Dijkerman and de Haan, 2007). Additionally, a recent lesion study proposed that the insula is causally involved in tactile perception through a pathway from S1 to insula via S2 (Preusser et al., 2015).

Cingulate cortex. The cingulate cortex is involved in complex sensorimotor functions as well as emotion, pain, and autonomic system (Caruana et al., 2018; Davis et al., 1995). In human, direct cortical stimulation (DCS) on this area elicits somatosensory responses of the contralateral body part without a clear somatotopical organization (Balestrini et al., 2015; Caruana et al., 2018). However, the functional role of this area in somatosensory processing remains to be elucidated.

Chapter 2: Electrocorticography

Electrocorticography (ECoG) is an invasive approach to record neuronal population activities of the cortex directly. It provides a unique opportunity to assess cortical functions with relatively low noise contamination, high sensitivity and temporal resolution; however, there exist several limitations of this method due to the procedure itself. In this chapter, I will briefly discuss general characteristics and recording procedures of ECoG. Additionally, I will deal with several characteristics of high-gamma (HG) band neuronal population activities, which can be robustly detected by ECoG, at the end of the chapter.

2.1. Intracranial Electroencephalography

Intracranial electroencephalography (iEEG), including ECoG, is an invasive monitoring method to directly record electrophysiological neuronal population activities from the cortex or deep brain structures by ECoG or depth electrodes. The main purpose of this monitoring method is to record electrophysiological neural activity from patients with drug-resistant epilepsy for finding the zones of epileptic origin. The iEEG as a clinical procedure was initially developed by Dr. Wilder Penfield and Herbert Jasper at Montreal Neurological Institute (MNI) in 1950. The identified epileptic zones during iEEG monitoring are then surgically resected from the patient's brain to treat the epilepsy. In a special

case, the iEEG is also used during surgery (intraoperative ECoG). In this section, I mainly focus on the ECoG, but the general characteristics are similar between ECoG and depth electrode.

ECoG shows very high spectral resolution compared to the electroencephalography (EEG) and magnetoencephalography (MEG), especially at higher (> 50 Hz) frequency (**Fig. 2-1**) (Crone et al., 2006). This characteristic of ECoG allows a better understanding of neuronal population activity compared to non-invasive electrophysiological methods. Like EEG, the ECoG is sensitive to the radial component of current source (from exposed cortical gyri) induced by neuronal population activity. In contrast, the MEG is more sensitive to the tangential component of that (from sulci). To record neural activity from the sulcus, the depth electrodes or intrasulcal ECoG grids/strips are inserted into the suspected sulcus for clinical purpose (Yanagisawa et al., 2009).

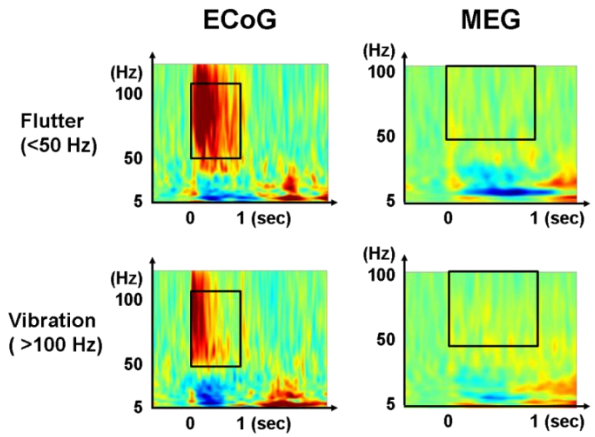

Figure 2-1. Difference in spectral resolution between ECoG and MEG. Stimulus properties were the same in both methods (delivered by piezoelectric vibrotactile stimulator; see Chapter 4). Data were recorded in S1. Results show the distinct difference in high-gamma (HG) band (>50 Hz) power level between two recording methods.

The spatial resolution of ECoG depends on the size of electrode, the inter-electrode distance, and the degree of intrinsic volume conduction effect of the cortex. The electrode diameter and inter-electrode distance of conventional ECoG electrodes are 3 to 4 mm and 10 mm, respectively. For special purposes, clinicians sometimes use high-density ECoG with an electrode diameter of 1 to 2 mm and an inter-electrode distance of 4 to 5 mm (Hiremath et al., 2017). The high-density ECoG has much better spatial resolution than conventional ones leading to obtain more detailed information about neural activity. Specifically, a recent study has suggested that spoken

sentences of patients can be successfully reconstructed by decoding articulatory movements using neural signals from high-density ECoG (Anumanchipalli et al., 2019).

Typically, epilepsy patients scheduled for resection surgery undergo the craniotomy for ECoG electrode insertion to monitoring epileptic seizure onset zone, prior to the lesionectomy. After craniotomy, the extraoperative ECoG monitoring procedure takes place for one or two weeks, and additional electrophysiological experiments with the patients' consent are then conducted. Conventional procedure in Seoul National University Hospital is illustrated in **Fig. 2-2**.

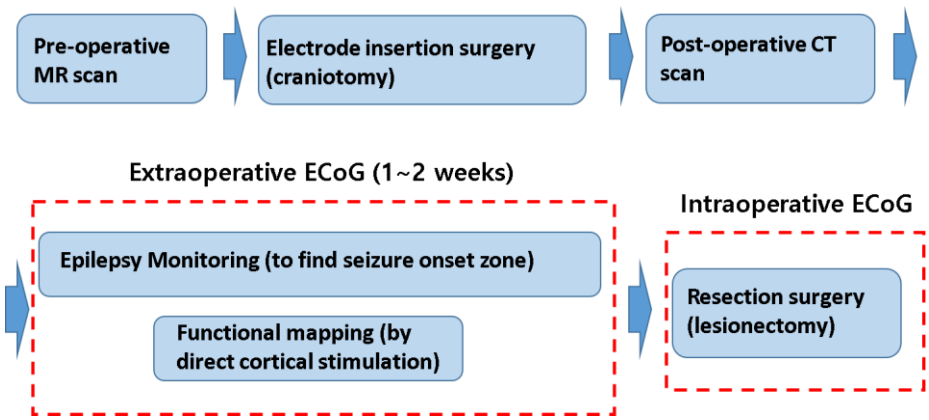

Figure 2-2. Conventional ECoG monitoring procedure in Seoul National University Hospital (SNUH).

Although the ECoG provides high quality neural population signals with robust spatiotemporal resolution compared to any type of non-invasive method, there are some limitations which are not considered in non-invasive studies. First, the location of electrodes is determined only for clinical purpose, leading to high individual variabilities of sampled areas across patients. In particular, this issue makes it difficult to investigate neuronal network among cortical regions by ECoG. Second, ECoG data are recorded from epilepsy patients who have some abnormalities in their cortices, thus a careful validation is needed when interpreting the result of these data. Third, the chances of ECoG recording for neuroscience research are limited and are affected by the patient's condition. Accordingly, it takes a relatively long time to get enough ECoG data for neuroscience research.

2.2. High-Gamma Band Activity

In ECoG recording, a broadband neuronal high frequency activity (>50 Hz), which is difficult to detect during EEG or MEG recording, is frequently observed during various sensory stimulation and cognitive tasks. Although its exact generating mechanism and functional roles are controversial, there has been a consensus that this high frequency neural activity, or HG, in the sensory

area may represent on-going neural computation for afferent sensory information. In the somatosensory cortex, high frequency neural activity is closely related to the intensity and quality of stimuli, and is directly or indirectly related to the neuronal spiking activity in the same area (Ray et al., 2008a; Rossiter et al., 2013; Ryun et al., 2017b).

Various time-frequency analysis methods have been used to investigate the spectro-temporal dynamics of HG activity. In this section, I introduce four types of techniques – short-time Fourier transform (STFT), wavelet transform (WT), matching pursuit (MP), and Hilbert-Huang transform (HHT).

The STFT is one of the simplest and fastest ways to analyze the non-stationary spectral dynamics of signals, but it has a fixed time resolution across frequencies, and vice versa. The WT overcomes this problem by utilizing variable window size depending on the frequency. Therefore, this method provides good temporal resolution while sacrificing frequency resolution at higher frequencies, and vice versa at lower frequencies. Generally, this approach is very efficient when investigating spectral characteristics of neuronal population activity because the neural activity at high frequencies (>50 Hz) often shows broadband responses with transient burst. However, there also exists sustained high frequency neuronal oscillatory activities with narrow frequency band, and it is difficult to simultaneously capture both transient and

narrow-band high frequency activities with good precision by the wavelet approach. Several techniques have been developed to improve time-frequency resolution beyond the wavelet transform. The MP is a greedy, or "brute force" algorithm for time-frequency analysis, and finds the best compromise between time and frequency resolution without *a priori* constraints of window size depending on the frequency (Ray et al., 2008b). The HHT, which is recently applied to neuroscience research, empirically decomposes the signal to obtain several intrinsic mode functions (IMF), and calculates Hilbert spectra of these IMFs. The calculated Hilbert spectra are then plotted onto the time-frequency plain. Methodological details of the HHT are in the literatures (Chandran et al., 2016; Huang et al., 1998). Figure 2-3 depicts the results of time-frequency analysis from these four techniques above.

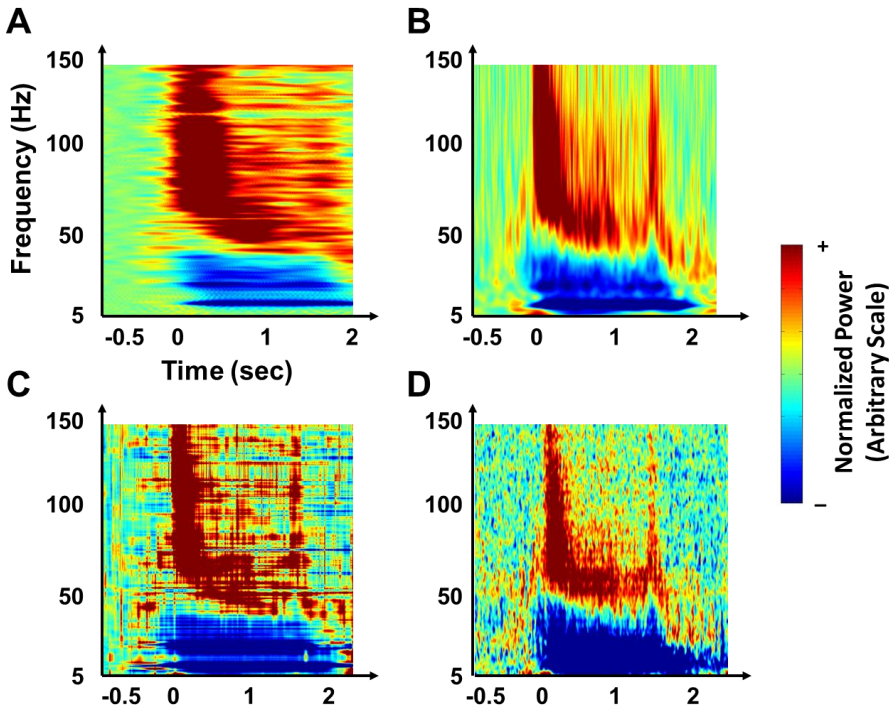

Figure 2-3. Time-frequency representations of HG activity in S1 from various techniques including (A) short-time Fourier transform (STFT), (B) complex Morlet's wavelet transform (WT), (C) matching pursuit (MP), and (D) Hilbert-Huang transform (HHT) methods during the same texture stimulation. Some degree of spectrotemporal smoothing was applied for averaging and visualization.

In this study, I used Morlet's wavelet transform to construct time-frequency representation for several reasons. First, although there exist some spectral blurring effects at high frequencies (>70 Hz), overall time-frequency pattern from WT is not very different from MP and HHT. In addition, the frequency resolution of WT at 50 to 70 Hz is sufficient to capture the narrow

band gamma oscillation given the intrinsic frequency variability of neural activation in this band (see Fig 2-3 B and D). Second, the MP and HHT methods extract the spectral energy from signals by iteration procedures and then add it to the time-frequency plain with zero values. In single-trial calculation, many points of time-frequency plain have zero values if the spectral energy of these points is not sufficient to be extracted by the iteration. This methodological limitation makes them difficult to perform conventional statistical tests. Third, in a practical aspect, these methods require numerous iterations due to the algorithm itself, making them inefficient when analyzing large datasets. Finally, since this study mainly focuses on the broadband high-gamma activity, precise spectral resolution is not necessary.

It is widely believed that generation of gamma oscillation is closely related to the rhythmic and coherent firing in inhibitory interneuron networks (Fries et al., 2007). However, there exists ongoing debate about whether the HG activity has mechanisms and functions similar to the conventional gamma band oscillation, or it reflects completely different nature of neural processing. I suggest that the higher component of HG activity has a different mechanistic role from conventional gamma oscillation, whereas the characteristics of the lower one is similar (or the same) to those of conventional gamma oscillation, for several reasons. First, a series of studies suggested that spikes of the S2 neurons during vibrotactile stimulation are highly coupled to the higher gamma

frequency activity (80 to 150 Hz), but are weakly coupled to the lower, or conventional gamma frequency (40 to 80 Hz) oscillatory activity (Ray et al., 2008a; Ray et al., 2008b). Second, the higher part of HG activity in S1 during mechanical stimulation shows robust transient bursts at the on/offset of the stimulus, and the onset timing of this activity is almost identical to those of the early component (N20) of event-related potentials (ERPs). In contrast, the induced gamma oscillatory activity at the same region exhibits delayed response pattern and lasts longer than the higher frequency activity. If the higher part of HG activity is generated by the networks of inhibitory interneurons, this activity should gradually increase over time because the firing rate of afferent neurons in S1 is attenuated after bursting at the stimulus onset (Musall et al., 2014; Tommerdahl et al., 1999a). Third, the "oscillation" implies the sustained rhythmic activity of neuronal population. In a single trial data, the higher part of the HG activity rarely shows such sustained responses, but rather intermittent spike-like responses. Regardless of whether the broadband gamma activity is generated by inhibitory interneuron networks, such transient burst activities cannot be categorized into the "oscillation".

Chapter 3: Purpose of This Study

In the present series of studies, I aim to reveal the macroscopic neural mechanism for perceptual processing of tactile and proprioceptive sensations in human.

In the first study, I test the hypothesis that neural processing for vibrotactile perception involves multi-regional co-operation between the S1 and the downstream regions such as the S2. To assess this issue, I investigate the macroscopic neural characteristics of various vibrotactile and texture stimuli including artificial and naturalistic ones in human S1 and S2 using ECoG. I also test whether the neuronal population activities show similarities between artificial vibrotactile stimuli and naturalistic texture stimuli, depending on the spectral compositions of stimuli.

In the second study, I focus on the high-gamma (HG) activities in S1 during movement execution. I test whether the movement-related HG activities in S1 mainly represent proprioceptive and tactile feedback from periphery or primarily indicate cortico-cortical neural processing for movement preparation and control. If the former is true, these activities mainly have information about proprioception, and can be interpreted as somatosensory encoding and further processing mechanism. Alternatively, these activities may be related to the motor intention and execution which can be used for features of brain-machine

interface (BMI) techniques.

In the final study, I assess the fundamental question that somatosensory processing for movement perception (related to the proprioception) and for tactile perception has different large-scale cortical network, or pathway. To do this, I construct cortical maps for proprioception and tactile sensations in two different ways – One is the direct cortical stimulation (DCS) mapping to identify cortical areas where the somatosensory perception is elicited, and the other is the cortical mapping of HG activities to somatosensory stimuli from the periphery.

Throughout these studies, I suggest that there exist intrinsic somatosensory neural streams governed by perceptual function and its purpose.

PART II. EXPERIMENTAL STUDY

Chapter 4: Apparatus Design

Unlike other sensory studies such as vision and audition, several sophisticated mechanical and electrical engineering techniques are absolutely required to perform the somatosensory experiment because the stimulus is delivered to our body directly by the external device with micro-level precision. Sometimes, however, these techniques are underestimated and not categorized as a critical procedure for study. Thus, I will devote an individual chapter to illustrate the design and specification of customized tactile stimulators used in this series of studies. Four devices including piezoelectric vibrotactile, magnetic vibrotactile, disc-type texture, and drum-type texture stimulators will be introduced with detailed description and their pros and cons.

4.1. Piezoelectric Vibrotactile Stimulator

The “piezoelectric” stimulator is the firstly designed tactile device for this series of studies. This stimulator was developed in collaboration with Korea University of Technology and Education. Basically, this stimulator utilizes a reverse piezoelectric effect which converts electrical energy (i.e., change in

applied electrical potential) into mechanical energy (i.e., change in length of material). In this study, a strip-type, customized piezoelectric actuator manufactured by APC International was used. This actuator covers the 1–500 Hz frequency range. In this actuator, two strips of piezoelectric ceramic are attached together. One is expanded and the other is contracted by the applied electrical input. The total deflection is evaluated by following equation:

$$\text{Total Deflection (mm)} = 2.2 \times 10^{-6} \times \left(\frac{{l_f}^2}{h^2}\right) \times V$$

where l_f is free length of actuator (mm), h is thickness of actuator (mm), and V is input voltage (l_f = 25 mm, h = 0.6 mm in this study). The magnitude of stimulus can be controlled by adjusting input voltage. For stimulation on fingertip, a bell-shaped, small plastic material (0.75 mm in diameter) was mounted on one end of the actuator strip. The opposite end of the strip was firmly fixed in a plastic box blocking the electrical noise from actuator (**Fig.4-1**, left). Stimulus frequency is controlled by micro controller unit (MCU) which also generates stimulus trigger to synchronize the timing between this system and the acquisition system. The stimulus waveform generated by MCU is amplified and the output is applied to the piezoelectric actuator. Experimental paradigm is controlled using customized software written in Python. To assess the noise level of this device during operation, a test magnetoencephalography (MEG) recording was performed in an electromagnetic shielded room. No significant noise induced by actuator was found during recording (**Fig. 4-1**,

right).

This stimulator is compact and portable enough to conduct experiments in the patient room. Although two large voltage supplies are required to operate, it is not a critical problem because the main module can be located outside the patient room. However, this device has a relatively low magnitude resolution (magnitude difference between calculated and observed values = ±30 %) due to the piezoelectric actuator itself. Moreover, the blocking force value (the maximum value of applied force to operate the actuator normally) decreases with decreasing the magnitude of stimulus, making it impossible to deliver a small magnitude of stimulus.

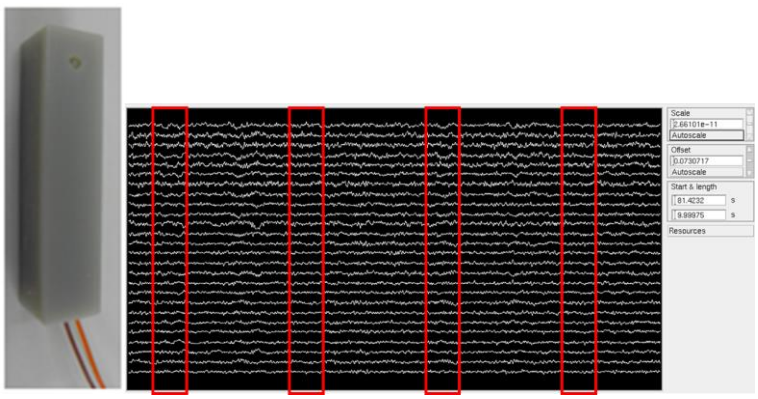

Figure 4-1. Piezoelectric actuator (left) and result of noise test (right). Noise test for this actuator was performed during MEG recording.

4.2. Magnetic Vibrotactile Stimulator

Although the piezoelectric vibrotactile stimulator reliably delivers single frequency stimulation from 5 to 400 Hz, this device is unable to generate complex stimulus patterns such as diharmonic waveforms and temporally modulated sinusoidal patterns because its magnitude resolution is limited (see previous section). Therefore, I designed an advanced version of vibrotactile stimualtor driven by magnetic actuator (Mini-shaker, model 4810; Brüel and Kjær).

This magnetic actuator covers a wide range of stimulus frequencies up to 18 kHz with strong resistance to the applied normal force by the fingertip. However, this actuator generates electromagnetic noise during operation. Therefore, the Mini-shaker were shielded by barrel-shaped stainless steel and aluminium materials to minimize electromagnetic artifact (**Fig. 4-2A**). Additionally, I inserted sound absorbing materials into the shielded barrel to reduce stimulus-related auditory noise. To stimulate a fingertip, a long plastic pin (2 mm in diameter; 100 mm in length) was mounted on the top of the Mini-shaker. Only the tip of the plastic pin was exposed to the top of the barrel lid with minimal indentation of skin (**Fig. 4-2B**).

Paradigm control, the generation of stimulus waveforms and trigger signals are conducted by custom-made software written by MATLAB. The generated digital signals are converted to the analog ones by digital-analog

converter (DAC) in the data acquisition and digital/analog output system (DAQ). To drive the magnetic actuator, these analog signals are amplified via power amplifier (PA; model 2718, Brüel and Kjær), and the amplified signals are applied to the Mini-shaker inside the shielded barrel through a micro baby Neill constant (micro-BNC) cable (**Fig. 4-2C** for system diagram).

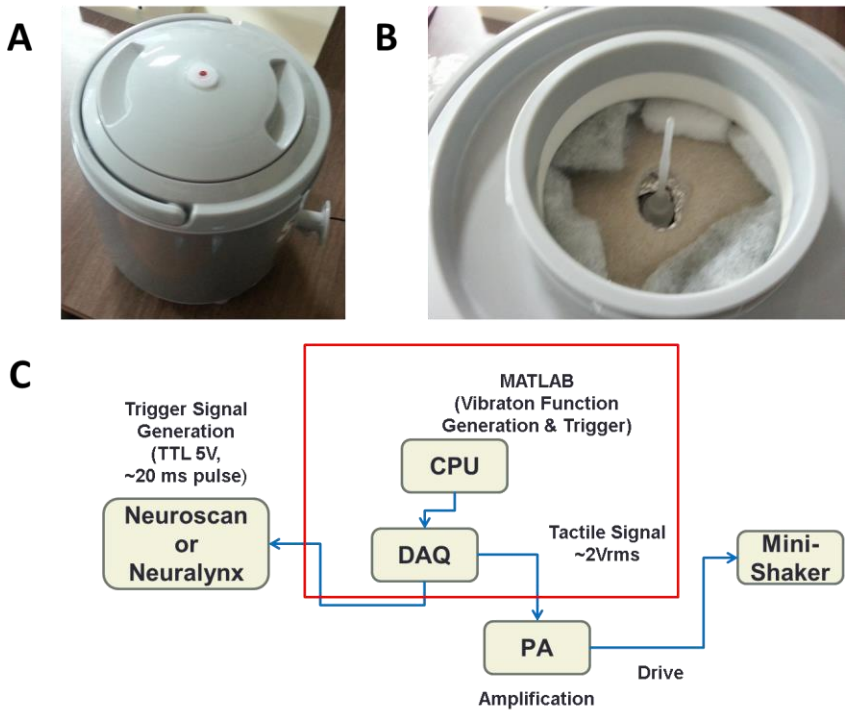

Figure 4-2. Magnetic vibrotactile stimulator (A and B) and the diagram of vibrotactile stimulation system (C). (Abbreviation: DAQ = data acquisition system and analog/digital output; PA = power amplifier; TTL = transistor-transistor logic)

Unlike piezoelectric stimulator, the magnetic one requires voltage-magnitude calibration to estimate the exact applied voltage corresponding to the desired stimulus magnitude. To do this, I used a Laser-Doppler Vibrometer (LDV; model AT3600, GRAPHTEC Corp., Japan), which can detect the displacement of vibrating object with no contact based on the Doppler effect on laser reflected by vibrating surface. Since the magnitude of the delivered stimulus varies with frequency at a given voltage, the calibration was performed at a frequency range of 5 to 800 Hz in 5 Hz intervals, and at a voltage range of 0.01 to 1 V in 0.01 V intervals. In each condition, a test sinusoidal signal was applied to the magnetic actuator during 1.5 s, and the velocity of wave signal was simultaneously recorded by DAQ. The velocity of wave signal was integrated between 0.25 and 1.25 s after stimulus onset, and then the Hilbert transform was performed to the integrated data. The absolute values of transformed data were taken to calculate the envelope, and then the median value of the envelope data was taken for stimulus magnitude of this condition.

The observed stimulus magnitudes contained some noise due to the unexpected vibration or electric devices in the recording room (**Fig. 4-3A**). Fortunately, a strong linear relationship between the input voltage and the observed at given frequencies (**Fig. 4-3A**, left). Therefore, after the interpolation at the 60 Hz electric noise frequency and its harmonics, the calibrated raw data at each frequency condition were linearly regressed, and the

calculated regression coefficients were saved as a matrix for later use. System diagram for stimulator calibration is depicted in **Fig. 4-3B**

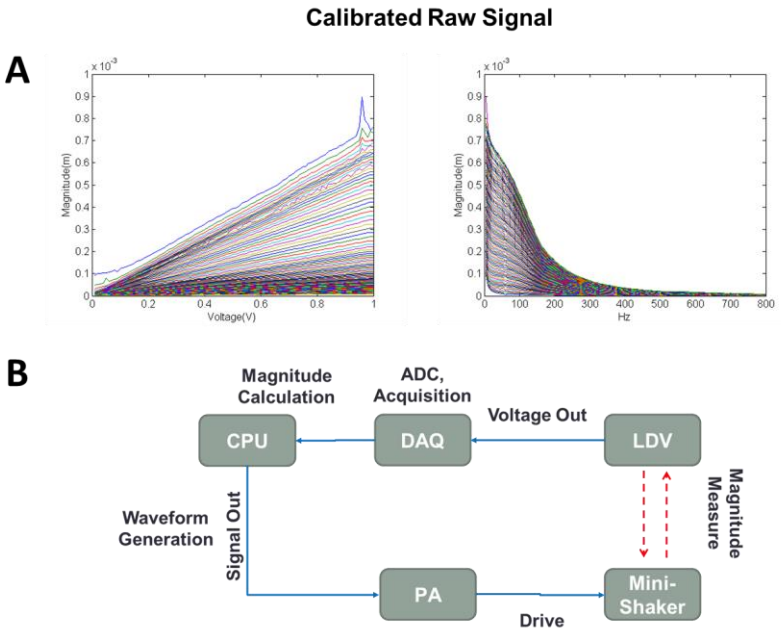

Figure 4-3. Initially calibrated raw signal (A) and diagram of calibration procedure. (abbreviation: ADC = analog-digital converter)

The developed stimulator can deliver almost any type of vibrotactile stimulation and the light pressure stimulation up to 4 mm indentation. However, this stimulator generates perceivable auditory noise at the resonance frequency of the shielded barrel (approximately 200 to 250 Hz). An auditory masking procedure is required when this stimulus frequency is delivered.

4.3. Disc-type Texture Stimulator

The pin-point vibrotactile stimulation enables to easily control the magnitude and frequency of stimulus; however, the delivered stimulus is far from the naturalistic one. Actually, the stimulus which we everyday experience through glabrous skin is two- or three-dimensional with temporal variation and stimulus direction – the texture perception. Thus, I initially designed a disc-type texture stimulator to deliver naturalistic texture stimuli to our fingertip. In fact, this type of texture stimulator has been widely used in cognitive psychological studies. However, unlike other experimental devices for psychological study, there are several technical considerations to design such device. First, the customized device should have appropriate size to perform ECoG experiment in the patient room. Epilepsy patients often perform their tasks on the patient bed, and the device should be located on the small table attached to the bed. Second, the device should be free of electromagnetic noise. Generally, most of commercial electric motors have permanent magnets generating huge electromagnetic noise when they rotate. Third, the device should be ergonomic. The patient often performs the tasks for 20-25 minutes with no movement, and the length and shape of the patient's finger are highly individual.

The custom-made disc-type texture stimulator is driven by an ultrasonic (US) motor (USR60 E3N; Shinsei Corp.). This motor is MR/MEG-compatible and consists of non-magnetic materials. To reduce other

electromagnetic noise, the main hardware of the stimulator including reduction gear, shaft, hand rest, and rotating disc were made of plastic. The US motor rotates the disc through a custom plastic gearbox with a 4:1 reduction ratio. For smooth contact between the finger and the surface of texture material, the stimulus on-/offset points were designed in a round hill shape (**Fig. 4-4A**). Hardware design was performed with Solidworks software (Dassault Systèmes SolidWorks Corp.).

A custom-made software written in embedded C was installed in MCU (Atmega 128; Atmel Corp.) to control the rotation speed and direction of disc via US motor driver (D6060E; Shinsei Corp.). The MCU recognizes the on-/offset time of stimulation and the current position of disc by detecting small gaps located on each quadrant of disc through the photo interrupter, and sends the information to the acquisition system and main computer. The MCU and main computer communicate via the universal asynchronous receiver/transmitter (UART). To control the MCU, a customized software written in MATLAB (MathWorks) was installed in the main computer. This software also controls the experimental paradigm.

The disc-type texture device has several limitations. First, this device cannot deliver more than two texture stimuli in one experimental session. Second, this device is unable to control the pressure on the finger during stimulation. Third, it is difficult to deliver the texture stimuli with periodic

patterns by this device because its sliding trace is circular. Such problems are solved in the drum-type stimulator.

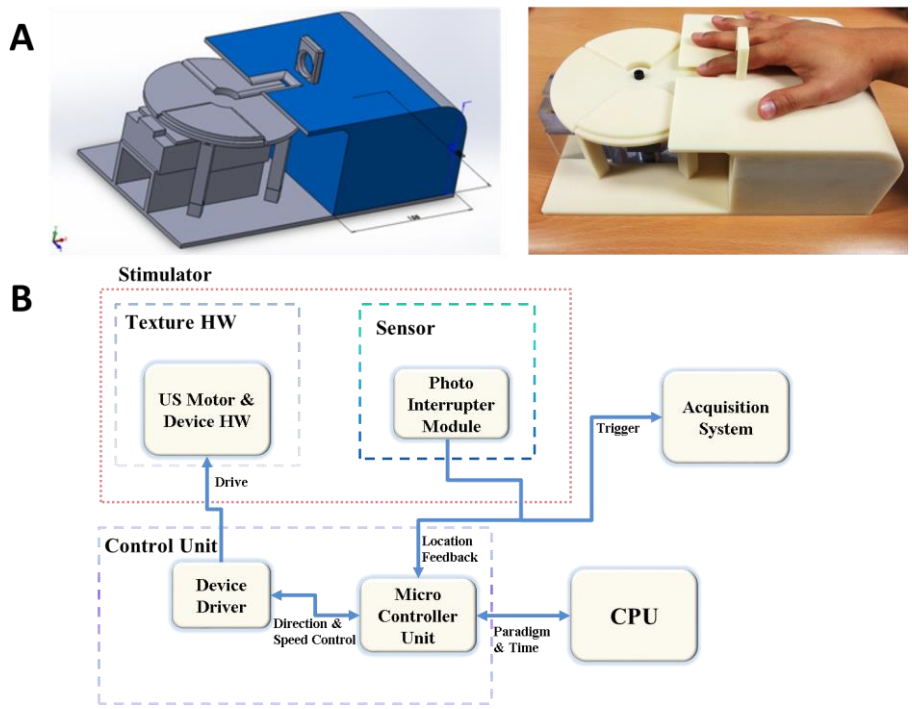

Figure 4-4. Hardware and system diagram of texture stimulator. 3-D design of disc-type texture stimulator (A, left) and its implemented version (A, right). In this figure, the position sensor module and texture materials are not yet installed and attached. (B) Diagram of texture stimulation system. The control unit and CPU are typically located outside the patient room.

4.4. Drum-type Texture Stimulator

The drum-type texture stimulator, inspired by the system in the Bensmaia's laboratory of Chicago university, was developed to overcome the limitation described in the previous section. This stimulator, an advanced version compared to the disc type one, was designed to pseudo-randomly deliver up to eight different textures with different normal forces (light touch to several hundred g wt.) (**Fig. 4-5**). Like the disc-type stimulator, I used the US motor to rotate texture drum through the custom-made gearbox with reduction ratio of 4:1. To reduce electromagnetic noise, moving parts during experiment including rotating drum (diameter: 190 mm), involute gears, and horizontal shaft were made of plastic. Stimulus on/offsets are detected by the photo interrupter and the trigger disc rotating with the drum (**Fig. 4-5D**). It works the same as the disc-type stimulator. Initially, I included real-time LDV recording module in the current system to precisely detect the stimulus on/offset and the frequency composition of ongoing stimulus. However, the module is not currently used for ECoG experiments because the entire system, including this module, is too bulky to be installed in the patient room.

To control the accurate horizontal movement of the texture drum, a geared encoder motor (reduction ratio = 600:1) and five photo interrupters detecting the boundary of the horizontal shaft (**Fig. 4-5F** and **H**) were used. Additionally, I used the rotation information of encoder motor with micrometer

precision to determine horizontal positions more precisely. I designed D-cut horizontal shaft to operate both rotating and horizontal movements. A customized round rack gear was attached at one end of the horizontal shaft. For smooth horizontal sliding of D-cut shaft, two linear bushing bearings were inserted into the vertical supports. To measure the normal force on the skin during stimulation, a small load cell was located under the plastic finger rest (**Fig. 4-5E**). The normal force between the finger and rotating drum is controlled by adjusting the knob of Lab Jack (SLJ-26; ScienceTown) located under the hand rest with micrometer precision. The hand rest was designed to deliver texture stimuli to the left or right index/middle fingers, regardless the shape of hand, and to change its position freely in the xy-plain (**Fig. 4-5G**).

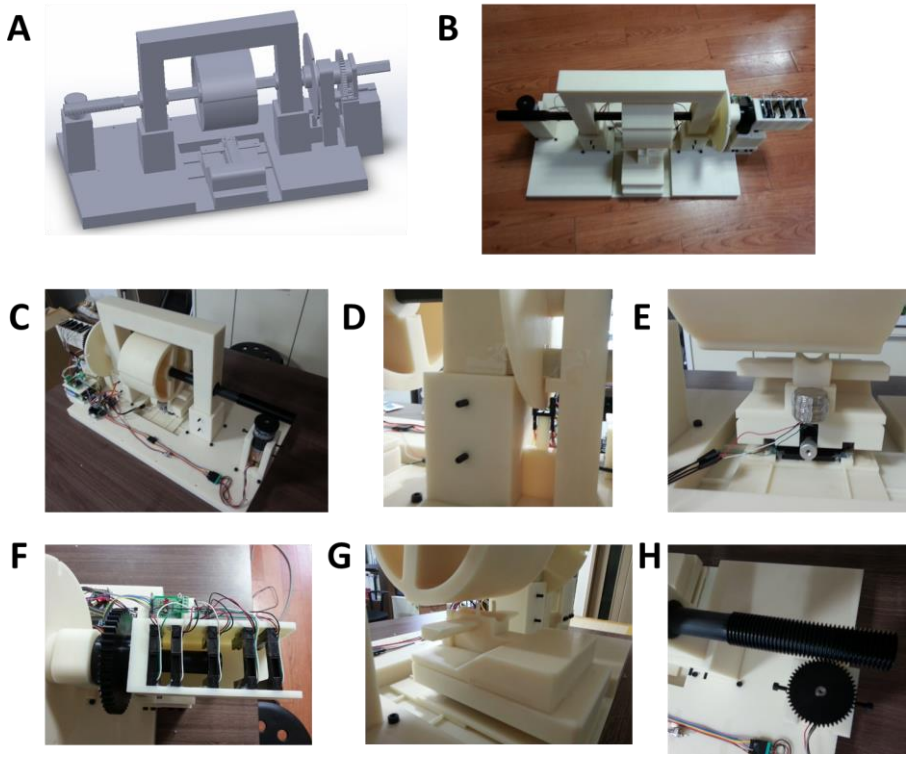

Figure 4-5. Drum-type texture stimulator. (A) 3-D design of texture stimulator hardware. Front (B) and rear (C) views of the implemented version. (D) Trigger disc and photo interrupter. (E) Lab Jack, weight sensor and finger rest. (F) Plastic gearbox and location sensors. (G) Hand rest and rotating drum. (H) Horizontal gear shaft and geared encoder motor.

The texture hardware module is directly controlled by 8-bit MCU (Atmega128; Atmel Corp.). Actually, most of signal processing for hardware control is conducted by the MCU in this system. The firmware installed in MCU was written in embedded C. The MCU counts pulses from the encoder of

the geared motor, and simultaneously detects the TTL signals from five location sensors, to calculate current horizontal position precisely. It also performs calibration between the number of encoder pulses and the horizontal displacement of shaft. It detects trigger signals from photo interrupter to estimate current state of the rotating drum, and then sends the state to the main computer. The MCU controls the movements of US and geared encoder motors via sending TTL signals to each driver module. The speed of both motors is manually controlled by adjusting the values of variable registers.

The main computer (CPU) performs paradigm control and data acquisition, sends commands about tasks programmed in MCU, and receives information about current status of hardware through the UART module. The weight sensor and LDV data are collected from the main computer through a DAQ device (USB 6002; National Instruments Corp.). The TTL trigger signal generated by the photo interrupter is transmitted to the acquisition system, DAQ, and MCU in parallel for time synchronization among them. The diagram of entire system is depicted in **Fig. 4-6**.

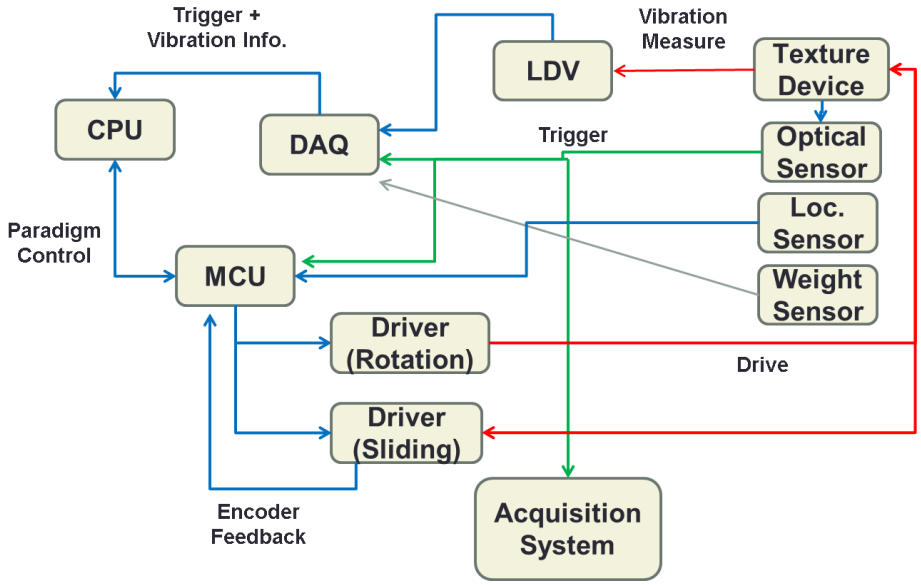

Figure 4-6. System diagram of drum-type texture stimulator.

Chapter 5: Vibrotactile and Texture Study*

*This chapter has been largely reproduced from an article published by Ryun, S., Kim, J. S., Lee, H., and Chung, C. K., Scientific Reports 7:15442 (2017).

*I thank H. Yeom, B. Kang for help with the ECoG experiments, and W. Jeong for providing MR and CT images.

Vibrotactile sensation is one of the important modalities in somatosensory perception for detecting dynamic mechanical fluctuations of our glabrous skin. Humans can perceive vibrotactile stimuli at a wide range of frequencies (up to several hundred hertz) by the information from several kinds of mechanoreceptors including Meissner and Pacinian corpuscles, but underlying macroscopic neural processing mechanisms in the neocortex are poorly understood. In this chapter, I investigated the macroscopic neural characteristics of various vibrotactile and texture stimuli including artificial and naturalistic ones in human S1 and S2 using ECoG. I found robust tactile frequency-specific high-gamma (HG, 50–140 Hz) activities in both S1 and S2 with different temporal dynamics depending on the stimulus frequency, especially at higher frequencies (>100 Hz). Stimulus-related HG activity in S1 exhibiting peaks with short latencies (50–100 ms), was attenuated more quickly

in vibration (>100 Hz) than in flutter (<50 Hz), and their attenuation patterns were frequency-specific within vibration range. In contrast, stimulus-related HG activity in S2, which was activated much later than that of S1 (150–250 ms), strikingly increased with increasing stimulus frequencies in vibration range, and their changes were much greater than those in S1. Furthermore, similar HG patterns of S1 and S2 were found in naturalistic stimulus conditions such as coarse/fine textures. These findings provide evidence that S2 is critically involved in neural processing for high-frequency vibrotaction. Therefore, I suggest that co-operation between S1 and S2 is crucial for a wide range of complex vibrotactile perception in human.

5.1. Introduction

Our ability to perceive mechanical fluctuations of glabrous skin plays critical roles in everyday life. It allows us to acquire information about the surface geometry of objects (Harvey et al., 2013), the roughness of textured objects (Hollins and Risner, 2000) and the relative fluctuation speed of our body parts (Romo and Salinas, 2003). However, our knowledge as to how the brain perceives various vibrotactile stimuli differently is largely limited. Several studies have suggested that stimulus-specific activity patterns of S1 cortical neurons might be related to various vibrotactile perceptions (Luna et al., 2005; Musall et al., 2014); however these neural correlates of certain tactile

information are also presented beyond the primary cortical region (Reed et al., 1996).

At the somatosensory periphery, the relatively fast (>5 Hz) mechanical fluctuations of the skin are mainly encoded by two specialized mechanoreceptors: Meissner (most sensitive in the flutter range, 5–50 Hz) and Pacinian (most sensitive in the vibration range, 100–400 Hz) corpuscles (Mountcastle et al., 1969). Due to the different frequency sensitivity of these two mechanoreceptors, it has been proposed that tactile information from them may be processed differently at the cortex level (Mountcastle et al., 1969).

The S1, the major neural entrance of somatosensory information, plays a critical role in the vibrotactile early processing. In primates, it has been suggested that the tactile flutter frequency is mainly encoded in the firing rate based patterns (Romo and Salinas, 2003; Salinas et al., 2000), whereas the vibration frequency is encoded in millisecond-precision spike timing (Harvey et al., 2013; Mackevicius et al., 2012). Although these studies have provided fundamental encoding mechanisms at the micro-level, it is still unknown how the encoded stimulus feature from these S1 neurons contributes to the specific vibrotactile perception including flutter and vibration in human. In fact, millions of neurons in various cortical regions are involved in vibrotactile processing. For instance, at the population level, more than 10% of cortical surface presents significant HG activation even in single-pulse median nerve

stimulation (Avanzini et al., 2016). Given this macroscopic aspect of neural characteristics, it is possible that vibrotactile perception may be gradually built up across a large-scale cortical network including S1, S2 and other sensorimotor-related areas. Specifically, the S2 may play a critical role in vibrotactile processing. Several previous human neuroimaging studies have suggested the stimulus-specific difference in blood oxygen level-dependent (BOLD) signals among vibrotactile frequencies including flutter and vibration in both S1 and S2 (Chung et al., 2013; Francis et al., 2000; Harrington and Downs III, 2001). However, the proposed results are controversial, and no direct electrophysiological evidence describing these phenomena has been reported. Furthermore, it remains largely unknown how the encoded information by the early processing in S1 is represented in the large-scale neuronal activation across various cortical regions in a submodality-specific (flutter and vibration) manner, with different spatiotemporal dynamics.

Scanning a textured surface with fingertip generates complex vibration pattern, and its frequency spectral characteristic is determined by the interaction between surface microgeometry of the texture and fingertip (Manfredi et al., 2014). Recent studies have indicated that neuronal firing activities of cutaneous mechanoreceptive afferents including Meissner and Pacinian fibers are closely related to the frequency composition of texture-elicited vibration (Bensmaïa and Hollins, 2005; Weber et al., 2013). However,

it is unclear how this encoded vibrotactile information is processed to elicit specific somatosensory perception at the human neocortex. Moreover, to my knowledge, it is largely unknown whether the neuronal responses to natural texture stimuli exhibit spatiotemporal characteristics similar to those of simplified artificial ones.

In the present study, I test the hypothesis that neural processing for specific vibrotactile perception involves co-operation among various cortical regions beyond the S1. Specifically, I investigate the tactile frequency-specific neuronal population activity in the human S1 and S2 during pin-point tactile flutter and vibration stimulation. Finally, I investigate the possibility that the neural activity patterns induced by the naturalistic texture stimulation are fundamentally related to those by the simplified artificial vibrotactile stimulation.

5.2. Materials and Methods

5.2.1. Patients

Six patients with intractable epilepsy were included in this study. Subdural electrode grids (Ad-tech Medical Instrument; electrode diameter of 4 mm; inter-electrode distance of 10 mm) were inserted into the cortical surface of patients to monitor electrocorticogram for clinical purpose. In Subjects 1, 4 and 6, additional intracerebral depth electrodes were inserted for monitoring subcortical activity. For electrode localization by co-registration, preoperative MR and postoperative CT images were acquired. All experiments and study procedures were approved by the Institutional Review Board of Seoul National University Hospital (H-1203-028-400). All subjects provided written informed consent before their participation (see **Table 5-1** for additional patient details).

Table 5-1. Demographics of all subjects

Subject	Age /Sex	Experiment	Electrodes location (Covered area)	# of electrodes	Diagnosis
#1	40/M	Pin-point	L (S1 and S2)	48	TLE
#2	24/M	Pin-point	L (S2)	54	OLE
#3	36/F	Texture	R (S2)	72	TLE
#4	31/M	Pin-point & texture	R (S1)	84	TLE
#5	34/F	Pin-point & texture	R (S1)	92	PLE
#6	25/M	Pin-point (2 sessions) & texture	L (S1)	58	PLE/TLE

Abbreviation: F, female; M, male; R, right; L, left; PLE = parietal lobe epilepsy, OLE = occipital lobe epilepsy, TLE = temporal lobe epilepsy.

5.2.2. Apparatus

Pin-point, sinusoidal vibrotactile stimuli were delivered by a customized piezoelectric actuator (stripe actuator; APC International, Ltd.) (**Fig. 5-1**). Detailed information about the apparatus is described in Chapter 4. For texture stimulation, the disc-type texture stimulator was used in this study. Stimuli were delivered through a rotating disc (diameter: 190 mm). Note that subject's index finger was located above the surface of the disc during the resting periods (**Fig. 5-1b**, top). Because the sliding speed varies depending on the distance from the

disc center, the subjects' fingertips were adjusted to be at the same position among subjects. Additionally, their fingers were fixed by the plastic ring mounted on the hand rest. Two different texture materials were attached to the opposite sides of each quadrant of the rotating disc (**Fig. 5-1b**, bottom).

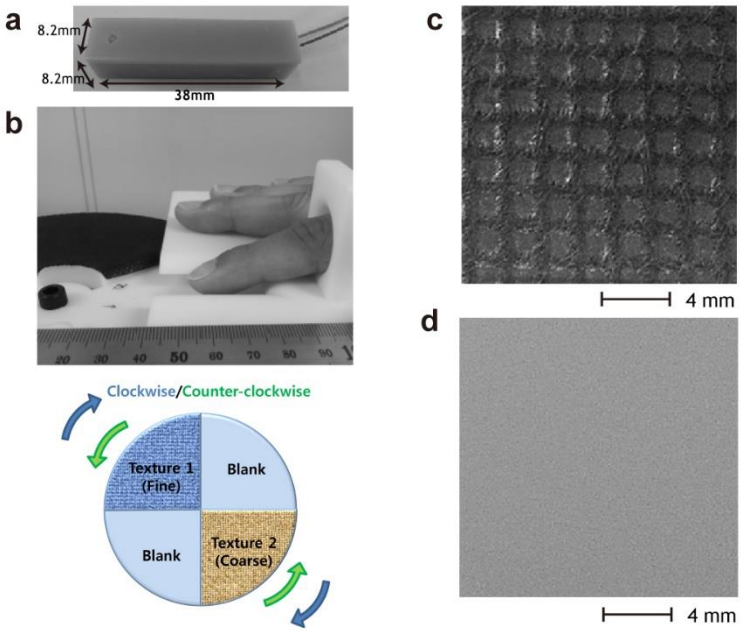

Figure 5-1. Stimulator design and surface of texture. (**a**) Pin-point vibrotactile stimulator. (**b**) Texture stimulator (top) and stimulation paradigm (bottom). No stimulus is delivered during blank periods. (**c**) Surface of the 2 mm grid texture for stimulating flutter frequency. (**d**) Surface of the fine texture for stimulating vibration frequency. (Adapted from Ryun et al., 2017b)

5.2.3. Experimental Design

Pin-point vibrotactile experiment. Stimuli were delivered to the index fingertip contralateral to the implantation site. Six different stimuli including flutter (5, 20 and 35 Hz) and vibration (100, 250 and 400 Hz) frequencies were pseudo-randomly delivered with 50 trials for each frequency (stimulus duration of 1 s with an inter-stimulus interval of 2.5, 3, or 3.5 s). No perceivable stimulus-related auditory sound was detected throughout the experiment. To compensate the inequality of the subjective intensity level depending on the frequency, I adjusted the stimulus amplitudes of the flutter (180 μm) and vibration (90 μm) based on previous literatures (Mountcastle et al., 1990; Verrillo et al., 1969).

Texture experiment. Two passive texture stimuli were delivered by the disc-type stimulator with a normal force of 15 to 30 g wt., a rotating speed of 10 rpm, a sliding speed of 63 mm/s (60 mm from the center of the disc), and a stimulus period of 1.5 s. Stimulation site was the same as that for vibrotactile experiment. A 2 mm grid texture (coarse texture) and a sandpaper-like fine texture (particle size < 50 μm, non-periodic particle pattern; made of acrylonitrile butadiene styrene) were used (**Figs. 5-1c and 5-1d**). The two texture materials were chosen according to the result of previous literatures, suggesting that coarse texture mainly activates SA1 (slowly adapting type 1), RA1 (rapidly adapting type 1) and PC (Pacinian corpuscle) afferents, whereas fine texture robustly activates PC afferents only (Bensmaïa and Hollins, 2005; Manfredi et al., 2014;

Weber et al., 2013). The expected peak frequencies elicited in the fingertip by the coarse and fine textures were 30–35 Hz (flutter range) and 200–250 Hz (vibration range), respectively (Manfredi et al., 2014). Stimuli were pseudo-randomly delivered with an inter-stimulus interval of 3.5, 4, or 4.5 s. Additionally, each texture stimulus was randomly delivered in a clockwise or counter-clockwise direction with 40 trials per direction to avoid a bias due to the scanning direction (**Fig. 5-1b**, bottom).

Throughout the experiment, the subjects were instructed to look at a fixation cross located far enough from the stimulator site to avoid the anticipation of stimulus on/offset. Additionally, the subjects were also instructed to pay attention to all of the stimuli because HG activities in somatosensory areas can vary depending on the degree of attention during the stimulus conditions (Steinmetz et al., 2000).

5.2.4. Data Acquisition and Preprocessing

A 128-channel amplifier system (Neuroscan) was used to record ECoG data with a sampling frequency of 1000 (for Subject 1) or 2000 Hz. Signals were band-pass filtered at 0.1–200 (for Subject 1) or 0.1–500 Hz. ECoG channels exhibiting pathological activities and abnormal fluctuations due to technical problems were excluded from further analysis. The recorded data were re-referenced to the common average reference (CAR). The re-referenced signals

were notch-filtered at 60 Hz and related harmonic frequencies with a finite impulse response (FIR) filter using the eegfilt function (EEGLAB), and epoched with a window of –1 to 3 s of stimulus onset. A semi-automatic MR-CT co-registration technique (CURRY software, version 7.0; compumedics neuroscan) was used to localize ECoG electrodes of each subject.

5.2.5. Analysis

All analyses were performed with Matlab. In the present study, it is extremely critical to determine the exact ECoG electrodes exhibiting the S1 and S2 activities. ECoG electrodes located on the hand knob, an anatomical landmark of hand area, and presenting well-known S1 tactile responses, such as strong ERP responses within 50 ms of stimulus onset and event-related desynchronization (ERD) responses were determined as S1 electrodes. Electrodes located on the upper limb of the sylvian fissure in the parietal region were designated as S2 electrodes, according to the previous findings (Allison et al., 1992; Disbrow et al., 2000; Frot and Mauguière, 1999).

For time-frequency representations, the epoched data were transformed to the data having time-frequency dimension by the continuous Morlet wavelet decomposition (the effective window length (95% confidence interval of the Gaussian kernel, seven cycles) of 80 ms at 50 Hz). The power levels of the transformed single-trial data were calculated by squaring each data

point, and then were normalized by the mean and standard deviation of the baseline power (–1 to 0 s of stimulus onset) of each frequency. For visualization, the single-trial normalized data were temporally smoothed (the window length of 50 ms) and then averaged across all trials. Note that the result of this procedure does not indicate the Z-score, but has an arbitrary unit.

To test the significance among stimulus conditions, the HG (50–140 Hz) power levels of each stimulus condition was averaged across the stimulus period (from 0.2 s after stimulus onset to 0.1 s (0.2 s for texture) before stimulus offset). The S1 HG activities of the transient stimulation period (50–100 ms after stimulus onset) were excluded from this analysis because their power levels of this period did now show the tactile frequency dependence during the pre-screening analysis. However, the overall results did not change when this period was included. The frequency range of HG band was initially determined according to previous studies (Avanzini et al., 2016; Canolty et al., 2006; Ray et al., 2008a). However, since the frequency boundaries of the HG band showed large inter-individual differences, the bandwidth was finely adjusted by visual inspection of the dataset (50–140 Hz). The on/offset times of the HG activities were determined according to the criteria from the literatures (Hotson et al., 2016; Ryun et al., 2017a). For significance testing, I used independent two-sample *t* test and one-way ANOVA for multiple conditions. For normality testing, the Lilliefors test was performed before significance testing ($P > 0.01$,

for all datasets). The Bonferroni correction procedure was applied to all multiple comparisons.

To investigate the temporal dynamics of the HG power during stimulation, the normalized single-trial HG time series data were temporally averaged within each 50 ms time bin with a time range from –0.4 to 1 s of stimulus onset. For visualization, these binned data were averaged across all trials, and were then smoothed by spline functions. To calculate a grand average of binned time series data from all S1 subjects, the data from each subject were divided into the maximum peak values of each data, and then averaged across subjects. The independent two-sample *t* test with Bonferroni correction was used to test the significance of the HG difference between the flutter and vibration at each time bin.

For classification among stimulus conditions, several single-trial HG features were extracted from two or three electrodes located on S1 or S2. A simple or multiclass linear support vector machine (SVM) algorithm with five-fold cross validation was utilized to determine whether the single-trial HG activity of the S1 or S2 contains sufficient information about vibrotactile stimulus frequencies.

5.3. Results

5.3.1. Frequency-specific S1/S2 HG Activities

To test whether neuronal population activities represent the information of vibrotactile stimulus frequencies including the flutter (5, 20 and 35 Hz) and vibration (100, 250 and 400 Hz) frequency range, I initially investigated the temporal-spectral aspects of neural activities in the S1 and S2 during stimulation. Overall, the stimulus-related HG power changes were observed both in S1 and S2, and their patterns were highly frequency-specific in vibration conditions. Interestingly, their decreasing/increasing patterns depending on the vibration frequency (>100 Hz) were clearly different between the S1 and S2 (**Fig. 5-2** and **5-3**).

In S1, prominent HG power increases were observed during all stimulus conditions. The HG activity in S1 started to increase at 27 ± 10 ms (mean ± SD) after stimulus onset and lasted until the end of stimulation. No significant difference in the onset timings was found between the event-related potentials (ERPs) and the HG activities in S1 (paired *t*-test; $t = 1.60$, $P = 0.13$). At the flutter range, the differences in HG power level among three conditions were relatively small and showed inconsistent patterns (**Fig. 5-2c** and **Table 5-2**). These trends were also observed in the 100 Hz vibration frequency condition; however, the increased HG power level was significantly attenuated with increasing the stimulus frequency above 100 Hz. These frequency-specific HG

attenuation patterns under the vibration conditions were consistently observed in all four subjects (**Fig. 5-2c**).

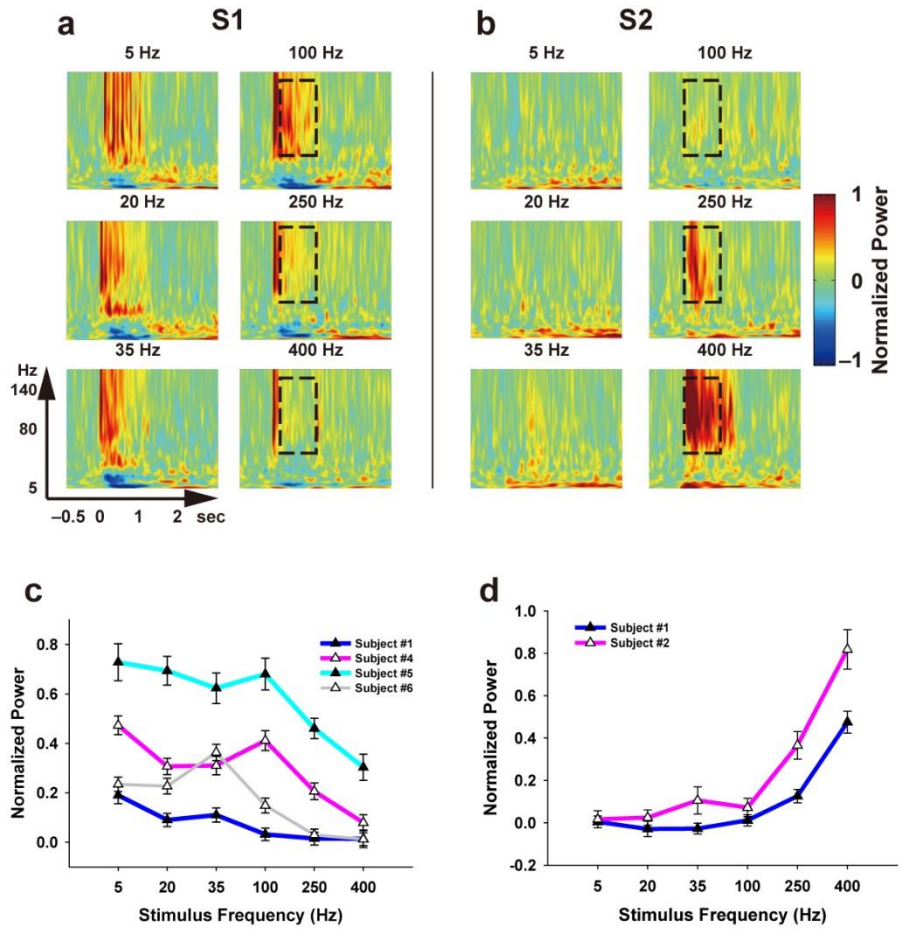

Figure 5-2. Representative time-frequency plots for flutter and vibration conditions (5, 20 and 35 Hz for flutter; 100, 250 and 400 Hz for vibration) in S1 (**a**, from Subject 4) and S2 (**b**, from Subject 2). Time t = 0 and t = 1 s indicate stimulus onset and offset, respectively. Dashed boxes indicate the time (0.2 to

0.9 s after stimulus onset) and the frequency range (50 to 140 Hz) which shows prominent HG power decreases in S1 (**a**), and increases in S2 (**b**) with an increase the stimulus frequencies above 100 Hz (**c** and **d**). Line plots for HG power levels from Subjects 1 (blue), 4 (pink), 5 (cyan) and 6 (gray) in S1 (**c**) and from Subjects 1 (blue) and 2 (pink) in S2 (**d**). Error bars in both (**c**) and (**d**) denote the s.e.m. Significance testing results among the various stimulus conditions are shown in **Table 5-2**. (Adapted from Ryun et al., 2017b)

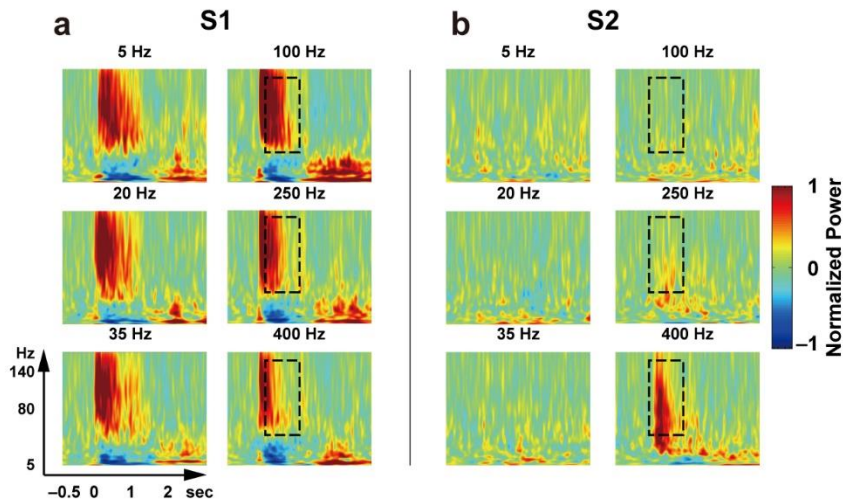

Figure 5-3. HG time-frequency plots from other subjects. Legends and dimensions are the same as **Fig. 5-2a** and **b**. (**a**) S1 HG results from Subject 5. (**b**) S2 HG results from Subject 1.

Table 5-2. Results of significance testing among various stimulus frequencies

Subject (S1/S2)	Within flutter	Flutter vs. 100 Hz	Flutter vs. 250 Hz	Flutter vs. 400 Hz	100 vs. 250 Hz	250 vs. 400 Hz	100 vs. 400 Hz
1 (S2)	0.69*	0.39*	5.57×10^{-4}	6.42×10^{-23}	0.049	8.94×10^{-7}	2.84×10^{-11}
	($F_{(2, 147)} = 0.38$)	($t_{198} = 0.85$)	($t_{198} = -4.03$)	($t_{198} = -11.5$)	($t_{98} = -2.76$)	($t_{98} = -5.70$)	($t_{98} = -7.90$)
2 (S2)	0.37*	0.67*	5.37×10^{-6}	4.62×10^{-20}	0.0023	0.0010	8.15×10^{-10}
	($F_{(2, 147)} = 1.01$)	($t_{198} = 0.43$)	($t_{198} = -5.11$)	($t_{198} = -10.5$)	($t_{98} = -3.72$)	($t_{98} = -3.95$)	($t_{98} = -7.21$)
4 (S1)	0.011	0.33	0.0020	1.1×10^{-9}	0.0014	0.057	3.80×10^{-8}
	($F_{(2,147)} = 6.84$)	($t_{198} = 1.08$)	($t_{198} = 3.70$)	($t_{198} = 6.75$)	($t_{98} = 3.88$)	($t_{98} = 2.70$)	($t_{98} = 6.40$)
5 (S1)	0.51*	0.98*	0.011	2.36×10^{-6}	0.032	0.13	1.19×10^{-4}
	($F_{(2, 147)} = 0.67$)	($t_{197} = 0.02$)	($t_{197} = 3.16$)	($t_{197} = 5.21$)	($t_{96} = 2.85$)	($t_{96} = 2.32$)	($t_{96} = 4.49$)
6 (S1)	0.021	0.0042	5.15×10^{-11}	4.11×10^{-12}	0.015	0.60*	0.0050
	($F_{(2,297)} = 5.94$)	($t_{398} = 3.46$)	($t_{398} = 7.06$)	($t_{398} = 7.45$)	($t_{198} = 3.12$)	($t_{198} = 0.52$)	($t_{198} = 3.45$)

Unit = *P* values (Bonferroni corrected; * = uncorrected *P* values).

S1 = primary somatosensory cortex; S2 = secondary somatosensory cortex.

No prominent HG response in S2 was found under the flutter conditions. Notably, however, the S2 HG power level strongly increased with increasing stimulus frequencies in vibration range (>100 Hz). Furthermore, the HG power level in S2 was more strikingly changed than that in S1 with opposite pattern. This trend was consistently observed in both subjects (**Fig. 5-2d**). The temporal characteristics of S2 HG response were considerably different compared to those of S1. The S2 HG responses showed maximum peaks at 150–250 ms after stimulus onset and lasted 250–300 ms after stimulus offset. The differences in HG power level among the vibration conditions were highly significant (**Table 5-2**), whereas those among flutter conditions were not statistically different. Similar patterns were also observed from Subject 1's intracerebral depth electrodes inserted near the S2 (**Fig. 5-4**). Interestingly, the HG power level of 100 Hz condition was almost the same as those of the flutter conditions, although this condition has conventionally been regarded as the vibration range.

I performed the same analysis for the other frequency bands including the theta (4–7 Hz), alpha (8–14 Hz), beta (15–30 Hz) and low-gamma (30–50 Hz). No consistent and significant difference across the subjects and conditions was found except the low-gamma band. It might be due to the signal leakage from the HG band. In the ERP analysis, no distinct tactile frequency-specific ERP peak pattern was found in S1. In S2, however, strong and long-latency HG

(150–250 ms after stimulus onset) peaks were observed in the 250 Hz and 400 Hz stimulus conditions (**Fig. 5-5**). They seemed to be closely related to the HG activity given the latencies and increasing patterns of these two properties.

The results of topographical mapping analysis indicate that prominent HG power differences are mainly found in S2 (the posterior part of the upper bank of the sylvian fissure) and S1 (**Fig. 5-6**). However, it does not guarantee that only the S1 and S2 areas are critically involved in the vibrotactile processing. This point will be investigated deeply in the Chapter 7.

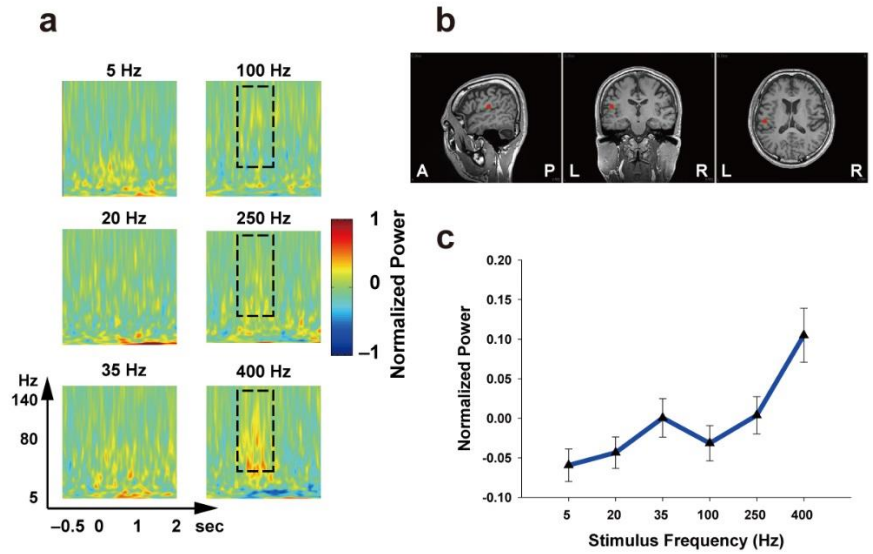

Figure 5-4. Frequency-specific HG activity in intracerebral electrode. (**a**) Time-frequency plots for various vibrotactile frequencies from Subject 1's intracerebral electrode. (**b**) Location of the intracerebral electrode. The

electrode contact was located at the parietal operculum. (**c**) Line plots of the HG activities among various stimulus frequencies. Their patterns were analogous to the results from the ECoG electrodes. Error bars indicate s.e.m.

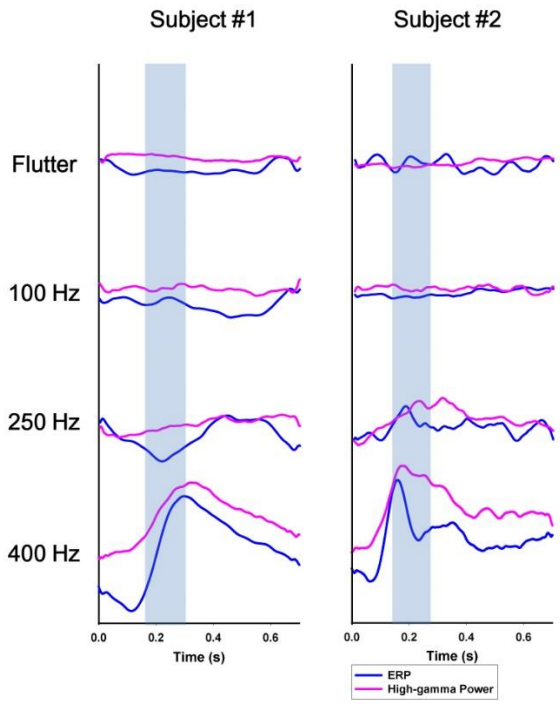

Figure 5-5. HG and ERP time series in S2. S2 HG time series (pink) and simultaneous ERP (blue) at various vibrotactile frequencies in Subjects 1 (left) and 2 (right). Y-axes of each condition have arbitrary units for matching the scale between them. The results show that their peak patterns in the high-frequency conditions have similar timescales.

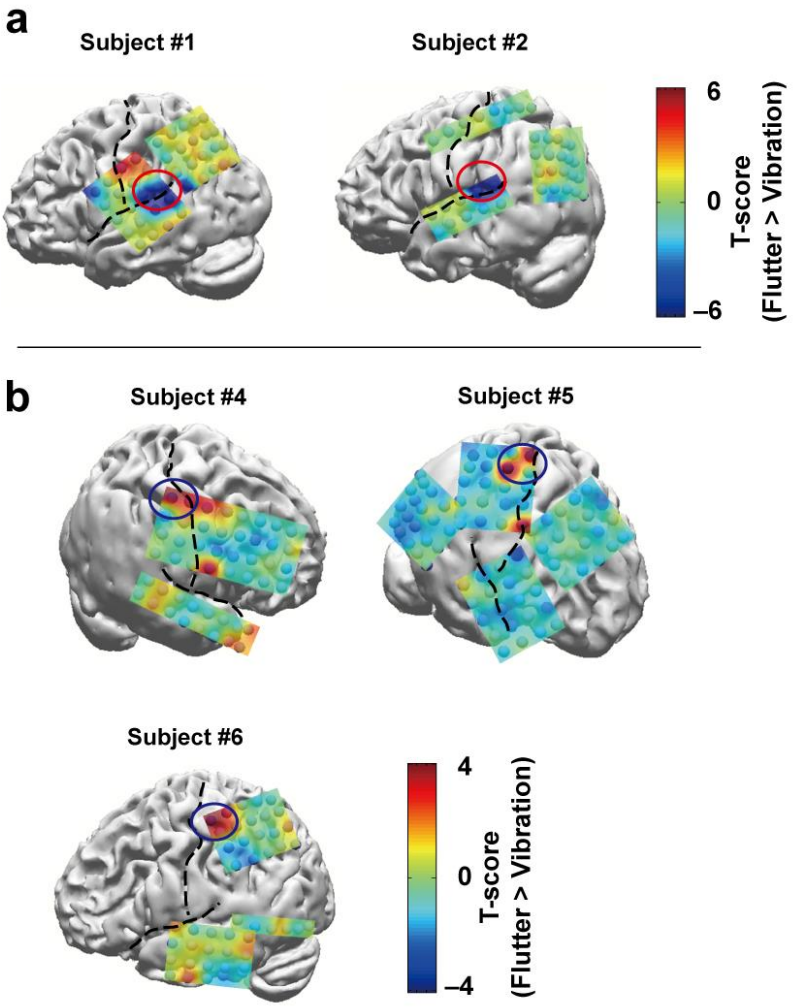

Figure 5-6. Topographical maps of the HG power differences between the flutter and vibration stimulus conditions. Dashed lines indicate the central sulcus and Sylvian fissure. The blue and red circles indicate the S1 hand and S2 area, respectively. The red/blue areas in the topographical map indicate that the HG powers in the flutter conditions are higher/lower than those in the vibration conditions. (**a**) Topographical maps of Subjects 1 and 2. Both subjects show a dominant power difference in the same region, S2. In Subject 1, a power

difference is also seen in the S1 region (red area). (**b**) Topographical maps of Subjects 4–6. These subjects' electrodes were located in the S1 region. Some electrode grids/strips were excluded because they were located at invisible sites.

5.3.2. S1 HG Attenuation during Flutter and Vibration

In the present section, I investigated the temporal dynamics of HG activity in S1 during stimulus period. As I shortly mentioned in the previous section, in terms of temporal dynamics, the magnitude of the HG power peaks, which was formed at 50–100 ms after stimulus onset, showed no significant difference between the flutter and vibration conditions in Subjects 5 and 6. Moreover, the magnitude of the HG peaks in vibration conditions was sometimes higher than that in flutter conditions (**Fig. 5-7b–d**). Based on these observations, I hypothesized that these differences in S1 are due to different degree of temporal attenuation in the HG power level between the flutter and vibration conditions. To confirm this, I calculated binned HG power time series for each stimulus condition. I found that HG power in flutter showed more sustained activity at the stimulus period (0.2 to 0.9 s of stimulus onset) than that in vibration. In contrast, the power in vibration was rapidly attenuated during that period (independent two-sample t test, $P < 0.001$, Bonferroni corrected) (**Fig. 5-7**). Importantly, the degree of HG power attenuation increased with increasing stimulus frequency within vibration condition, whereas no difference was found among flutter conditions (**Fig. 5-7a**). In this analysis, the S1 HG data

from Subject 1 was excluded because its signal-to-noise ratio was extremely low.

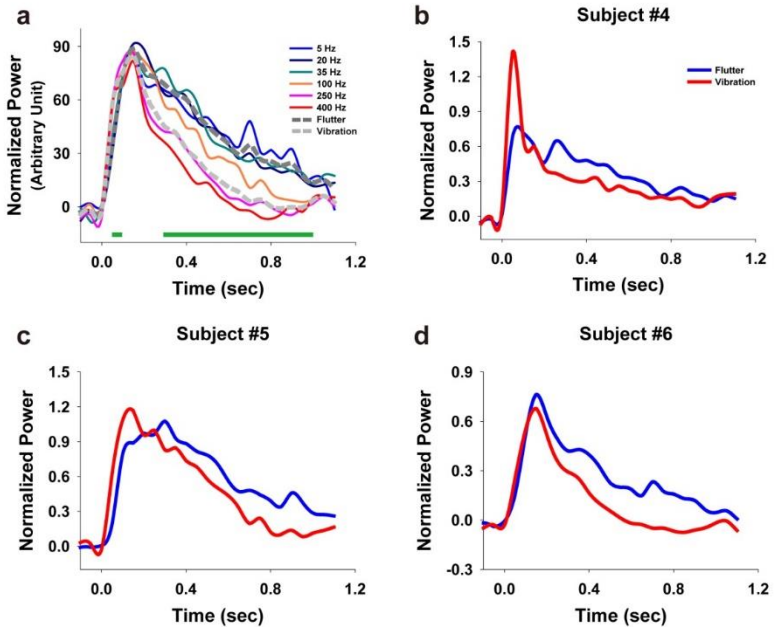

Figure 5-7. S1 HG power time series under the flutter and vibration stimulus conditions. Time t = 0 s denotes stimulus onset. (**a**) Average power time series plots across all three subjects (Subjects 4, 5 and 6). Each line indicates the 5 (blue), 20 (dark blue), 35 (dark cyan), 100 (orange), 250 (pink) and 400 Hz (red) conditions. Dashed dark gray and gray lines denote the average flutter and vibration conditions, respectively. The green bars indicate the time bins exhibiting significant power differences between the flutter and vibration conditions ($P < 0.001$, Bonferroni corrected). (**b–d**) HG power time series of individual subjects. The blue and red lines represent the flutter and vibration

conditions, respectively. (Adapted from Ryun et al., 2017b)

5.3.3. Single-trial Vibration Frequency Classification

The results of previous section suggest that HG power changes in the S2 area during vibration stimuli are more prominent than those in S1, and their frequency-specific patterns are highly significant. Given these results, I tested whether the stimulus frequencies can be discriminated by the stimulus-related HG activity from single-trial ECoG data with high accuracy. To do this, I extracted HG features from single-trial data with two or three electrodes, and then calculated the classification accuracy using the simple and multiclass linear SVM. I initially evaluated condition-by-condition classification accuracy to compare the performance among three possible pairs. All condition pairs were classified with high accuracy (69.0–96.2%; chance level = 50%), and the highest classification performance was achieved with the 100 vs. 400 Hz condition (96.2% from Subject 1, 86.0% from Subject 2) (**Fig. 5-8a**). Classification accuracies over the three conditions were 72.0 and 63.3% (chance level = 33%) in Subjects 1 and 2, respectively (**Fig. 5-8b**, left). I also evaluated the classification performance using the HG features from S1. Their accuracies were lower than those in S2, although they were above the chance level (**Fig. 5-8b**, right).

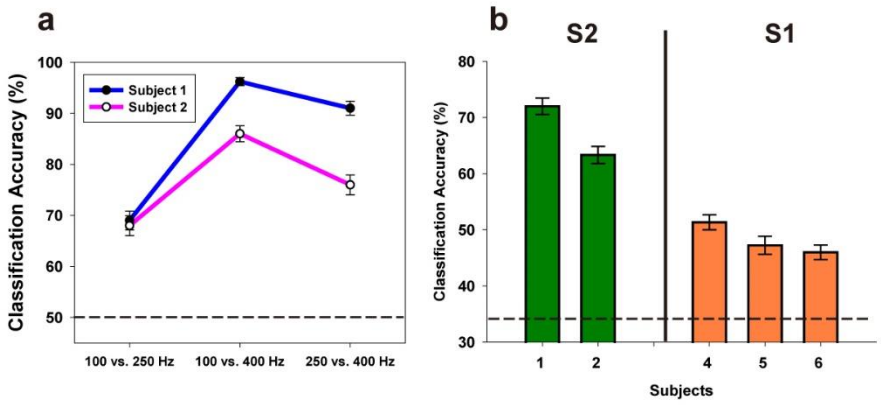

Figure 5-8. Classification results. (**a**) The accuracy of the stimulus frequency classification by simple SVM using single-trial HG features from S2. The x axis indicates three possible stimulation pairs. Dashed line indicates the chance level (50%). (**b**) The accuracy of the stimulus frequency classification by multiclass SVM using the single-trial HG features from S2 (left, green bars) and S1 (right, orange bars). The dashed line indicates the chance level (33 %). Error bars in both (**a**) and (**b**) indicate the s.e.m. (Adapted from Ryun et al., 2017b)

5.3.4. S1/S2 HG Activities during Texture Stimuli

In this section, I test whether the neural response characteristic for the naturalistic tactile sensation such as surface scanning for natural textures through the glabrous skin can be explained by the result of the previous section. Although a previous study indicated that Pacinian (PC) afferents at the peripheral level are highly sensitive in both coarse and fine texture stimulations (Weber et al., 2013), in terms of population activity, the relative activation ratios

between RA1 and PC afferent populations in coarse and fine texture stimulations might be similar to those in our pin-point flutter and vibration stimulations. Interestingly, I found that HG power decreasing/increasing patterns in S1 and S2 during coarse/fine texture stimulations are analogous to those from the pin-point vibrotactile experiment (**Fig. 5-9a**). In S1, HG power level of the coarse texture condition was significantly higher than that of the fine texture condition across all three subjects (**Fig. 5-9b**). Notably, a significant increase in S2 HG power level was observed in the fine texture condition compared to the coarse one (**Fig. 5-9c**). The temporal characteristics of HG activity in S2 were similar to the results from pin-point stimuli (200–300 ms after stimulus onset). Furthermore, these distinct S1/S2 HG patterns between the coarse and fine textures were consistently observed regardless of the scanning direction (two-way ANOVA; interactions: texture × direction; $F_{(1, 156)} = 0.83$, $P = 0.36$ in Subject 3; $F_{(1, 156)} = 0.02$, $P = 0.89$ in Subject 4; $F_{(1, 156)} = 0.73$, $P = 0.40$ in Subject 5; $F_{(1, 316)} = 0.07$, $P = 0.79$ in Subject 6). Note that the texture-specific difference in HG power level was only found in the S2 area (**Fig. 5-10**).

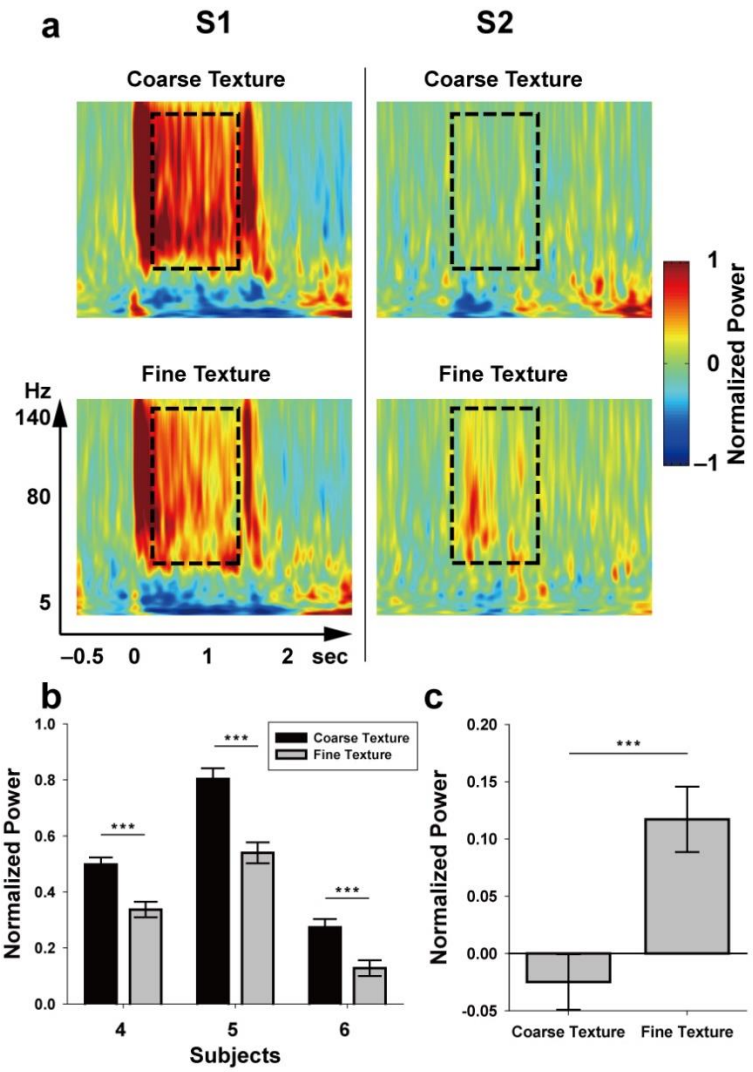

Figure 5-9. (a) Representative time-frequency plots for coarse (top) and fine (bottom) textures in S1 (left column, from Subject 5) and S2 (right column, from Subject 3). Time t = 0 and t = 1.5 s indicate stimulus onset and offset, respectively. Dashed boxes indicate the time (0.2 to 1.3 s after stimulus onset) and frequency range (50 to 140 Hz). Bar plots denote the HG power levels in S1 (b) and S2 (c, from subject 3) during coarse and fine texture stimulations.

Error bars indicate the s.e.m. The power differences between the two conditions were significant across all subjects ($P < 0.001$). (Adapted from Ryun et al., 2017b)

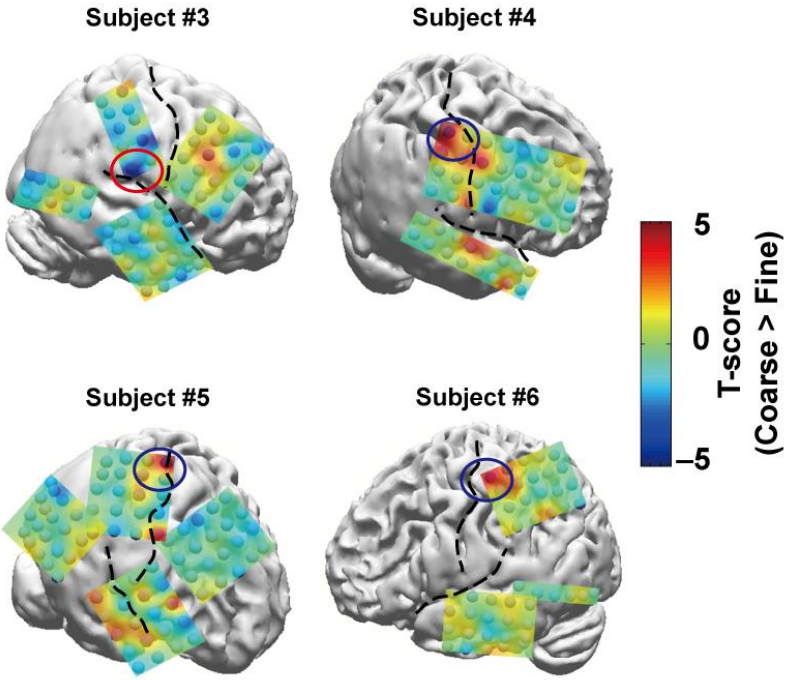

Figure 5-10. Topographical maps of HG power level differences between the coarse and fine texture conditions. Dashed lines indicate the central sulcus or Sylvian fissure. The blue and red circles indicate the S1 hand and S2 area, respectively. The red/blue areas in the topographical map indicate that the HG power levels in the coarse texture conditions are higher/lower than those in the fine texture conditions.

5.4. Discussion

5.4.1. Comparison with Previous Findings

Previous single unit recording and optical intrinsic signal (OIS) imaging studies suggested that there are prominent decreases in the mean firing rate and absorbance during 200 Hz vibration stimuli as compared to 20 Hz flutter stimuli in S1 (Tommerdahl et al., 1999a; Tommerdahl et al., 1999b). These studies also indicated that the firing rates of the initial stimulation period (or transient period; 100 to 300 ms) are very similar between both conditions, but then rapidly decrease in the vibration condition. In the present study, I found similar neural response patterns for vibrotactile stimulation at the population level. Indeed, recent studies have indicated that the temporal evolution associated with local field potential (LFP) HG activities are tightly correlated with the time-series of the average firing rate (Ray et al., 2008a; Ray et al., 2008b). Although such strong relationship between the HG and spiking activities is not always true (Scheffer-Teixeira et al., 2013), the present findings suggest that frequency-specific neural attenuation for tactile processing in S1 is not only the result of micro-level computation but also the macroscopic phenomenon in human.

5.4.2. Tactile Frequency-dependent Neural Adaptation

In this study, frequency-dependent attenuation patterns of HG activities in S1 were exclusively observed within the vibration conditions whereas no significant difference was found within the flutter conditions. If the HG activity on vibrotactile stimulation is closely related to the firing rates of the neuronal population (Ray et al., 2008a; Ray et al., 2008b), the present results in S1 can be explained in relation to the evidence of micro-level studies. Although HG band is only one component of the neural oscillatory activities in S1, the present result may stem from 1) the differences in the distribution and frequency sensitivity between the RA and PC neurons in S1, or 2) the stimulus frequency-dependent adaptation property of the S1 neuronal population. In fact, RA neurons are densely distributed in the S1 area, whereas the distribution of PC neurons is relatively sparse (Lebedev and Nelson, 1996; Mountcastle et al., 1990). Accordingly, the increases in activities of RA neurons may induce a more dominant effect on the HG activity compared to those of PC neurons. Because the sensitivity of RA neurons gradually decreases with increasing stimulus frequencies in the vibration range (Merzenich and Harrington, 1969), the overall amount of afferent neuronal activity can be subsequently decreased in this frequency range. In the present result, however, the S1 HG responses at the transient period (0 to 200 ms of the stimulus onset) were not statistically different between flutter and vibration conditions. It is mainly due to the fact

that most of the touch-sensitive afferent neurons in the S1 area tend to be highly activated at the first transient stimulus of the stimulus train (Delmas et al., 2011). In terms of the attenuation of HG activity at the sustained period, it is reasonable to hypothesize that there exist different adaptation properties depending on the stimulus frequency in the vibration range. Indeed, in the rat barrel cortex, the increase in stimulus frequency increases a degree of neuronal adaptation in the flutter range, and this phenomenon is closely related to the frequency discrimination performance (Khatri et al., 2004; Musall et al., 2014; von der Behrens et al., 2009). In this study, no frequency-specific HG adaptation was observed in the flutter range. However, it may be due to the fact that the mean firing rates of the S1 afferent neurons also increase with increasing stimulus frequencies in the flutter range (Luna et al., 2005). In light of this, it is possible for the overall neural population activities not to present any distinct differences among these frequencies. In contrast, in the vibration range, the firing rates of S1 afferent neurons are almost independent of the stimulus frequencies (Harvey et al., 2013). Therefore, the present results may represent large-scale, frequency-dependent neuronal adaptation in the vibration range.

5.4.3. Serial vs. Parallel Processing between S1 and S2

The present findings may provide insight into the ongoing debate about the serial versus parallel processing of somatosensory system including S1 and S2 (Kalberlah et al., 2013; Zhang et al., 2001). Given the present results, it seems that the HG activity in S2 does not directly represents the early response for high-frequency vibrotactile information. Rather, for several reasons, these activities may depend on the information from the primary area, such as S1, and be induced by the result of the interaction between RA1 and PC neurons in S1. First, the HG responses in S2 showed a relatively long latency (150–250 ms) compared to those in S1 (50–100 ms), and lasted 250–300 ms after stimulus offset. This indicates that the S2 HG responses are not induced by the direct input from thalamus but by the cortico-cortical information transfer. This mechanism, the serial processing, is strongly supported by many previous findings (de Lafuente and Romo, 2006; Inui et al., 2004; Pons et al., 1987). Second, the S2 HG activity on vibration frequency does not represent the well-known frequency sensitivity patterns of the PC afferents (most sensitive around 200–250 Hz) (Mountcastle et al., 1969; Verrillo et al., 1969). Third, in the texture stimulation, robust HG activities were found only in the fine texture condition. A previous finding indicated that both coarse and fine texture stimuli strongly activate PC afferent neurons (Weber et al., 2013). If the HG activities in S2 solely represent the information from PC afferents, significant S2

activities should be observed in both conditions. Therefore, given the present findings and previous literatures, I propose that the frequency-specific S2 HG activity is induced by the cortico-cortical, or hierarchical processing, and this activity may represent a higher-level tactile processing such as tactile perceptual categorization. Indeed, several studies have indicated that S2 area is involved in the tactile roughness perception (Pruett et al., 2000; Sathian, 1989), and shape perception (Connor and Johnson, 1992; Weber et al., 2013).

5.4.4. Conclusion of Chapter 5

Findings in this chapter provide important insights into the macroscopic neural processing for vibrotactile sensation. Unlike micro-level studies, the present findings suggest that human vibrotactile sensation involves macroscopic multi-regional hierarchical processing in the somatosensory system, even during the simplified stimulation. This implies that human tactile perception cannot be determined by the neural activities of specific cortical region, but by the neural ensemble of sensory-related cortical networks. This point will be demonstrated further in Chapter 7.

Chapter 6: Somatosensory Feedback during Movement*

*This chapter has been largely reproduced from an article published by Ryun, S., Kim, J. S., Jeon, E., and Chung, C. K., Frontiers in Neuroscience, 11:408 (2017).

In the previous chapter, I discussed the macroscopic neural processing mechanism of the passive tactile somatosensation. In this chapter, I will demonstrate the other important somatosensory function – proprioception. Indeed, proprioceptive feedback plays essential roles in control of our body movement. However, its underlying neural mechanism in our brain is largely unknown. It is mainly due to the fact that it is almost impossible to separate proprioception from motor behavior, especially in human study. Likewise, during active movement, it is very difficult to distinguish which neural activities represent the motor command and which ones represent the proprioceptive feedback. Furthermore, when assessing this issue, an internal feedback mechanism, efference copy, should be considered throughout active movement. In this study, I suggest that S1 HG activity during active movement mainly represents the neural activation for somatosensory feedback, and this activity is less relevant to the cortico-cortical feedback information before

movement such as efference copy.

6.1. Introduction

Somatosensory feedback during any type of movement is an essential function for precise and dexterous motor control. It is well-known that loss of somatosensory feedback causes severe deficits of movement control (Jenmalm and Johansson, 1997; Rothwell et al., 1982; Sanes et al., 1984). Since our body always receives somatosensory feedback consciously or unconsciously, it is very difficult to imagine the environment without somatosensory feedback. Without this, however, we would not be able to perform most everyday actions such as walking, chewing and any type of hand manipulation. In human brain, the S1 mainly receives proprioceptive inputs from periphery and processes the cortico-cortical feedback information induced by motor command, including efference copy (Christensen et al., 2007). It also modulates the proprioceptive and tactile input by sending a top-down signal to the dorsal horn, which is not modulated by primary motor cortex (M1) (Armand et al., 1997; Lemon, 2008).

Somatosensory feedback signals generated by mechanoreceptors of the periphery generally reach the S1 within tens of milliseconds. In the cortex level, the early component of the event-related potentials (ERPs) in S1 is considered the primary response of somatic afferents, and event-related de-

synchronization (ERD) is regarded one of the induced component of such primary response (Lim et al., 2012; Wiest and Nicolelis, 2003). Additionally, in invasive recording such as ECoG and microelectrode recordings, prominent HG responses are detected in the sensorimotor-related area both during passive and active somatosensory stimulation (Avanzini et al., 2016; Miller et al., 2007; Ray et al., 2008a). Specifically, the HG activity in S1 is possibly related to the movement-related somatosensory feedback (Chestek et al., 2013). In terms of the functional characteristics of HG activity in somatosensory area, several studies indicated that HG activities are tightly correlated to the population of neuronal firing and the intensity of somatosensory stimulation (Ray et al., 2008b; Rossiter et al., 2013; Zhang et al., 2012).

Active movements also induce strong HG activities in the sensorimotor area (Cheyne et al., 2008; Crone et al., 1998). Since HG activities show the motion-specific activation patterns in the sensorimotor area, features from these activities have often been used for ECoG-based brain-machine interface (BMI) which decodes actual movement. However, it is still unclear as to whether HG activities in the sensorimotor area during active movement mainly represent the movement itself or sensorimotor feedback induced by movement. This issue is important for present BMI research. Indeed, several studies have indicated the inflation of the movement decoding performance by

unexpected HG activity due to the somatosensory feedback (Bleichner et al., 2016; Chestek et al., 2013). Furthermore, it is essential to figure out how much the HG activity induced by somatosensory feedback contributes to the overall HG activity in the primary sensorimotor area. From a practical point of view, the majority of BMI candidates would be people having sensorimotor deficits, and they cannot receive the sensory feedback by peripheral nervous system directly. Consequently, macroscopic HG-based BMI system without considering this issue may not be suitable for decoding movement intention from those people.

Emerging evidence indicates that neuronal activation in S1 can be modulated by the premotor cortex (PM) and M1 during preparation or planning of movement (Adams et al., 2013; Christensen et al., 2007). Although it is unclear whether the S1 HG activity is related to this top-down mechanism, several recent findings have proposed that S1 HG activity before a cued movement may represent the cortico-cortical top-down feedback, or the efference copy (Branco et al., 2017; Hotson et al., 2016; Sun et al., 2015). However, these results have not been verified in a fully voluntary movement condition, and with electromyography (EMG) to effectively detect the undesirable movement such as isometric contraction of muscle during resting period.

To address these issue, I investigated the characteristics of HG activity

in several cortical areas including the S1 and M1, during voluntary or cued movement from eleven ECoG patients. I initially investigate whether the overall HG activities in the primary sensorimotor area mainly come from S1 or M1 during active movement. Several classification analyses are performed to assess how the movement-related HG activity in the S1 area affects the performance outcome of movement type classification. Finally, I investigate whether the HG activity in S1 mainly represents somatosensory feedback or whether it also represents pre-movement cortico-cortical interactions.

6.2. Materials and Methods

6.2.1. Subjects

In this study, eleven patients (6 male, 21–36 years) with intractable epilepsy were included. ECoG electrode grids or strips (Ad-tech Medical Instrument, Racine, WI, USA; electrode diameter of 4 mm, inter-electrode distance of 10 mm) were inserted into the subdural space of patients to localize the seizure onset zone. The electrodes of each patient covered both the M1 and S1. To localize ECoG electrodes, preoperative MR and postoperative CT images were obtained and then MR-CT co-registration procedure was performed. For visualization, electrodes from each patient were projected to individual 3-D brain structures using the CURRY software (version 7.0, Compumedics Neuroscan, Charlotte, NC, USA). The exact locations of each electrode were visually identified according to the co-registration data above. If the electrode was located between the S1 and M1, the closest one was chosen. All experimental procedures were approved by the Institutional Review Board of Seoul National University Hospital (H-0912-067-304). All patients signed informed consent forms before their participation. See **Table 6-1** for detailed clinical profiles.

Table 6-1. Clinical profiles

Subjects	Experiment	Electrode Location/Number	Diagnosis
1	HG, EF	L hemisphere/72	FLE
2	HG, EF	R hemisphere/52	TLE
3	HG, EF	L hemisphere/48	TLE
4	HG, EF	R hemisphere/68	OLE
5	HG, EF	L hemisphere/82	PLE
6	HG, EF	L hemisphere/64	TLE
7	HG, EF	R hemisphere/64	OLE
8	HG, EF, V	R hemisphere/84	TLE
9	Reaching	L hemisphere/50	FLE
10	Reaching	Bilateral/68	FLE
11	Reaching	R hemisphere/56	TLE

Abbreviation: M, male; F, female; HG, hand grasping; EF, elbow flexion; V, vibrotactile stimulation; L, left; R, right; FLE, frontal lobe epilepsy; PLE, parietal lobe epilepsy; TLE, temporal lobe epilepsy; OLE, occipital lobe epilepsy.

6.2.2. Tasks

Eight patients were asked to perform self-paced, voluntary hand grasping and elbow flexion tasks contralateral to the implantation site, as illustrated in a previous study (Ryun et al., 2014). Patients were instructed to move their hands and arms at approximate intervals of 5 to 10 s, but not to count the number of seconds to avoid movement execution by other cognitive cues (mean interval: 10.43 ± 5.09 s; mean ± SD). Before each movement, patients placed their hands or arms on the table with their palms upward. For hand grasping task, patients

were instructed to perform grasping motion with no object (1 to 2 s), and then release their hands after grasping motion with minimal force. For elbow flexion, patients were asked to completely flex their arms, and extend them with minimal force. Before the first session, patients were asked to practice each task for 2 minutes. Patients performed 2 to 4 sessions per each movement type, and each session consisted of 17 to 51 trials. The mean durations of motions were 2.84 ± 1.01 s and 3.63 ± 1.06 s for hand grasping and elbow flexion, respectively. For movement on/offset detection, EMG data was recorded from the opponens pollicis for hand grasping and from the biceps brachii for elbow flexion. To monitor the task performance, all tasks were recorded on video. Among all sessions from all subjects, 3 of 46 sessions were excluded because the signal-to-noise ratio of EMG was extremely low. One patient also participated in a pin-point vibrotactile experiment. Task paradigm of vibrotactile experiment was the same as described in the previous chapter.

Three patients performed a reaching movement task. The details of the task paradigm were described in the previous work (Yeom et al., 2013). Briefly, patients were instructed to move their arms from the resting position to the target after visual cues indicating the target location in the 3-D space which is presented pseudo-randomly in each of four directions. In each session, patients performed 30 trials for each direction. A three-axis accelerometer (KXM52, Kionix, NY, USA) attached to the index finger was used for movement

detection and trajectory reconstruction. The sensor and ECoG signals were simultaneously recorded. EMG data was not recorded in this experiment.

6.2.3. Data Acquisition and Preprocessing

ECoG data was recorded by the 128-channel Natus Telefactor (Telefactor Beehive Horizon with an AURA® LTM 64 & 128-channel amplifier system, Natus Neurology, West Warwick, RI, USA) or Neuroscan (Neuroscan, Charlotte, NC, USA) amplifier systems. The ECoG electrodes exhibiting abnormal fluctuations due to epileptiform activities and technical problems were excluded from further analysis. ECoG signals were digitized at 200 (Subject 1), 400 (Subjects 2 and 3), 1000 (Subjects 6 to 11) and 1600 Hz (Subjects 4 and 5) with analog anti-aliasing filtering ranging from 0.1 to 80, 150, 200 and 400 Hz, respectively.

For hand grasping and elbow flexion, the on/offset points of movement were initially determined using both a threshold-based automated detection method and visual inspections. EMG data were band-pass filtered (20–70 Hz) and then a Hilbert transform was performed to the filtered data. To extract envelope of EMG data, the absolute value of the transformed analytic signal was calculated. The on/offset points were roughly selected using the automated method above, and the data were epoched with a window of 2.5 s before onset to 2.5 s after offset. After which, the exact on/offset points were

determined by careful visual inspection. EMG envelope data were normalized by those of resting period (–2 to –1 s of movement onset). Trials showing low signal-to-noise ratios of EMG were discarded (97 of 1342 trials, 7.23 %; 1245 valid trials). See **Table 6-2** for detail.

Table 6-2. Behavior information. The number of valid movements per session and the interval between the movements of all subjects.

Subject	Hand Grasping			Elbow Flexion		
	Number of sessions	Valid trials per session	Interval(s) (Mean ± SD)	Number of sessions	Valid trials per session	Interval(s)
1	3	46/48/27	7.43±4.40	3	42/34/38	7.78±1.05
2	3	26/24/18	13.8±4.17	3	23/19/19	14.55±5.15
3	2	17/38	10.31±6.05	3	32/36/28	9.42±1.75
4	4	33/31/31/36	9.92±4.07	3	14/38/28	9.31±4.78
5	3	35/46/36	7.81±2.59	2	33/34	9.37±1.85
6	2	34/27	10.08±6.05	3	35/22/31	10.33±2.33
7	3	39/30/26	9.17±2.33	3	19/19/24	15.18±6.03
8	2	28/19	21.15±6.88	1	27	22.48±6.29

6.2.4. S1-M1 HG Power Difference

All analyses were conducted using MATLAB (MathWorks, Natick, MA, USA). ECoG data were re-referenced to the CAR, and then notch-filtered with a zero-phase-lag infinite-impulse response (IIR) filter to remove electrical device noise at 60 and 120 Hz. Epoching was performed to the filtered data with a time window of 2 s before onset to 1 s after offset. To extract the HG power, a complex Morlet wavelet transform was applied to the epoched data, with a frequency range of 5 to 100 Hz (80 Hz for Subject 1), and then the transformed data were squared to calculate power. The data were then normalized by the data of each frequency of the baseline period (–0.75 to –0.25 s). The single-trial HG power data were extracted by averaging the data across 50 to 100 Hz (80 Hz for Subject 1) and the on-going movement period.

To generate a HG power difference map between resting and movement conditions, the HG power values from each electrode were averaged across all trials, and were then divided the maximum value into the power values of each electrode. To test the difference in HG power levels between M1 and S1 during hand grasping and elbow flexion, the electrodes which showing maximum HG power levels in each S1 and M1 area were chosen. The mean HG power levels of M1 and S1 areas were also calculated for comparison between them. To do this, electrodes located 1.5 cm from the central sulcus were included. A Wilcoxon signed-rank test was performed for significance

testing.

6.2.5. Classification

To validate the HG activities from M1 and S1 contain task-specific information, a single-trial movement-type classification analysis was performed with a linear SVM. Averaged HG power values of each S1 and M1 during single-trial movement were used for features. In S1 and M1, the same numbers of features were extracted to avoid bias due to the different numbers of features between them. A ten-fold cross validation method was performed to evaluate classification performances.

6.2.6. Timing of S1 HG Activity

To investigate the temporal characteristics of HG activities in S1, electrodes exhibiting the most dominant changes in HG power level were chosen from each subject. The time from –2 to –1 s of movement onset was defined as the baseline period, and then all HG and EMG data were normalized by the data from this period. To avoid effects due to subtle movement before the onset, trials when the EMG data before the movement onset exceeded 4 SD were discarded (total discarded trials = 305, 7.09 trials per session). Because it is extremely difficult to extract the exact onset time of the HG activity from a single-trial data, I used averaged HG and EMG data of each session for

comparison. The averaged data were smoothed with a window of 100 ms to minimize the effect of any transient burst of HG activity before movement. Note that this smoothing method generally shifts the data point to the –x direction (x = time). The smoothed EMG and HG data were then normalized using the same method above. Finally, the time point at which the data exceeds 2 SD was defined as the HG onset time, based on previous studies (Branco et al., 2017; Hotson et al., 2016). For further comparison, this procedure was repeated by including the 4 SD trials above.

The same procedure was applied to the data for reaching movement task with accelerometer signals. To determine the movement onset from accelerometer signals, the sum of square of the three-axis accelerometer data was calculated, and then the vertex between resting and transient period was defined as the movement onset. S1 electrodes exhibiting the highest HG activation during the task in each subject were used for this analysis. In this analysis, I did not consider the direction of reaching movement because I only focused on the onset timing of HG activity during movement (120 trials per subject).

6.2.7. Correlation between HG and EMG signals

To calculate the correlation between HG and EMG fluctuations before movement, the SDs of the normalized HG power and EMG envelope time

traces before the movement periods (–0.75 to –0.1 s) were calculated for each session. Since the SDs of both normalized data are 1 in the baseline period (–2 to –1 s), the Pearson correlation between the two SD datasets can be directly calculated. The same analysis was performed for the condition including the 4 SD trials above.

6.3. Results

6.3.1. HG Activities Are More Dominant in S1 than in M1

Eight subjects performing hand grasping and elbow flexion were included in this experiment. Overall, the changes in HG power levels in S1 during active movements were greater than those in M1. This phenomenon was consistently observed regardless of the movement type and subjects (**Fig. 6-1**). The maximum HG activities were detected primarily in the S1 area in all subjects and conditions (**Fig. 6-1**, green triangle). Although the HG power levels were significantly increased both in the S1 and M1 during movement, the maximum HG power levels in S1 were much greater than those in M1. These differences were highly significant in most conditions (14 of 16) across all movement types and subjects (paired *t*-test: the highest $p = 0.012$, median $p < 0.0001$). Additionally, all patients (except one subject, Subject 8) reported somatosensory or motor experiences of hand, finger and arm during the direct cortical stimulation (DCS) for clinical purpose, and their locations seemed to be closely related to the area where the HG power level increased strongly (**Fig. 6-2**). This issue will be extensively investigated in Chapter 7.

The results of time-frequency analysis from S1 hand and near elbow areas during each movement indicated that HG activities exhibit movement type specific spatiotemporal dynamics, consistent with previous findings

(Branco et al., 2017; Miller et al., 2007). Specifically, the temporal dynamics of S1 HG activity seemed to represent the sequence of movements (i.e., grasping-releasing and flexion-extension sequences).

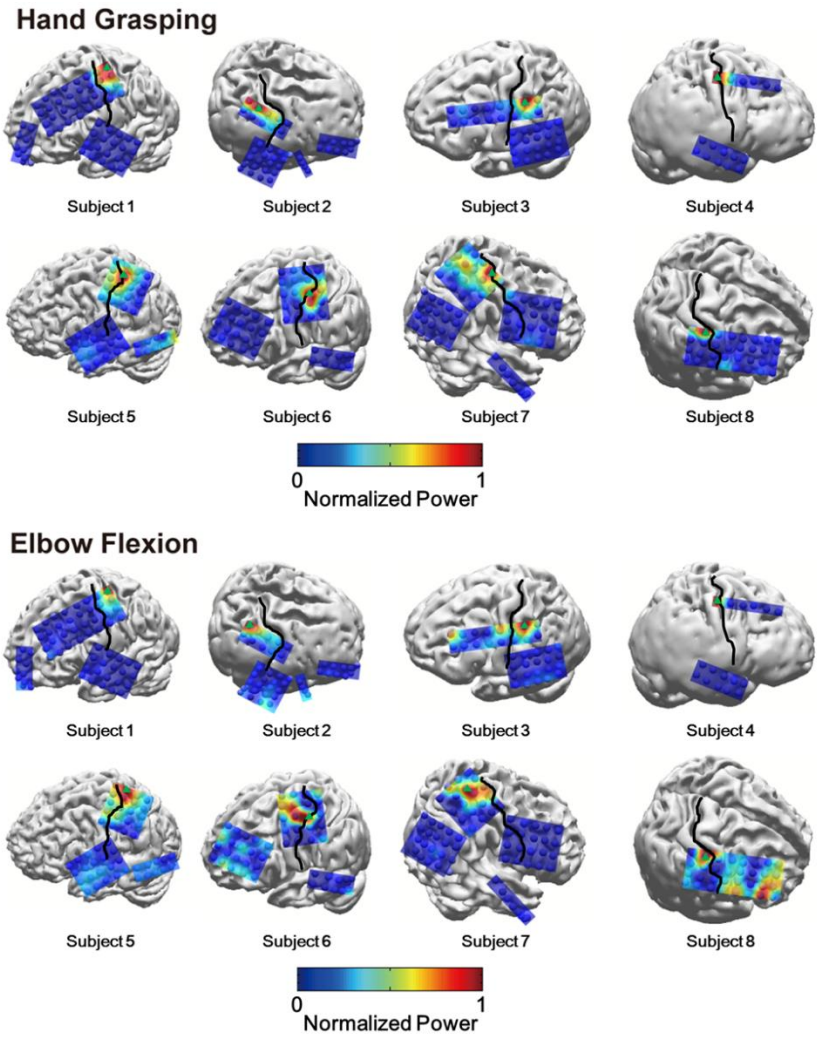

Figure 6-1. Topographical maps of HG activities during hand grasping (top)

and elbow flexion (bottom). Black lines denote the central sulcus. Green triangles represent the electrode exhibiting the greatest HG power level among all electrodes. Some electrodes are not shown because they were located on invisible sites. (Adapted from Ryun et al., 2017a)

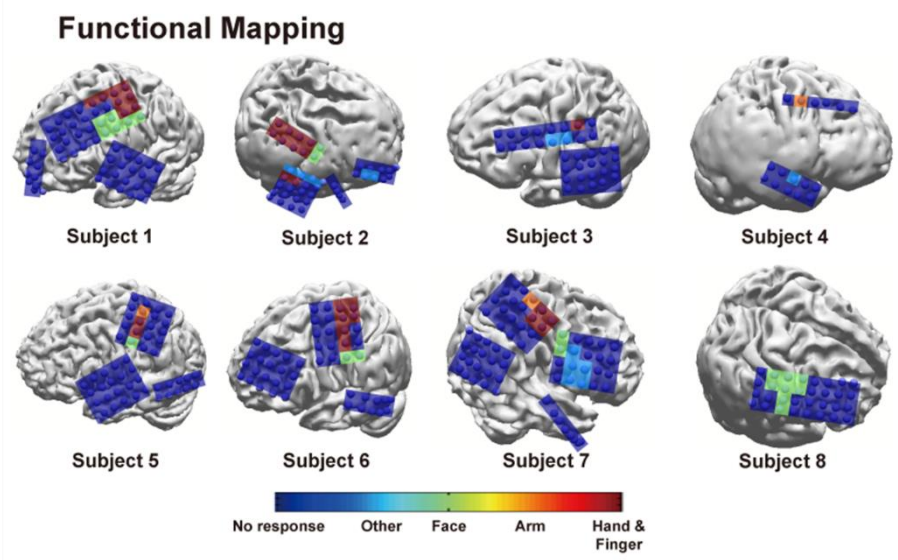

Figure 6-2. Topographical maps of functional mapping results by direct cortical stimulation. Each color indicates the corresponding type of sensorimotor experience.

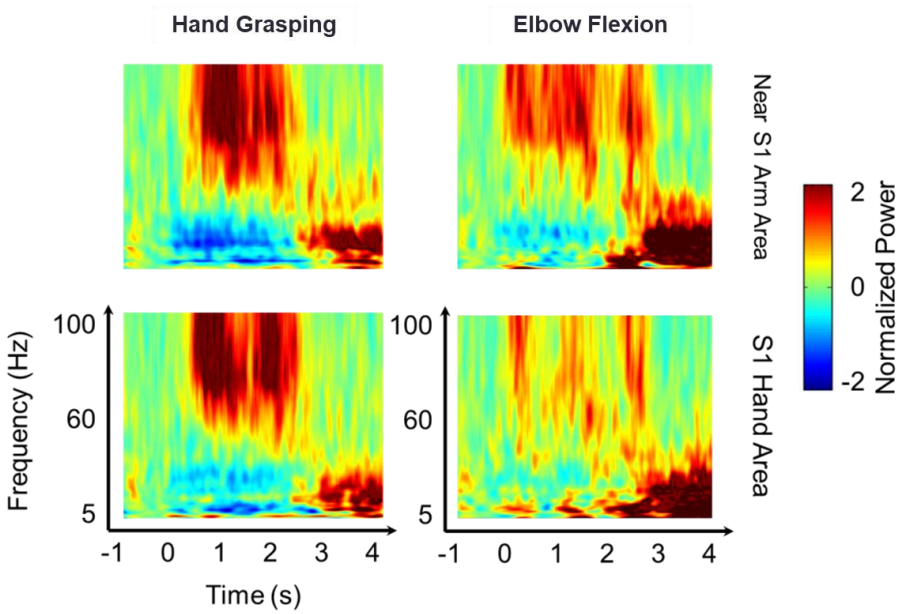

Figure 6-3. Spatiotemporal dynamics of HG activities during two conditions. Representative time-frequency plots during hand grasping (left) and elbow flexion (right) in near the S1 arm area (top) and in the S1 hand area (bottom) from Subject 2. The 60 Hz power line noise was removed after frequency-by-frequency normalization. (Adapted from Ryun et al., 2017a)

Although the results were consistent across subjects, the area showing maximum level of HG power can be changed depending on the experimental condition, for instance, the placement of ECoG electrode grid. Thus, I tested whether the overall HG power levels from each S1 and M1 electrodes also show the same trend above. Among all subjects, the mean HG power levels from S1 electrodes were higher than those from M1 electrodes regardless of the task conditions, except for one subject (**Fig. 6-4A** and **B**).

Next, I assessed how much the HG activities in S1 contain critical information for decoding of movement type compared to those in M1. To do this, single-trial HG features were extracted from each area, and then the classification accuracies in each area were calculated by the linear SVM classifier with ten-fold cross validation. Consistent with the results above, the overall classification accuracy from S1 features was significantly higher than that from M1 features (**Fig. 6-4C**; Wilcoxon signed-rank test (n = 8), $p < 0.05$). The mean values of classification accuracy over M1 and S1 across all subjects were 68.79 ± 4.48 % (mean ± SE) and 80.22 ± 3.69 %, respectively.

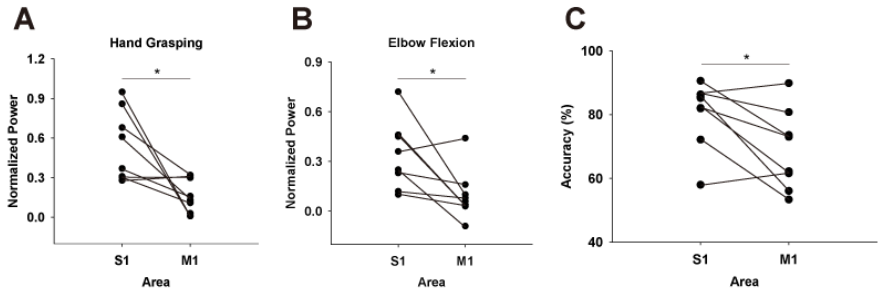

Figure 6-4. Mean HG power differences and movement classification accuracy. Mean HG power differences between S1 and M1 electrodes across all subjects during (A) hand grasping and (B) elbow flexion (mean power values across all subjects: S1 hand grasping = 0.54 ± 0.095 (mean ± standard error), M1 hand grasping = 0.17 ± 0.044, S1 elbow flexion = 0.34 ± 0.073, M1 elbow flexion = 0.011 ± 0.054). Power values of all sessions from each subject were averaged. The y-axis (normalized power) uses an arbitrary unit scale. (C) Differences in

classification accuracies between S1 and M1 features across all subjects. Black dots indicate the respective power or accuracy level of each subject. *: $p<0.05$ (Wilcoxon signed-rank test) (Adapted from Ryun et al., 2017a)

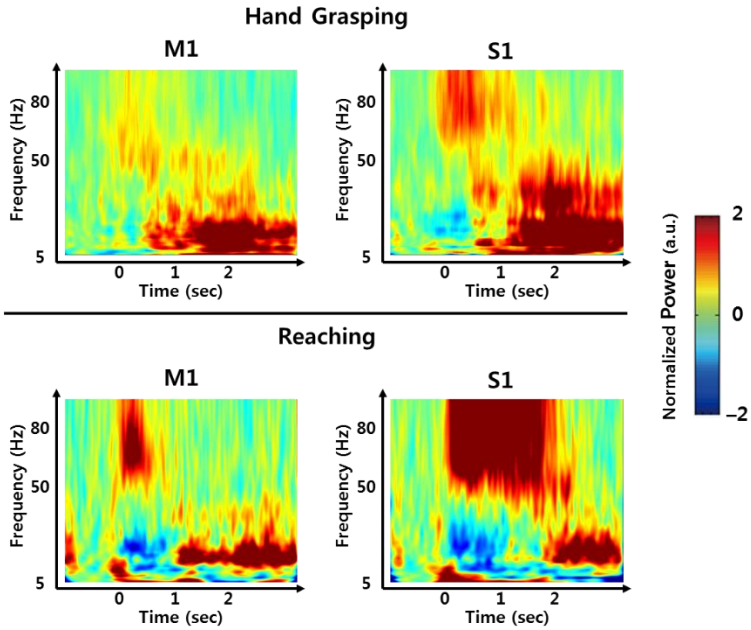

Figure 6-5. Representative time-frequency plots during hand grasping (top) and reaching tasks in the M1 and S1. HG activities in S1 were stronger and lasted longer than those in M1.

6.3.2. HG Activities in S1 Mainly Represent Somatosensory Feedback

Recent electrophysiological studies have proposed that significant S1 HG

power increases are found before movement, and these activities represent the neural processing beyond somatosensory feedback (Branco et al., 2017; Hotson et al., 2016; Sun et al., 2015). However, it is controversial as to whether HG activity in S1 before movement is related to the cortico-cortical neural processing for movement preparation. To test this suggestion, I initially tried to replicate the previous findings by investigating the timing of HG activity from the present data recorded during the cued, 3-D reaching movement tasks. Throughout the tasks, the movement onset time was defined using three-axis accelerometer attached to the index finger. Indeed, similar results were obtained from S1 areas of all three subjects (**Fig. 6-6**). The HG activities in S1 started to increase significantly at 140, 130 and 10 ms before the onset of movement in Subjects 9, 10 and 11, respectively. However, with this external sensor, it is difficult to detect subtle muscle activities prior to the movement, which leads to the undesirable change in HG activity. Moreover, the visual cue itself can act as a confound factor when evaluating HG activation before movement. Therefore, I re-tested this issue by recording EMG data during fully voluntary movement.

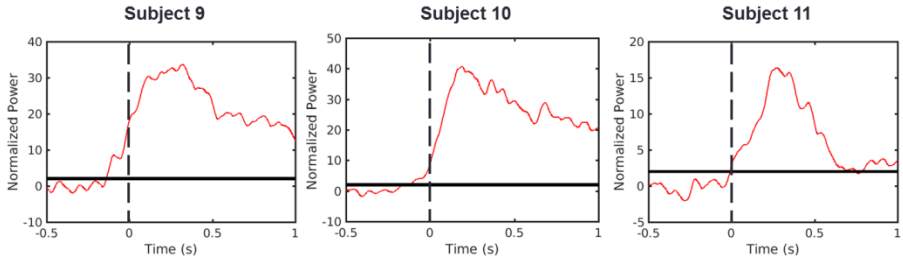

Figure 6-6. HG power time traces during cued movements. Red lines denote averaged HG time traces. Dashed line represents the movement onset as determined by the accelerometer signal. Solid black lines indicate the chance levels (2 SD) of the HG power increases. Calculated onset time points from all subjects were lower than zero (Subject 9 = –0.14 s, Subject 10 = –0.13 s, Subject 11 = –0.01 s). (Adapted from Ryun et al., 2017a)

Using EMG data, the HG time series data in 43 sessions of 8 subjects during voluntary hand grasping and elbow flexion were precisely aligned at the exact movement onset. Trials which the normalized EMG signals before movement exceed 4 SD compared to the baseline signals were excluded from this analysis. The HG activity began to increase significantly later than the start of movement (mean HG onset time: 49 ± 25 ms (mean ± SE); one-tailed t-test ($n = 43$), $p < 0.027$; **Fig. 6-7A**). The same analysis was also performed, including the rejected trials above (**Fig. 6-7B**). The time series of HG activity was shifted slightly in the –x direction compared to the previous result (**Fig. 6-7C**). However, the averaged onset of HG activity still occurred later than that of movement (31 ms after movement onset), although this time difference was

not significant. Moreover, there was no difference in HG onset timing between voluntary movement and passive tactile stimulation conditions (two-sample t-test, n = 93, p = 0.92; **Fig. 6-7D**).

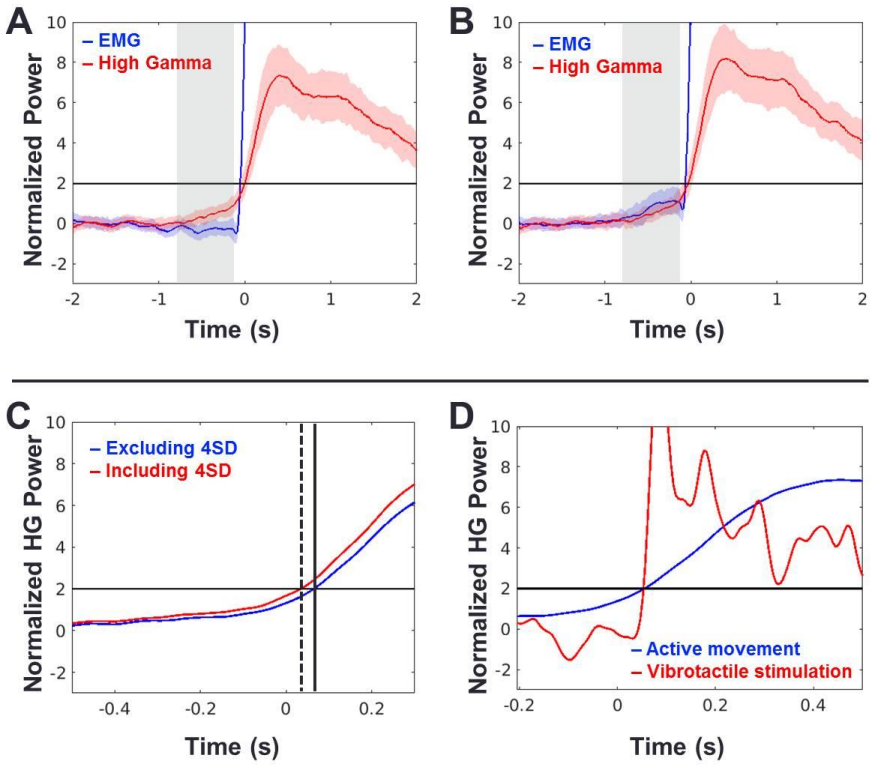

Figure 6-7. HG onset timing. (A, B) Time traces of grand-averaged EMG (blue) and HG power (red) across all movement types, sessions and subjects when the 4 SD trials were excluded (A) and included (B). Black horizontal lines indicate the chance levels (2 SD) of the EMG and HG power increases. Shaded areas with the color corresponding to the respective conditions denote 95 %

confidence intervals. Shaded areas shown in gray indicate periods of –0.75 to –0.1 s of the movement onset used in the further analysis. (C) Time shift of HG onset between (A; blue) and (B; red) conditions. Time t = 0 indicates the movement onset time-point determined by the EMG signal. Dashed and solid vertical lines indicate the HG onset time-points of (A) and (B) conditions, respectively. (D) HG power time traces of (A; blue) and vibrotactile stimulation (red). Time t = 0 indicates the movement onset or vibrotactile stimulus onset. Note that the HG onset timings of these two conditions are virtually the same. (Adapted from Ryun et al., 2017a)

Although I showed that the HG activity in S1 follows the related movement, the evaluated HG onset time may vary depending on the detection criteria used. In addition, there was a tendency for the HG power level to slowly increase before the movement onset, although it did not exceed the significant threshold level (see the shaded area in **Fig. 6-7A**). Therefore, I investigated the relationship between this HG fluctuation and the EMG signal to verify that this activity is also related to the somatosensory feedback induced by subtle movement. Interestingly, a significant correlation was found between them (**Fig. 6-7**, black; n = 43, r = 0.35, p = 0.02). Moreover, the correlation between them increased when the 4 SD trials above were included (**Fig. 6-8**, red; r = 0.47, p = 0.0015). These results suggest that the increase in HG activity during pre-movement period is mainly due to the subtle muscle contraction.

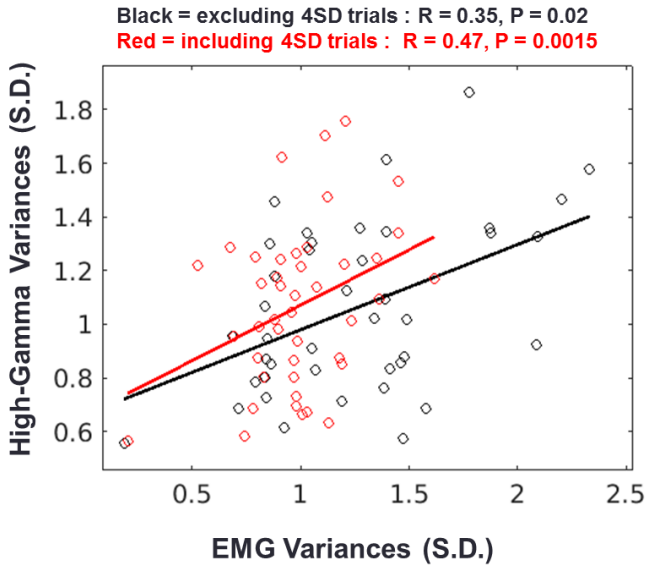

Fig. 6-8. Relationship between HG and EMG fluctuations during the pre-movement period. Result of regression analysis when the 4 SD trials are excluded (black) or included (red). Each circle represents the standard deviations of the HG power and EMG signal from one session. Solid lines indicate the regression slopes from the two conditions. (Adapted from Ryun et al., 2017a)

6.4. Discussion

In this study, I found that HG activities are more prominent in S1 than in M1 during active, voluntary movement. The results of movement classification analysis suggest that HG activities in S1 contain more informative features than those in M1 during active movement. Based on these results, I suggest that movement-related sensorimotor HG activities mainly come from S1 area, not from M1 area. Although recent ECoG studies have proposed the possibility of this phenomenon (Branco et al., 2017; Pistohl et al., 2012), I confirmed and quantified it from a large number of datasets (8 subjects, 43 sessions). Additionally, given the S1 dominance of HG activity in sensorimotor area the present study suggests that somatosensory feedback processing in S1 during movement may have more critical roles than originally expected.

6.4.1. S1 HG Activity Mainly Represents Somatosensory Feedback

In this study, I found that the onset time of S1 HG response follows that of the related movement and that the slowly increasing HG activation pattern before the actual movement is correlated with the EMG fluctuation due to the subtle muscle contraction. Based on these results and the additional reasons given below, I suggest that HG activities in S1 during active movement mainly represent the neuronal computation for somatosensory feedback from the

periphery. First, the HG activity in S1 during passive tactile stimulation is as strong as that during actual movement (Avanzini et al., 2016; Hotson et al., 2016). I also confirmed this point in the previous chapter. Although it is known that the HG activity in S1 can be modulated by attention or other cognitive processes (Bauer et al., 2006; Canolty et al., 2006; Ray et al., 2008c), the main generator of the S1 HG activity is the somatosensory information from the periphery, given the results of previous findings and Chapter 5 (Ray et al., 2008b; Rossiter et al., 2013; Womelsdorf et al., 2006). Second, previous studies on the patients with tetraplegia indicated that the S1 HG activity of the tetraplegic patient during attempted movement is substantially lower than that of the healthy control during active movement (Wang et al., 2013; Yanagisawa et al., 2012a). These results imply that the sensorimotor interaction such as efference copy does not induce robust HG activation during movement. Third, given the present result of onset timing, it is unlikely that the S1 HG activity before movement is less related to the movement preparation. Therefore, HG activity in S1 during active movement mainly represents the neural processing for somatosensory information from the periphery.

6.4.2. Further Discussion and Future Direction in BMI

Present findings suggest that the HG fluctuation before movement onset is less related to the cortico-cortical sensorimotor interaction for movement planning and preparation. However, these findings do not imply that the S1 HG activity only represents the somatosensory feedback itself throughout movement. Specifically, this activity may be related to other neural processing, such as the efferent modulation of the somatosensory input via corticospinal tract, although the relationship between HG activity and this efferent modulation mechanism has not been elucidated yet (Lemon, 2008).

Although the present results indicate the possibility of BMI performance inflation caused by S1 activity representing somatosensory feedback, the HG activities in S1 without somatosensory feedback would contain informative features for movement decoding. As mentioned above, weak but distinct HG activity was observed in the S1 area during attempted movement in patient with tetraplegia (Hochman et al., 2013; Yanagisawa et al., 2012b). Furthermore, a previous study suggested that the S1 receives movement-related information from the PM during voluntary movement, even in the absence of somatosensory feedback (Christensen et al., 2007). Nevertheless, however, it still remains to be elucidated as to whether the S1 HG activity during movement also contains information about cortico-cortical sensorimotor feedback or interaction, such as an efference copy, and thus,

further investigations are needed to address this issue.

6.4.3. Conclusion of Chapter 6

In this chapter, I suggested that movement-related HG activities in S1 strongly represent the somatosensory feedback from the periphery. Although it is possible that population activities such as HG are the sum of neuronal activities for various cortical functions, in terms of the major role of the S1, the present finding emphasizes the importance of feedback mechanism during motor control. Until now, however, how our brain processes the movement-induced feedback signals such as proprioception is largely unknown. The present finding related to the functional properties of HG activity in S1 may be the basis for investigating the neural processing for proprioception. In the next chapter, I will also address this issue in the macroscopic aspect.

Chapter 7: Cortical Maps of Somatosensory Function

Tactile and proprioceptive perceptions are crucial for our daily lives as well as survival. Since their major roles in human behavior are functionally different, theoretical studies based on the anatomical and neurophysiological evidence have proposed that there may exist distinct neural streams depending on their perceptual purposes and functions, similar to the dorsal and ventral streams in visual system. However, it is challenging to confirm this theoretical suggestion because somatosensory processing for perception involves complex co-operation among multiple brain areas with millisecond precision. Furthermore, converging evidence suggests that somatosensory perception is largely affected by specific neural activation of many cortical regions beyond the conventional sensorimotor areas. In the present study, I tackle this issue by combining direct cortical stimulation (DCS) data for eliciting somatosensation and high-gamma band (50 to 150 Hz) mapping data during tactile stimulation and movement tasks. To do this, I generated normalized functional maps of the elicited somatosensation by DCS on subdural ECoG electrodes from 51 patients with intractable epilepsy. Additionally, I constructed four-dimensional (4-D) cortical maps of ECoG high-gamma (HG) activities during various sensorimotor tasks including hand grasping, elbow flexion, vibrotactile and

texture stimulation from 20 (for movement tasks) and 31 (for tactile tasks) epilepsy patients. I found that the artificial somatosensory perception is elicited not only from conventional somatosensory-related areas such as the primary and secondary somatosensory cortices (S1 and S2, respectively), but also from widespread network including superior parietal lobule (SPL), inferior parietal lobule (IPL) and premotor cortex (PM). Interestingly, the distributions of electrode locations elicited somatosensation showed distinct spatial differences depending on the quality of somatosensation. Namely, the DCS on the dorsal part of the fronto-parietal area (SPL, dorsal IPL and dorsal PM) often induced action-related somatosensation such as proprioception, whereas that on the ventral part of fronto-parietal area (ventral IPL, S2 and ventral PM) generally elicited tactile sensation. Furthermore, the 4-D HG mapping results of movement and passive tactile stimulation tasks indicate considerable similarity in spatial distribution between HG and DCS functional maps. These findings suggest that macroscopic neural processing for somatosensation has distinct pathways depending on their perceptual functions. Additionally, the results provide evidence for the "perception and action" related neural streams of somatosensory system.

7.1. Introduction

Tactile and proprioceptive perceptions are crucial for our daily life as well as survival. They allow localization and characterization of somatosensory information, motor action-related somatosensory feedback about location and status of our body and limbs, and generation of body scheme which leads to a sense of body ownership (Dijkerman and de Haan, 2007). Although many perceptual functions require complex interactions between them, there has been a consensus that tactile sensation is mainly involved in object recognition and discrimination, whereas proprioception is tightly linked to movement- or action-related perceptual processing (Delhaye et al., 2018; Dijkerman and de Haan, 2007). However, their underlying neural mechanisms in the human neocortex still remain to be elucidated.

As a major neural entry of the somatosensory information in the cortex, primary somatosensory cortex (S1) plays an indispensable role in early somatosensory processing for perception. Since lesions in S1 can cause devastating perceptual disorders such as paralysis, numerous studies mainly focused on the perceptual relevance of neuronal activities in S1 by various neurophysiological techniques. For several decades, however, converging evidence has suggested that perceptual processing for somatosensation is a neural orchestration of sensory-related networks in our brain, including S1 and other sensory-related cortical areas. Many studies have indicated that lesions

other than S1 also cause severe perceptual disorders including tactile agnosia (Reed et al., 1996), impairments in tactile discrimination (Murray and Mishkin, 1984) and various sensorimotor-related deficits (Freund, 2001). Moreover, a recent human intracranial recording study indicated that more than 10 % of cortical areas, including S1, neighboring primary motor (M1), premotor (PM), and inferior parietal regions, are activated during a single median nerve stimulation, although their perceptual relevance remains to be elucidated (Avanzini et al., 2016).

Since the major roles of tactile and proprioception in human behavior are functionally different, theoretical studies based on the anatomical and neurophysiological evidence have proposed that there may exist distinct neural streams depending on their perceptual purposes and functions, similar to the dorsal and ventral streams in visual system (Dijkerman and de Haan, 2007; Freund, 2001; Gardner, 2010). Although the specific functional roles of the proposed pathways are still controversial (Dijkerman and de Haan, 2007; Disbrow et al., 2003), it has been suggested that the ventral stream, from the S1 via the S2, surrounding inferior parietal areas or posterior parietal cortex (PPC) to the insula is closely related to the tactile perception, tactile object recognition and discrimination (Preusser et al., 2015; Reed et al., 2005), whereas the dorsal stream, from S1 to PPC (either directly or via S2) is tightly linked to the movement-related processing including reach and grasp (Buneo and Andersen,

2006; Delhaye et al., 2018; Westwood and Goodale, 2003). However, to the best of my knowledge, no electrophysiological study has addressed this issue by directly comparing these two perceptual processes from the perspective of large-scale cortico-cortical networks, especially in human.

In human study, direct cortical stimulation (DCS) and electrocorticography (ECoG) recording can be promising techniques to assess this issue. The DCS provides a unique opportunity to identify the somatosensory perception-related areas directly with a wide coverage of cortical surface in human. Although its robustness is not as good as that of intracortical microstimulation (ICMS) (Armenta Salas et al., 2018; Flesher et al., 2016; Hiremath et al., 2017), DCS on the sensory-related area often elicits specific somatosensation and the human subject can verbally report the quality of sensation (Balestrini et al., 2015). However, the DCS does not always guarantee that the elicited perception is actually caused by DCS-induced neuronal activation in that area, because DCS can potentially affect nearby cortico-cortical fiber tract, leading to neural activation of other cortical areas. Conversely, ECoG recording during somatosensory perception immediately detects ongoing neural activations in the located region, whereas this method is relatively difficult to assess their perceptual relevance.

Taking these issues together, the present study combines DCS data for eliciting somatosensory perception and high-gamma (HG) band (50 to 150 Hz)

mapping data during various somatosensory-related tasks by using the same neuroimaging techniques in human. I investigate the macroscopic neural processing of the movement-related (mainly including proprioception) and tactile sensations by assessing the spatiotemporal differences in their DCS responses and HG activation patterns from 51 (for DCS mapping) and 46 (for HG mapping) patients with intractable epilepsy. Here, I show that large-scale neural processing for somatosensory perceptions has distinct streams depending on their functions – tactile and proprioceptive perceptions.

7.2. Materials and Methods

7.2.1. Participants

For DCS study, I retrospectively investigated 239 patients (113 female, 30.02 ± 10.21 yr; mean ± SD; 12,038 electrodes from 258 hemispheres, left = 123, right = 135) who underwent implantation of subdural electrodes for epilepsy monitoring and functional cortical mapping with DCS from the database of Seoul National University Hospital between January 2005 and December 2018 (618 patients). Among them, 111 patients (46.4 %) reported sensorimotor-related experiences. Finally, fifty-one patients (21.3 %) who reported sensory-only experiences without objective motor symptoms were included for further analysis.

For four-dimensional cortical HG mapping, 46 patients with intractable epilepsy participated in this study (17 left hemisphere, 25 right hemisphere, 4 bilateral). Among them, twenty patients (1256 electrodes), 22 patients (1388 electrodes) and 29 patients (1696 electrodes) participated in the hand grasping/elbow flexion, texture stimulation and vibrotactile stimulation tasks, respectively (**Table 7-1**). The subdural ECoG electrodes (Ad-tech Medical Instrument and PMT Corp.) had diameters of 4 mm (2 mm for high-density ECoG) with an inter-electrode distance of 10 mm (4 mm for high-density ECoG). Pre-operative MR and post-operative CT images were obtained

from each participant. All experimental procedures were approved by the Institutional Review Board of Seoul National University Hospital (1905-156-1035 & 1610-133-803). All patients who participated in the experiments provided written informed consent before participation.

Table 7-1. Demographics of the subjects (HG Mapping)

Patient No.	Age	Sex	Number of Electrodes	Experiment	Electrodes location	Sampling Frequency (Hz)	Diagnosis
1	25	F	72	Hand, Elbow	Left	200	FLE
2	30	F	88	Hand, Elbow	Bilateral	400	TLE
3	36	M	52	Hand, Elbow	Right	400	TLE
4	26	F	48	Hand, Elbow	Left	400	TLE
5	25	M	68	Hand, Elbow	Right	1600	OLE
6	26	F	82	Hand, Elbow	Left	1600	PLE
7	37	M	58	Hand, Elbow	Right	400	TLE
8	28	F	58	Hand, Elbow	Right	1600	TLE
9	28	M	72	Hand, Elbow	Left	1000	TLE
10	44	F	54	Hand, Elbow	Left	1000	TLE
11	26	F	46	Hand, Elbow	Left	1600	FLE
12	31	F	68	Hand, Elbow	Left	1000	TLE
13	19	F	68	Hand, Elbow	Left	1000	FLE
14	35	M	54	Hand, Elbow	Left	1000	TLE

15	40	M	48	Hand, Elbow, V	Left	1000	TLE
16	21	M	68	Hand, Elbow, V	Right	1000 (Hand, Elbow), 2000 (V)	OLE
17	27	M	62	V	Right	2000	TLE
18	24	M	54	V	Left	2000	OLE
19	27	M	32	Hand, Elbow, V	Right	1000 (Hand, Elbow), 2000 (V)	TLE
20	16	M	64	Hand, Elbow	Left	1000	TLE
21	36	F	72	Hand, Elbow, T	Right	1000 (Hand, Elbow), 2000 (T)	TLE
22	34	M	12	V, T	Right	2000	PLE
23	31	M	84	Hand, Elbow, V, T	Right	1000 (Hand, Elbow), 2000 (V, T)	TLE
24	23	M	36	T	Right	2000	TLE
25	34	F	92	V, T	Right	2000	PLE
26	44	M	64	V, T	Left	2000	TLE
27	21	F	50	V	Left	2000	FLE
28	26	M	68	V, T	Bilateral	2000	FLE
29	27	M	56	V, T	Right	2000	TLE
30	25	M	58, 96*	V, T (2 sessions each)	Left	2000	PLE/TLE

31	27	M	58	V, T	Right	2000	TLE
32	27	F	66	V, T	Right	2000	FLE
33	28	F	48	V, T	Right	2000	TLE
34	33	M	46	V, T	Right	2000	FLE
35	34	M	50	V, T	Right	2000	FLE
36	27	F	26	V, T	Left	2000	TLE
37	30	F	68	V, T	Bilateral	2000	TLE
38	16	M	66	V, T	Bilateral	2000	FLE
39	35	M	32	V	Right	2000	FLE
40	24	F	40	V, T	Right	2000	TLE
41	25	F	56	V, T	Left	2000	TLE
42	58	F	28	V	Right	2000	TLE
43	24	M	96	V, T	Right	2000	TLE
44	50	F	42	V	Right	2000	TLE
45	41	F	34	V, T	Right	2000	FLE
46	30	F	96	V, T	Right	2000	PLE

Abbreviation: M = male, F = female, V = vibrotactile experiment, T = texture experiment PLE = parietal lobe epilepsy, OLE = occipital lobe epilepsy, TLE = temporal lobe epilepsy, FLE = frontal lobe epilepsy.

*The patient underwent electrode insertion surgery twice with different electrode locations.

7.2.2. Direct Cortical Stimulation

Functional cortical stimulation mapping was performed as part of clinical procedure. DCS was delivered with GRASS S12 or S12X cortical stimulator (Natus, Warwick, RI, USA). During the pre-surgical functional mapping, 0.5 to 16.5 mA of bipolar electrical stimulation was applied to each electrode (pulse train duration of 5 s, pulse width of 0.3 ms, stimulus frequency of 50 Hz with alternating polarity). Patients were asked to verbally report any abnormality they feel. Only the verbal feedbacks without actual motor activity were included as subjective somatosensations and were considered in this study. Stimulated electrodes eliciting after-discharge or other pathological responses were discarded. Additionally, intracerebral electrodes located on the white matter were excluded from further analysis. Among fifty-one patients, DCS was performed by using two adjacent electrodes (23 patients), or choosing one reference electrode far from the target one (1 patient), or both (27 patients). For DCS using two adjacent electrodes, each electrode site was counted separately because one electrode was usually stimulated at least twice with different pairs of adjacent electrodes. If the patient reported the same sensory experience when the same site is stimulated with different types of stimuli (neighboring and reference-based bipolar stimulations), this case was considered once. Some patients reported sensory reports differently depending on the type of stimulation. These sensory reports were recorded as different cases (14

electrodes). I finally devised a dataset containing 297 verbal reports from 283 different electrode positions.

7.2.3. Classification of Verbal Feedbacks

The verbal reports were classified by the location of sensation and by the quality of sensation. The locations of sensations were categorized into 6 categories: (i) hand/finger and arm; (ii) face and head; (iii) lips; (iv) tongue; (v) torso including front, back, shoulder, neck and trunk; and (vi) leg and foot. The qualities of sensations were initially categorized into 6: (i) proprioception including moving sense and other motor-related sensations; (ii) tingling; (iii) electrifying; (iv) paresthesia or numbness; (v) pressure; (vi) et cetera. Additionally, to compare the movement-related and cutaneous sensations, I merged (ii) to (v) into one category.

7.2.4. Localization of Electrodes

Electrode positions were obtained from co-registration of the preoperative MR and the postoperative CT images using CURRY software (version 7.0; Compumedics Neuroscan). These positions of individual coordinates were subsequently converted to MNI coordinate system, and projected to the hemisphere-unbiased MNI surface template consisting of 81.924 nodes, constructed by CIVET pipeline (ver. 1.1.7, MNI) (Kim et al., 2005; Lyttelton et

al., 2009). For each electrode position, the nearest node on the cortical surface was chosen based on the Euclidean distance. To construct probabilistic maps, I used a 5 mm circular mask with binary values based on the geodesic distance from each electrode position at the individual level, and these masked maps were then summed across all patients. The electrodes located in the right hemisphere were projected to the corresponding nodes in the left hemisphere because the electrode sampling densities of some experimental conditions were sometimes relatively low in the opposite hemisphere. In this study, therefore, I did not focus on the hemisphere differences, but on the spatial distribution within the hemisphere.

To identify the brain region of each node, the automated anatomical labeling (AAL) atlas for the present surface template was used. Additionally, I constructed the surface map of Brodmann's area (BA) by directly comparing with previous studies (Papademetris et al., 2006; Xia et al., 2013). The anatomical boundaries between dorsal and ventral premotor cortices (BA 6), and S2 area were determined according to the literatures (Eickhoff et al., 2006; Tomassini et al., 2007). In this study, OP1 (opercular region) and the posterior part of OP4 were defined as S2 area.

7.2.5. Apparatus

For texture stimulation, I used custom-made disc/drum type stimulators driven

by ultrasonic motors (USR60E3N; Shinsei Corp.). Specifications of disc/drum type stimulators were described in Chapter 4, 5 and the literature (Ryun et al., 2017b). For drum-type texture stimulator, the rotating speed of the drum was 10 rpm, with a diameter of 190 mm, a stimulus duration of 1.5 s, a texture width of 25 mm, and a normal force of 38 ± 17 g wt. (mean ± SD).

For vibrotactile stimulation, I used custom-made pin-point piezoelectric and magnetic vibrotactile stimulators. The specification of piezoelectric vibrotactile stimulator is the same as used in Chapter 5. The pin-point magnetic vibrotactile stimulator, driven by Mini-shaker (model 4810; Brüel and Kjæ r), was designed for various complex vibrotactile and light pressure stimulations. A detailed description of the piezoelectric and magnetic vibrotactile stimulators is in Chapter 4.

7.2.6. Tasks

Twenty patients (10 female, 16–40 years) performed self-paced, fully voluntary hand grasping and elbow flexion movements, as described in Chapter 6 and previous studies (Ryun et al., 2017a; Ryun et al., 2014). Patients were instructed to grasp/flex their hands/arms with no object at approximate intervals of 5 to 10 s. Note that these types of motions are less related to the goal-directed movement. To determine the onset/offset of each movement, I recorded electromyogram (EMG) from the opponens pollicis for hand grasping and from

the biceps brachii for elbow flexion tasks. Tasks were video-recorded for monitoring performance and sequence of movement. The mean durations of each task were 2.34 ± 1.08 s and 3.12 ± 1.20 s for hand grasping (1880 valid tasks) and elbow flexion (1620 valid tasks), respectively.

Texture and vibrotactile stimulation tasks have previously described in detail (see Chapter 5). Twenty-two patients (10 females, 16–44 years) performed texture stimulation tasks. To do this, I used customized disc-type (for 17 patients) and drum-type (for 5 patients) texture stimulators. For disc-type texture stimulator, two different textures (2 mm grid and <50 μm fine textures) were pseudo-randomly delivered to the contralateral index finger (80 trials per each texture). For drum-type texture stimulator, eight different textures were pseudo-randomly delivered, but I considered only two textures (2-mm grid and <50 μm fine textures) for consistency (30 to 32 trials per each texture). The stimulus period was 1.5 s for both stimulators. Note that there was no static indentation during resting period.

For twenty-nine patients (12 female, 16 to 58 years), pin-point, sinusoidal vibrotactile stimuli were delivered to the contralateral index finger by customized piezoelectric (22 patient; 1 s of stimulus duration; 50 trials per each condition) or magnetic vibrotactile stimulator (7 patients; 1.5 s of stimulus duration; 40 trials per each condition). I delivered various vibrotactile stimuli including 5 to 400 Hz sinusoidal and combined (flutter + vibration) stimuli, but

I used 33 or 35 Hz (flutter; 120 μm for 33 Hz, 180 μm for 35 Hz) and 350 or 400 Hz (vibration; 60 μm for 350 Hz, 90 μm for 400 Hz) stimuli for further analysis given the previous finding (Ryun et al., 2017b). Throughout experiments, a voltage-displacement calibration procedure was performed at each stimulus frequency by using Laser-Doppler Vibrometer (LDV; model AT3600, GRAPHTEC Corp., Japan). Note that I conducted all experiments only when patients' electrode grids were located on the sensorimotor-related areas. Therefore, I was able to obtain maps with relatively high sampling densities in these areas.

7.2.7. Data Recording and Processing

ECoG data were recorded with the 128-channel Natus Telefactor (Telefactor Beehive Horizon with an AURA® LTM 64 & 128 channel amplifier system, Natus Neurology, West Warwick, RI, USA) or Neuroscan (Neuroscan, Charlotte, NC, USA) or Neuralynx ATLAS (Neuralynx, Bozeman, MT, USA) systems at 200, 400, 1000, 1600 or 2000 Hz (see **Table 7-1**) with analog anti-aliasing filtering ranging from 0.1 to 80, 150, 200, 400, and 500 Hz, respectively. ECoG channels which show abnormal fluctuations due to technical problems were preferentially excluded from further analysis. The data were re-referenced to a common average reference (CAR), and then the re-referenced data were notch-filtered with a zero-phase-lag infinite-impulse response (IIR) filter to

remove systematic noise at 60 Hz and related harmonics. Data epoching was performed with a window of –2 to 3 s of movement or stimulus onset. Epoched data from all electrodes were decomposed into time-frequency representation using complex Morlet's wavelet transform. The HG power ranging from 50 to 150 Hz frequency band (except one patient (50 to 80 Hz), due to the low sampling rate) was extracted with 50 ms bins. The binned HG power was compared with that of baseline period (–1.5 to –0.5 s of stimulus/movement onset) using a t-test.

7.2.8. Mapping on the Brain

To build a four-dimensional functional map across all patients, I initially generated a t-value based functional map of each patient. Since the sampling densities of each brain region were inhomogeneous, I adjusted the t-values of each electrode using the following equations:

$$T_{i,j} = \begin{cases} 0 & if \;\; s_{i,j} = 1 \\ \dfrac{t_{i,j}}{s_{i,j}} & otherwise \end{cases} ; i = 1, \ldots, M; j = 1, \ldots, N_i$$

$$s_{i,j} = \; 1 + \sum_{k} A_{i,j,k} \, ; \qquad k = 1, \ldots, i-1, i+1, \ldots, M$$

where t is the t-value from each electrode, s is the spatial weight, T is the adjusted t-value from each electrode, M is the number of patients, N_i is the

number of electrodes of each patient i, and $A_{i,j,k}$ is the number of electrodes of other patient k within 5 mm geodesic distance from target electrode j of patient i. Note that the adjusted t-value T is 0 if there is no surrounding electrode (within 5 mm) from other patients (the value of this electrode was discarded to minimize false-positive ratio).

For each node indicating electrode location, the values of the target and surrounding nodes (within 5 mm) were masked with the adjusted t-values of each electrode. To reduce edge effect at the boundary of mask, a repetitive linear interpolation based on the path length was performed for all nodes (effective distance from target node: 5 to 10 mm). Finally, the adjusted t-values of all nodes were summed across all patients.

Nodes with adjusted t-values exceeding a given threshold in at least three time bins within 0 to 1 s of stimulus/task onset were considered as significant ones. This criterion was also used for calculating three-dimensional HG significance maps. To determine the significant threshold level, I repetitively simulated the whole procedure above (1000 iterations) with the same electrode configuration for arbitrary z-value (from standard normal distribution) time series of each node, as increasing the threshold level. The critical point when the probability that all nodes are completely rejected (no false positive) by given threshold is above 95% from 1000 iterations was determined as the significant threshold level (generally, threshold Thr = 1.76-

1.79, I selected *Thr* =1.8 as the significant threshold of all conditions for consistency).

7.2.9. ROI-based Analysis

To analyze the peak delays of HG activities from several ROIs (S1, SPL, dIPL, vIPL, vPM and S2), I initially extracted the electrodes of each ROI in the surface template, and then calculated t-value time-series of each electrode with 10 ms bins using the same method described above. To reject electrodes with non-significant HG peaks, only electrodes with t-values exceeding 2.5 ($p \approx 0.01$) in at least three consecutive time bins during 0 to 1 s of stimulus onset were selected.

7.3. Results

7.3.1. DCS Mapping

In this study, I included epilepsy patients who reported somatosensations without movement during DCS functional mapping procedure (51 of 239 patients). Overall, I collected 297 verbal reports from 283 different electrode positions. Patients reported various somatosensory experiences including movement-related (joint move (12.5%), tremor (25.5%) and other muscle sensations (8.1%)), tingling (20.2%), electrifying (13.1%), paresthesia or numbness (9.1%), pressure (0.7%), and unclassified (10.8%) sensations at various body parts (finger/hand/arm = 55.4%, face/neck = 18.3%, tongue/oral/lip/throat = 17.0%, leg/foot = 4.3%, torso/front/back = 5.0%). I divided them into three categories, (i) movement-related sensations, (ii) tactile sensations, and (iii) unclassified. All sensations were elicited on the contralateral side of the stimulus site. Pain (unclassified) was reported only one electrode (located on the secondary somatosensory cortex, S2) among all electrodes of the exposed cortical sites. Since the sampling density of medial parts (inside the inter-hemispheric and Sylvian fissures) was relatively low (< 5% of total valid electrodes), I mainly focused on the exposed cortical sites. All valid electrodes eliciting somatosensory experiences were projected to the hemisphere-unbiased MNI surface template. Brain atlas of the current surface

template is illustrated in **Fig. 7-1**.

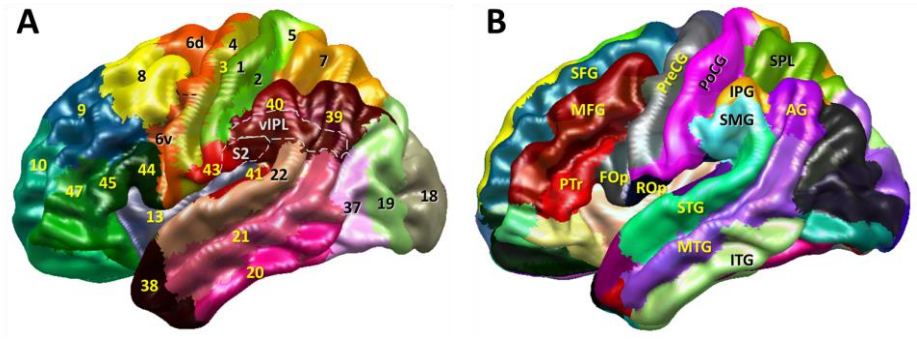

Figure 7-1. Brain atlas used in this study. (A) Atlas of the template surface based on Brodmann's area (BA). Black dashed line indicates the boundary between BA 6d and 6v. Gray dashed lines denote boundaries of S2 and vIPL. The boundary of vIPL was functionally determined based on the result of present study. (B) AAL-atlas of the template surface. (Abbreviation: S2 = secondary somatosensory cortex, vIPL = ventral part of inferior parietal lobule, PreCG = precentral gyrus, PoCG = postcentral gyrus, SPL = superior parietal lobue, IPG = inferior parietal gyrus, SMG = supramarginal gyrus, AG = angular gyrus, ROp = Rolandic operculum, FOp = frontal operculum, PTr = pars triangularis, SFG = superior frontal gyrus, MFG = middle frontal gyrus, STG = superior temporal gyrus, MTG = middle temporal gyrus, ITG = inferior temporal gyrus) (Not all atlas labels were shown)

Artificial somatosensory perceptions were elicited not only from conventional somatosensory-related areas such as the S1 (BA 3, 1 and 2) and S2, but also from widespread network including inferior parietal lobule (IPL), superior parietal lobule (SPL), and PM (**Fig. 7-2A**). The highest proportion of valid electrodes was present in S1 (40.4%), followed by M1 (15.4%), SPL (13.9%), IPL (10.0%), PM (9.62%) and S2 (4.62%). Interestingly, the distributions of electrode locations with elicited somatosensation showed distinct spatial differences depending on the quality of somatosensation. The DCS on the dorsal part of the parietal area including the SPL, and the dorsal part of IPL (dIPL; nearby the intraparietal sulcus, IPS), mainly induced movement-related somatosensation such as proprioception whereas that on the ventral part of the parietal area including S2 and the adjacent ventral part of IPL (vIPL), generally elicited tactile sensation (**Fig. 7-2B and C**). Note that no movement-related sensation was reported in the posterior S2 and adjacent vIPL regions, despite twenty-three valid electrodes were located on these areas. This tendency seemed to be unrelated to the represented body parts (see finger/hand/arm, face/neck and tongue/oral/lip/throat conditions in **Fig. 7-3** and **7-5**). Additionally, a significant right hemisphere dominance was found in the S2 and vIPL in the tactile condition from entire body parts (permutation test, $p = 0.003$, uncorrected, see **Fig. 7-4**). No significant hemisphere dominance was found in the movement-related condition. However, it is possibly due to the fact

that clinicians mainly focus on the language function during DCS on the inferior parietal area of dominant hemisphere, and thus, further investigation is needed to verify this issue. In this study, I focused on the spatial distribution within the hemisphere.

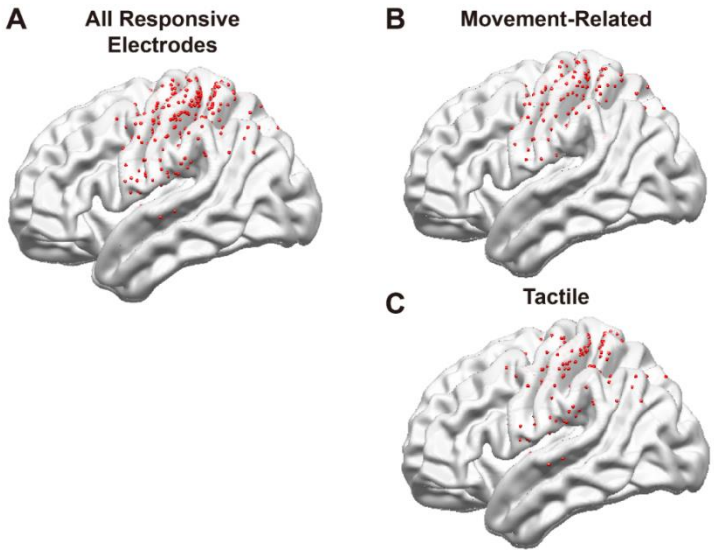

Figure 7-2. 3-D DCS functional maps. (A) Electrode locations which elicited somatosensation during DCS from entire body parts regardless of sensory quality. (B and C) Electrode locations whose stimulation elicits (B) movement-related and (C) tactile sensations.

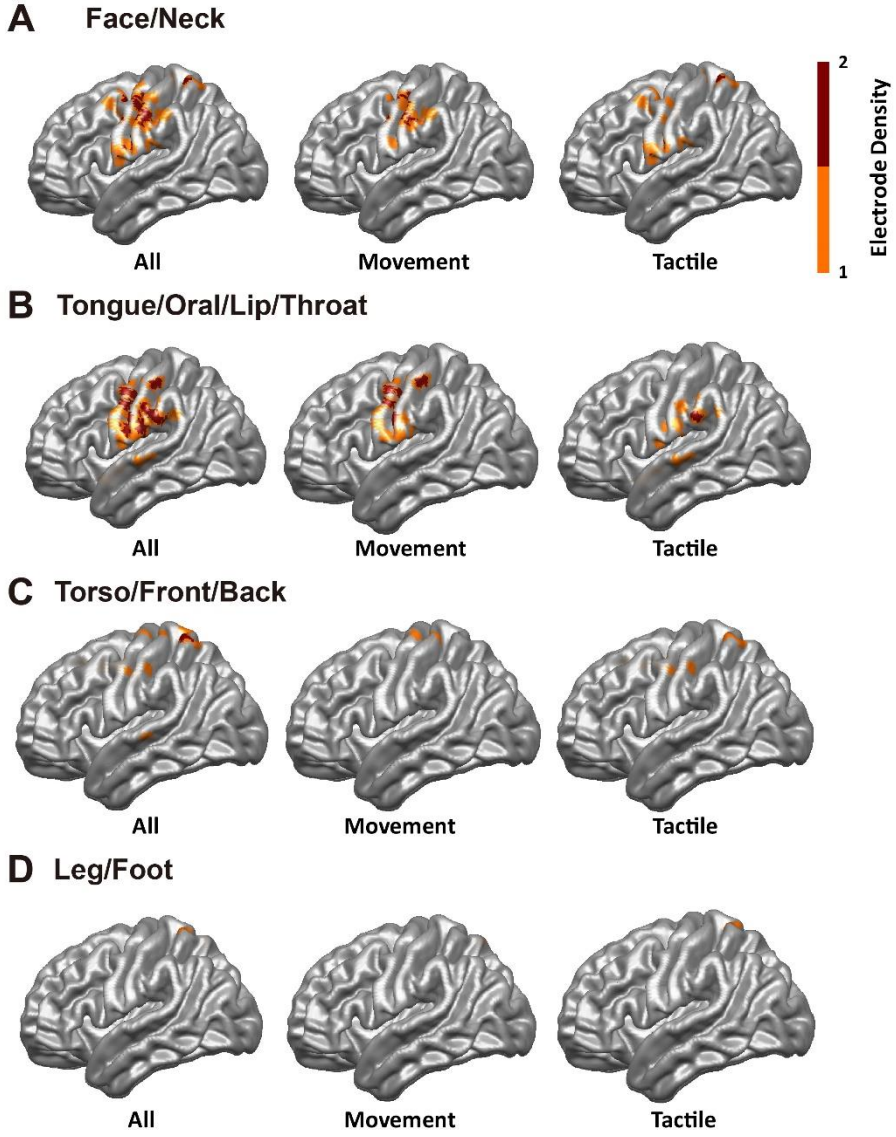

Figure 7-3. 3-D DCS functional maps of each body part.

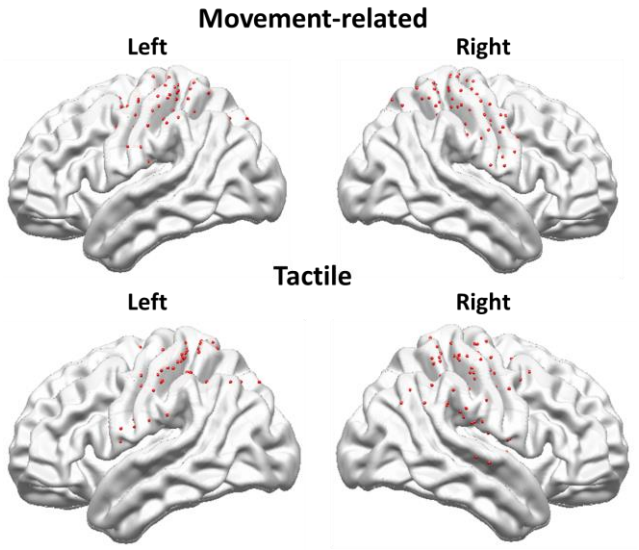

Figure 7-4. Differences in spatial distributions of electrodes between left and right hemispheres under the movement-related and tactile conditions from entire body parts.

Next, I focused on the elicited sensation of the finger/hand/arm areas for detailed quantification and direct comparison with further HG results below. Note that the corresponding somatotopy of these body parts in S1 is sufficiently far from the ventral fronto-parietal area including S2, vPM and vIPL, avoiding spatial ambiguity due to the intrinsic resolution of my approach. As mentioned above, in the finger/hand/arm condition, the difference in spatial distribution between movement-related and tactile sensations was prominent in dorsal and ventral fronto-parietal areas (**Fig. 7-5A** and **B** and **Fig. 7-6**). Beyond the primary sensorimotor area, movement-related sensations were mostly elicited

by the stimulation on SPL and dPM, whereas that on IPL, vPM and S2 almost exclusively generated tactile sensations (**Fig. 7-5D**; Fisher's exact test for six regions, p = 0.0059; permutation tests for dorsal (SPL and dPM) and ventral (S2, vPM and vIPL) areas, $N = 100000$, $p < 0.001$). Additionally, the stimulation on SPL induced both sensations with the highest proportion, suggesting that SPL is involved in both tactile and proprioceptive perception, consistent with previous literatures (Dijkerman and de Haan, 2007; Pause et al., 1989; Stoeckel et al., 2004).

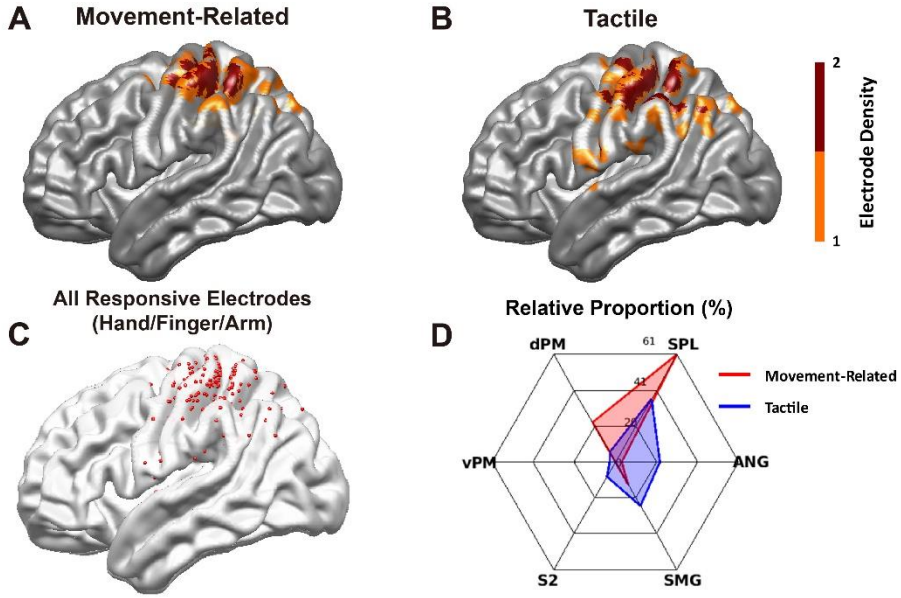

Figure 7-5. 3-D DCS functional maps based on the quality of sensation ((A) movement-related and (B) tactile sensations). Corresponding body part of the

maps is the hand/finger/arm. (C) Distribution of electrode where patients reported any somatosensation in hand/finger/arm. (D) Radar plots represent the relative proportion of the number of electrodes in each area for movement-related (red) and tactile (blue) sensations. Electrodes in S1 and M1 were excluded.

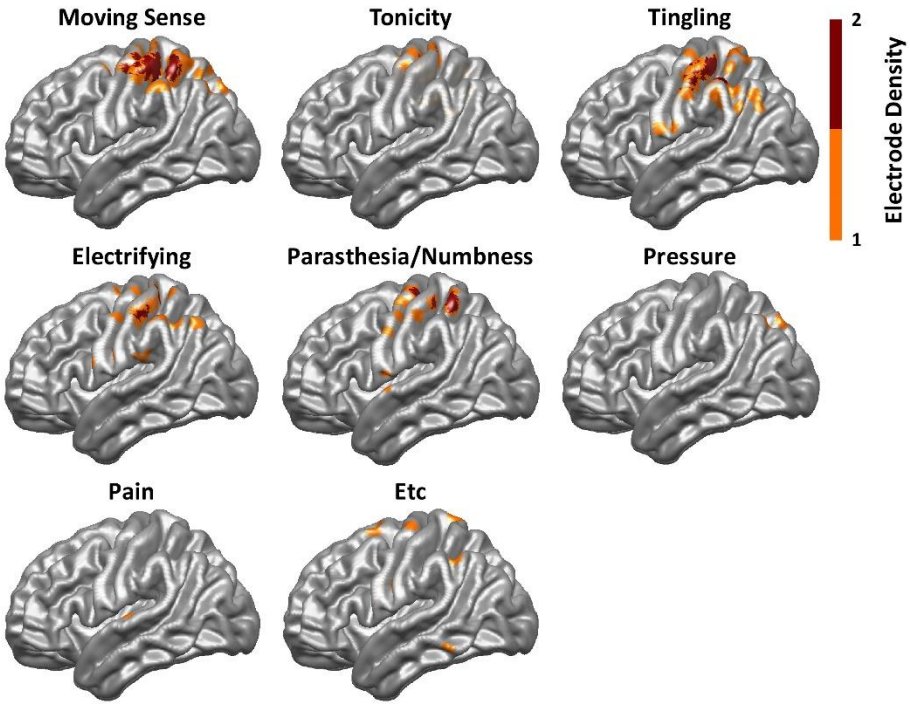

Figure 7-6. 3-D DCS functional maps for qualities of sensations elicited felt in the hand/finger/arm.

7.3.2. Three and Four-dimensional HG Mapping

Although the DCS results indicated that there is a distinct spatial difference between movement-related and tactile perception, it is possible that somatosensory perception was induced by top-down streams from non-primary areas. In the preliminary analysis, however, I observed significant HG activities during passive tactile stimulation from the electrode located on the non-primary areas, where the patient reported tactile sensation during DCS (**Fig. 7-7**). To generalize this observation that these non-primary areas are actually activated by such sensations, I constructed three- and four-dimensional brain maps for actual movement and passive tactile stimulation tasks. Forty-six epilepsy patients were participated in this study (20 patients for hand grasping and elbow flexion tasks (1256 electrodes), 22 for coarse/fine texture stimulation tasks (1388 electrodes for both conditions), 29 for flutter/vibration stimulation tasks (1696 and 1650 electrodes, respectively)). The sampled electrode maps indicate a sufficient coverage of the exposed cortical sites, especially the cortical crowns of sensorimotor-related brain regions (**Fig. 7-8**). In contrast, the cortical areas of medial side and frontal pole were poorly sampled, except the supplementary motor area (SMA) and medial temporal lobe. The mean spatial weights, indicating the number of electrodes of other patients within 5 mm geodesic distance from each electrode (see Method and Materials for detail), were 3.75 ± 2.21 (mean ± SD) for movement tasks, 3.81 ± 2.05 for texture stimulation

tasks, and 4.58 ± 2.53 for vibrotactile stimulation tasks. Additionally, those of sensorimotor-related areas (S1, M1, S2, SPL, IPL, and BA 6) were 4.22 ± 2.25 for movement tasks, 4.32 ± 1.97 for texture stimulation tasks, and 5.33 ± 2.44 for vibrotactile stimulation tasks.

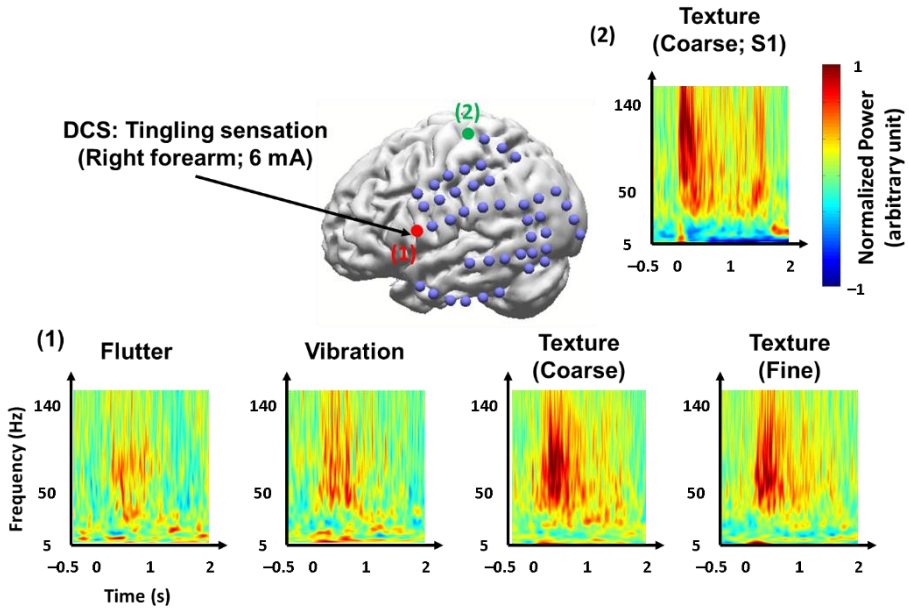

Figure 7-7. Individual sensation report and time-frequency plots for tactile stimulation. Patient reported tingling sensation in right arm and hand during DCS on the ventral PM area (1). Recorded HG activities in (1) during flutter, vibration, and coarse/fine texture stimulations. HG activity pattern in S1 (2) during texture stimulation.

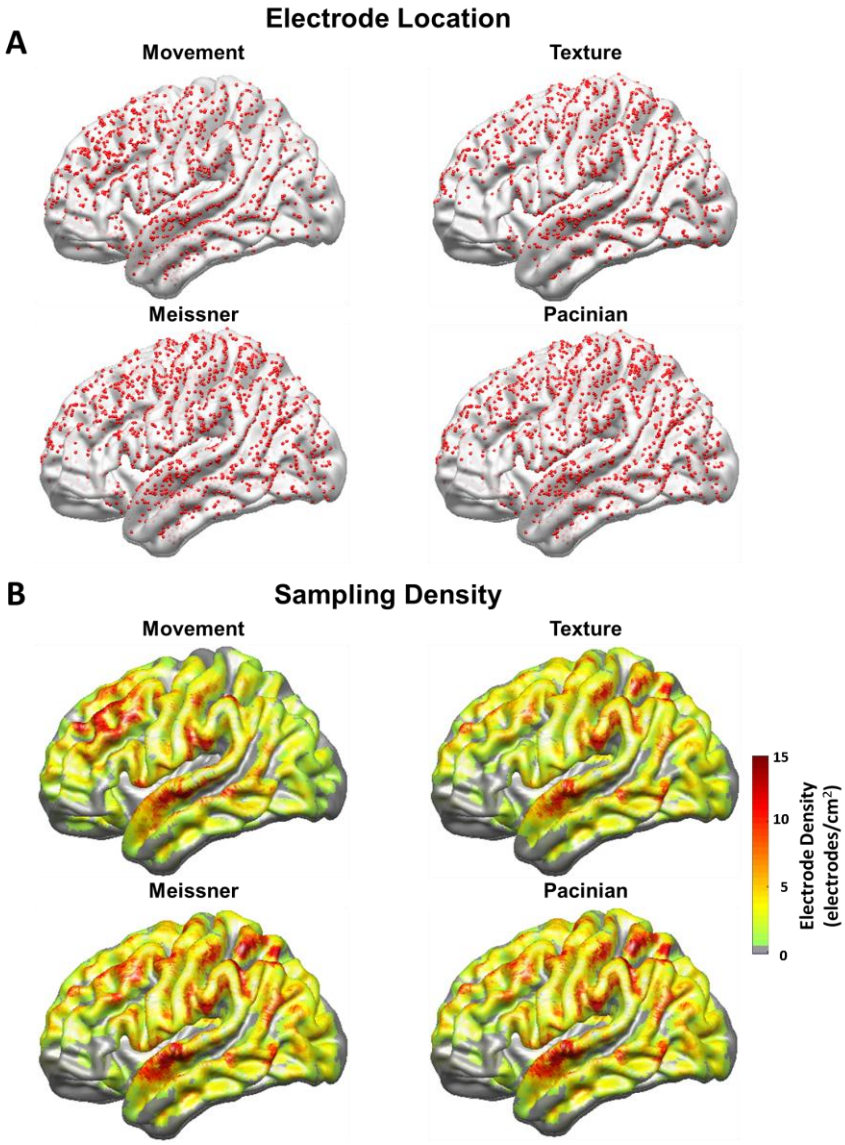

Figure 7-8. (A) Locations of all electrodes and (B) sampling densities of electrodes, in each experimental condition. Note that electrodes covered most of parietal lobe, M1, and PM regions with sufficient sampling densities.

Significant HG activities were observed in various cortical regions including S1, M1, SPL, IPL, BA 6 ventral (vPM), BA 6 dorsal (dPM and SMA), and S2 within 0 to 1 s of task onset (**Fig. 7-9**). In both hand grasping/elbow flexion and coarse/fine texture conditions, S1, M1, SPL and BA 6 areas were consistently activated, whereas the HG activities in S2 and adjacent IPL (representing supramarginal gyrus, SMG) areas exhibited a marked difference between two conditions (**Fig. 7-9** and **7-15**). Unlike the result of DCS mapping, the posterior part of IPL (angular gyrus, ANG) showed less dominant HG activity under both conditions. Interestingly, strong HG activities in ventral PM were consistently observed regardless of task conditions. In texture conditions, significant HG activations were found in the medial part of BA 5, the medial part of S2 and insula regions, but these areas could not be compared with the movement conditions due to the low sampling density. I also found weak but significant HG activity in the middle temporal region, consistent with previous finding (Avanzini et al., 2016).

Similar tactile-specific spatial patterns were observed in the vibrotactile stimulus conditions (flutter and vibration), although the amounts of changes in HG activities under these conditions were relatively small due to the narrow stimulation site and weak stimulus intensity (**Fig. 7-10**). Furthermore, these distinct spatial patterns of HG activities during movement-related and tactile conditions were more apparent at the individual level (**Fig. 7-11**). ROI

analysis revealed that ventral SMG, S2, and dorsal BA 6 areas show significant differences in the proportion of the responsive electrodes (electrodes with t-values exceeding 2.5 in at least three time bins (50 ms bins) during 0 to 1 s of task onset) of each ROI between two conditions (**Fig. 7-12A**). The difference in dorsal BA 6 area is possibly due to the augmented neural population activity related to the movement execution and control.

I also performed the same analysis using neural activity at different frequency bands such as theta (4 to 7 Hz), alpha (8 to 14 Hz), beta (15 to 30 Hz), and low gamma (30 to 50 Hz). Event-related desynchronization (ERD) of the beta and alpha band activities was spatially correlated with increase in HG activity, but with exceptions (i.e. vPM and vIPL; Fig. 7-13). In the tactile condition, bursting activities in the theta band were found at the stimulus onset, but the activated area was generally restricted to S1 and M1. However, in the movement conditions, such bursting activities in the sensorimotor area were not significant although the patterns were often found at the individual level. It may be due to the signal leakage from the alpha-beta ERD, which seems to have started before movement execution. Irregular activation patterns were observed in the low gamma band. It is due to the fact that activation of this frequency band is affected by both the lower boundary of HG band and the upper boundary of beta band activities which exhibit opposite activation patterns.

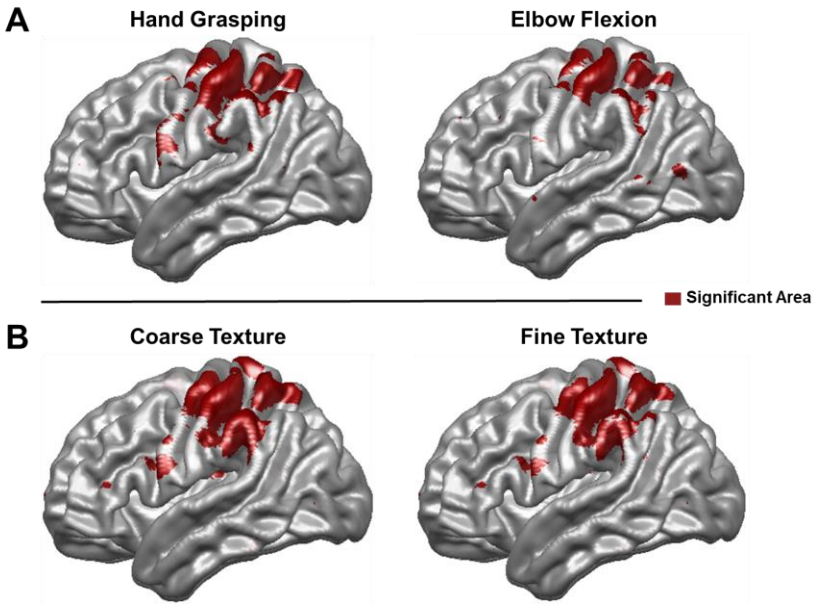

Figure 7-9. Three-dimensional HG significance maps. (A) HG significance maps for hand grasping (left) and elbow flexion (right) conditions, and (B) those for coarse texture (left) and fine texture (right) conditions.

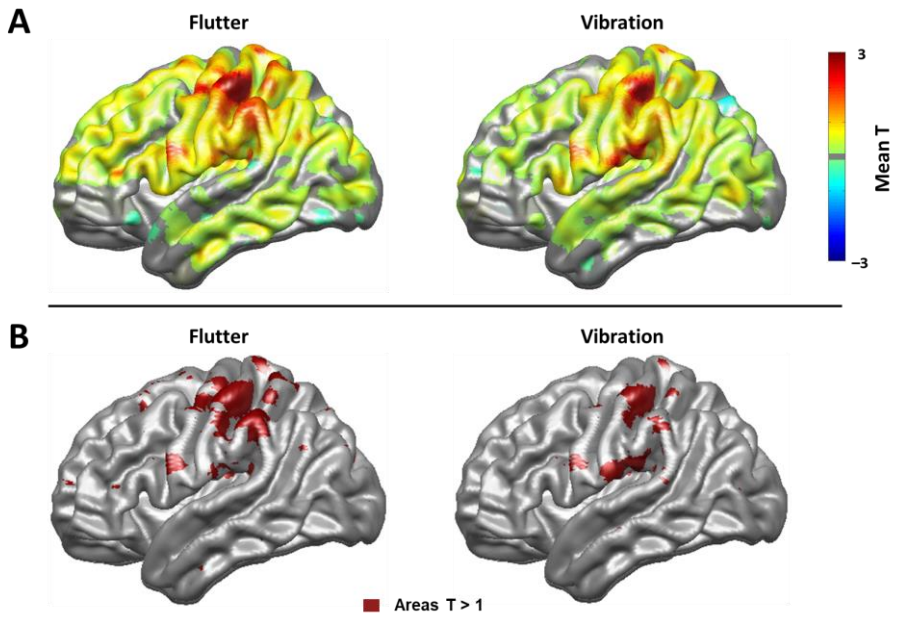

Figure 7-10. HG maps for vibrotactile stimuli. (A) Mean adjusted t-value maps for flutter (left) and vibration (right) stimulation. (B) Masked (threshold = 1) cortical maps of HG activities. Although areas identified by this threshold level is not significant based on the criteria, overall spatial patterns are similar to that for texture conditions

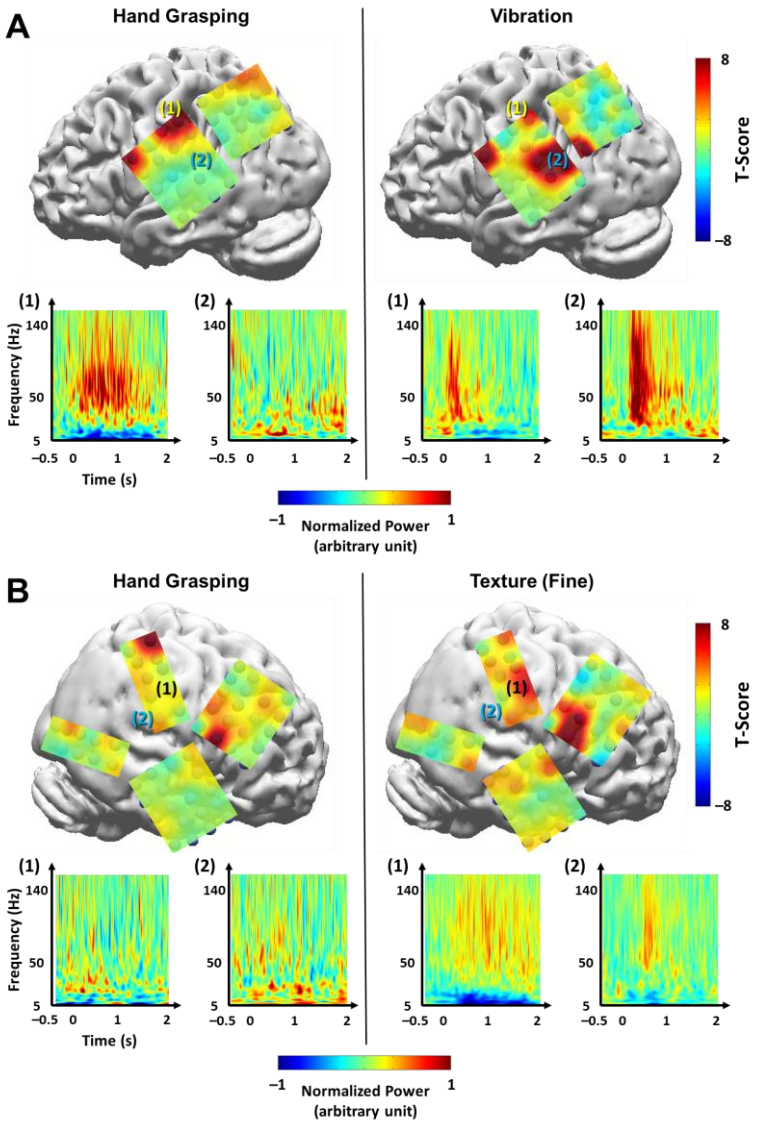

Figure 7-11. Differences in HG activities at the individual level. (A) Topographical maps of HG activities during hand grasping (left) and vibration stimulation (right) from Subject 15. Areas (1) and (2) indicate the S1 and S2, respectively, and corresponding time-frequency representations of each area are shown at the bottom. (B) The same maps during hand grasping (left) and fine

texture stimulation (right) from Subject 21. Areas (1) and (2) indicate IPL and S2, respectively. Corresponding time-frequency representations of each area are depicted below. Note that strong HG activities were consistently found in vPM of both subjects, regardless of task types.

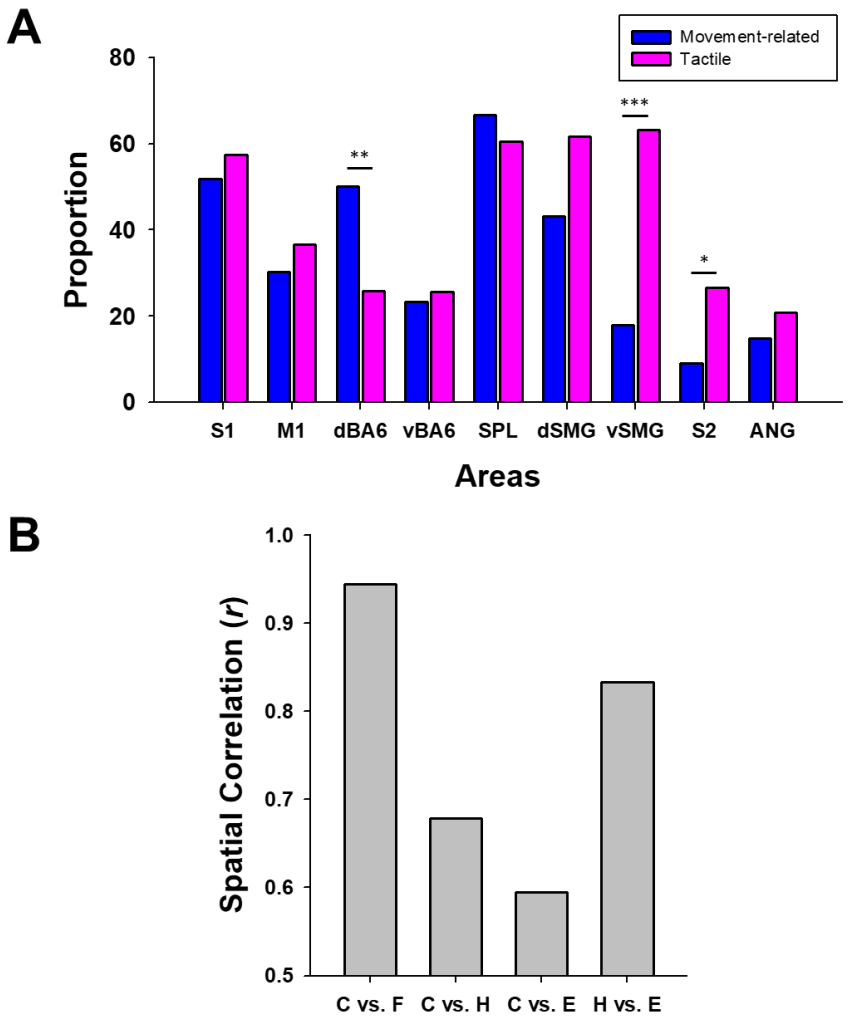

Figure 7-12. (A) Difference in the number of responsive electrodes between movement-related (blue) and tactile (pink) conditions (*: $p < 0.05$; **: $p < 0.01$;

***: p<0.001; FDR corrected) (Abbreviation: dSMG = dorsal supramarginal gyrus; vSMG = ventral supramarginal gyrus). (B) Spatial correlation of HG significance maps between conditions. (Abbreviation: C = coarse texture; F = fine texture; H = hand grasping; E = elbow flexion)

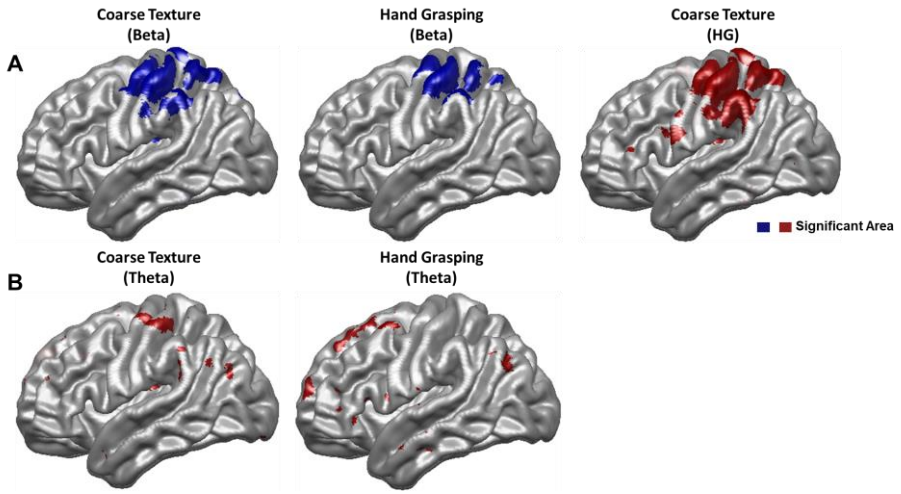

Figure 7-13. Beta and theta band maps of coarse texture and hand grasping conditions. (A) Maps of significant beta ERD from coarse texture (left) and hand grasping (middle), and HG maps from coarse texture (right) for comparison. (B) Maps of significant theta activity from coarse texture (left) and hand grasping (middle).

The significant cortical area was much wider in the texture condition (number of significant nodes = 2267 in coarse texture, 1932 in fine texture, 1777 in hand grasping, 1103 in elbow flexion), although the maximum adjusted

t-value was greater in the movement condition (mean adjusted t-values of top 100 significant nodes = 4.70 ± 0.08 in coarse texture, 3.80 ± 0.06 in fine texture, 7.75 ± 0.1 in hand grasping, 3.85 ± 0.05 in elbow flexion). The spatial distributions of adjusted t-values were very similar between coarse and fine texture stimulus conditions (spatial correlation r = 0.94). In contrast, the spatial correlations between hand grasping/elbow flexion and texture stimulus conditions were relatively low (**Fig. 7-12B**). Additionally, mean adjusted t-values (0 to 1 s of stimulus onset) of coarse texture condition from the sensorimotor-related areas were generally greater than those of fine texture condition, except the lateral part of S2, consistent with a previous finding (Ryun et al., 2017b) (**Fig. 7-14,** see also **Fig. 7-10A** for flutter vs. vibration).

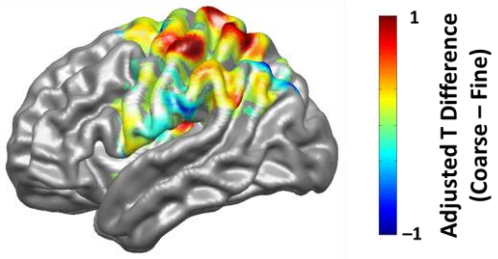

Figure 7-14. Cortical maps of the HG differences between the coarse and fine texture conditions in somatosensory-related areas.

Four-dimensional mapping analysis revealed that significant somatosensory-related regions are activated with different temporal dynamics (**Fig. 7-15**). Early HG responses (within 100 ms of task onset) were observed in the S1, M1, SPL, and dorsal IPL both in movement-related and tactile conditions. The increased S1 HG activities gradually decreased until the end of the task, but were still significant throughout the task. Additionally, a transient HG burst in S1 was observed at the task offset. This indicates that the neurons in the S1 are sensitive to the transient changes of somatosensory inputs. Prominent spatial differences in HG activation between the two conditions were found after approximately 200 ms of task onset. HG activations in the ventral part of the IPL became significant after 150 to 200 ms of task onset in the tactile condition, and these activities appeared to gradually propagate into the lateral S2 area. In contrast, no dominant HG activity was observed within 400 ms of task onset in the movement-related condition. Interestingly, significant HG activities in vPM were consistently found regardless of task conditions. In the tactile condition, HG activities in the S2 area became significant after 350 to 400 ms of task onset, after which it lasted about 450 ms. In the hand grasping and elbow flexion condition, weak but significant S2 HG activities were observed after 500 to 550 ms and 1600 ms of task onset, respectively. It might be due to the neural response of isometric contraction period during hand grasping (300 to 400 ms after task onset) and elbow flexion (1 to 1.2 s after task

onset).

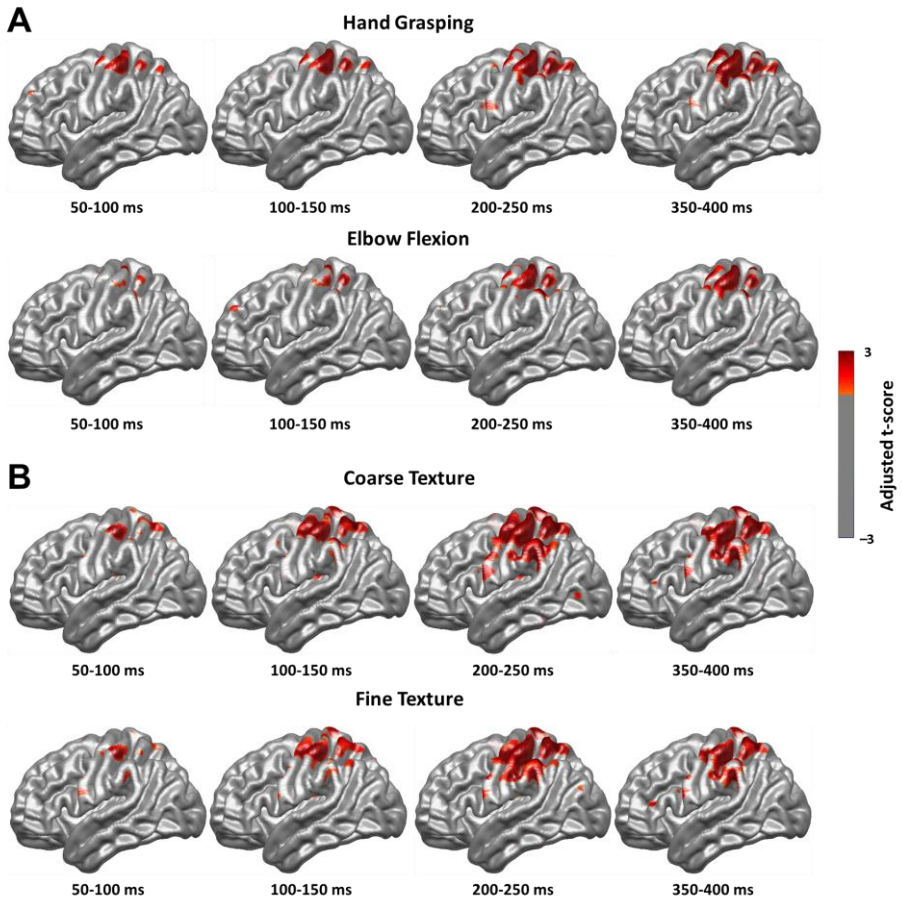

Figure 7-15. Four-dimensional HG maps for (A) movement and (B) texture conditions. Cortical regions where significant HG activities were observed at each time bin were marked.

7.3.3. Neural Characteristics among Somatosensory-related Areas

To quantify the temporal directionality of HG activities among the identified regions, I investigated peak latencies of HG activities of each ROI. In this analysis, I focused on the texture condition because this condition activated the largest cortical area (compared to the movement condition) with high signal-to-noise ratio (compared to the vibrotactile condition). Furthermore, the kinematics of the movement task change within a task period (i.e., grasp-isometric contraction-release) making it difficult to evaluate the exact timing of HG peaks from the task onset.

Results of HG peak latencies revealed that somatosensory-related cortical areas are sequentially activated with different peak timings (**Fig. 7-16** and **7-17**). The HG activity in S1 reached the peak first, followed by SPL, dorsal part of IPL, ventral part of IPL, vPM, and S2. Interestingly, the HG peaks in vPM and S2 showed high individual variability among electrodes in each region, suggesting that neuronal population responses in these regions have unique characteristics such as long-lasting HG activity, compared to other regions (see **Fig. 7-16A** and **7-17A**).

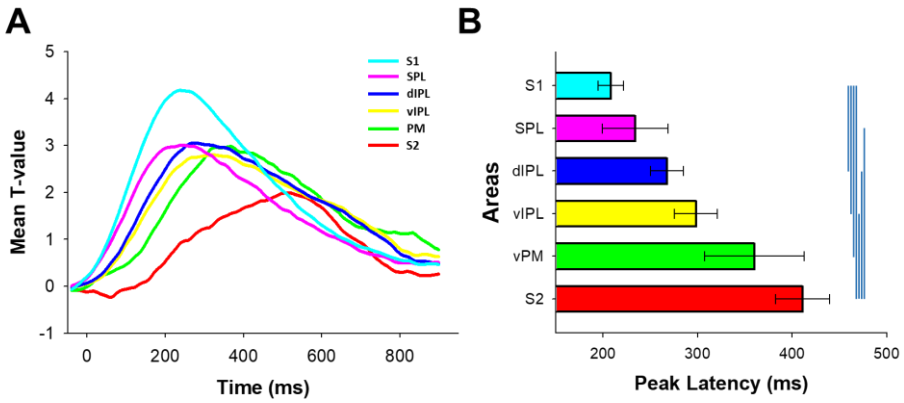

Figure 7-16. HG temporal dynamics of each area. (A) Grand means of HG temporal dynamics in various somatosensory-related areas during fine texture stimulation. (B) HG peak latencies among areas in (A) from responsive electrodes of each ROI. Vertical blue lines indicate significant pairs (FDR corrected; $p < 0.05$). Error bars denote SE of mean.

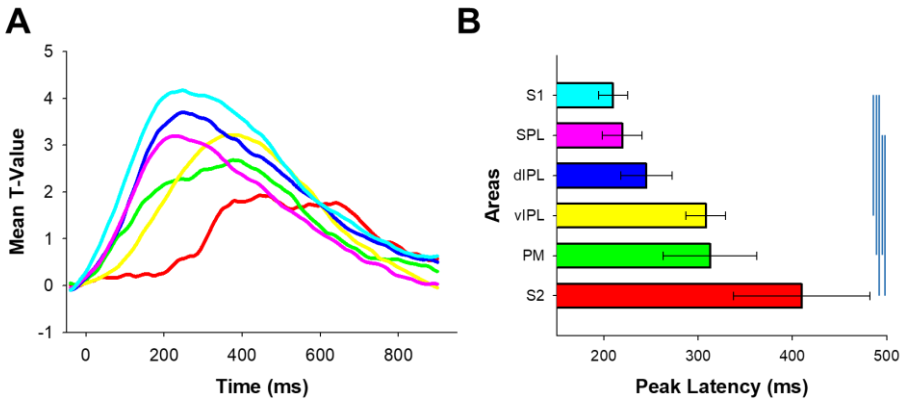

Figure 7-17. HG temporal dynamics of each area during coarse texture stimulation. Legends are the same as in **Fig. 7-16**.

7.4. Discussion

In this study, I found that somatosensory perception is elicited from widespread somatosensory-related network in the cortex, as well as from the S1 and S2. The cortical regions which elicited somatosensory perception by DCS were tightly linked to the areas where strong HG activities were observed during actual somatosensory stimulation. Specifically, the results of DCS and HG mapping revealed that functional cortical maps from these two approaches show distinct spatial distributions depending on the somatosensory functions. In addition, somatosensory related cortical areas were sequentially activated with distinct temporal dynamics in each region. These results demonstrate that macroscopic neural processing for somatosensation has distinct hierarchical networks depending on their perceptual functions.

7.4.1. DCS on the Non-Primary Areas

Somatosensory perceptions were elicited not only by DCS on the primary area, but also by that on the downstream areas. Previous findings have reported that DCS on the medial structures of parietal lobe and cingulate cortex also elicits somatosensory perceptions (Balestrini et al., 2015; Caruana et al., 2018). These findings and the present results indicate that neuronal somatosensory processing which generates specific perception occurs in

various high-order somatosensory-related brain areas. In light of this, it may not exist one core region which governs entire somatosensory perception. Rather, perceptual experiences may be formed by large-scale cortical networks responsible for specific somatosensory functions.

The current results demonstrate that there exist considerable similarities in spatial distribution between DCS and HG maps. It has been suggested that HG activities in sensorimotor areas more closely reflect cortical processing of various sensorimotor functions than event-related de-/synchronization (ERD/ERS) in other oscillatory activities such as alpha and beta band (Crone et al., 2006; Ryun et al., 2017b). Additionally, the spatial pattern of HG activity in the primary sensorimotor area is highly somatotopy-specific, and this pattern correspond well to the results of DCS mapping. Owing to the characteristics above, HG functional mapping has been considered an alternative to the DCS mapping in identifying eloquent area before resection surgery (Qian et al., 2013). The current study indicates that such spatial correspondence is also conserved in widespread somatosensory-related cortical areas, beyond the primary sensorimotor area. Therefore, the present results suggest the possibility that HG mapping can be applied to estimate deficits in high-level perceptual functions in surgical planning or the assessment of prognosis.

7.4.2. Two Streams of Somatosensory System

Several studies have proposed the existence of two distinct neural pathways which process the somatosensory perception for recognition and perception for action (Delhaye et al., 2018; Dijkerman and de Haan, 2007; Gardner, 2010). One is from the S1 to insula via lateral parietal region such as S2, representing the neural processing for perceptual recognition such as tactile perception. Another one is from the S1 to the dorsal parietal regions including SPL, representing neural processing for movement-related perception. Although there are slight differences in the areas of the two pathways compared to the previous suggestions, the present results indicate that there exist distinct networks reflecting somatosensory processing for movement-related and tactile perceptions in human. In addition, the results of HG peak latency analyses reveal the hierarchical process of human somatosensory system among various somatosensory-related cortical regions including S1, S2, SPL, IPL, and PM. Based on these findings, I suggest that large-scale cortical network involving the S1, M1, SPL, PM, and dorsal IPL reflects somatosensory stream for movement-related perceptual processing, whereas the S1, M1, SPL, vPM, S2 and adjacent IPL areas consists another network reflecting stream for tactile perception. Anatomically, these areas are densely connected each other, and project output to frontal regions via parieto-frontal pathway for decision or action (see Chapter 1 and (Delhaye et al., 2018; Dijkerman and de Haan, 2007)

for review).

The SPL was involved in both perceptual processing; however, this area seems to be more related to the movement-related perceptual processing. In the present study, DCS on SPL mainly elicited movement-related somatosensations. Furthermore, previous lesion studies showed that lesions of SPL cause mild deficits in tactile perception and discrimination, but induce significant abnormalities in the movement tasks (Padberg et al., 2010; Pause et al., 1989).

In this study, the S2 and adjacent ventral IPL were not significantly involved in the movement-related somatosensory processing. Several studies have suggested that the S2 is also related to the proprioception, because this area also receives input from proprioceptive afferents, and is connected to the cortical areas related to the movement control such as PPC (Disbrow et al., 2003; Friedman and Murray, 1986). In human studies, the S2 is activated during passive movement, and the S2 activation is modulated by movement (Huttunen et al., 1996; Xiang et al., 1997). Likewise, in monkey study, neurons in the IPL respond during not only somatosensory stimulation, but also during movement (Rozzi et al., 2008). Additionally, the IPL is strongly linked to the movement intention and illusion (Desmurget et al., 2009).

However, although the S2 receives proprioceptive information from thalamus and other cortical regions, and the IPL is involved in the movement

processing, it is unlikely that the S2 and adjacent ventral IPL are significantly involved in the neural processing for proprioceptive perception. First, in this study, no movement-related sensation was induced by DCS on these regions. All twenty-three somatosensory reports in these areas were tactile sensations. This result implies that received proprioceptive information in these regions are less related to the conscious perception for proprioception, and that does not send output for perceptual information of proprioception because DCS possibly induces activation of other cortical regions through the corticocortical fiber tract. Rather, these areas may receive proprioceptive information not to consciously perceive the movement itself, but to completely identify the object being touched, as complementary information. Second, several studies have showed that lesions in the S2 and IPL cause severe tactile deficits including tactile agnosia and impairment of texture and shape discrimination, but do not affect the motor skills and proprioception (Murray and Mishkin, 1984; Reed and Caselli, 1994; Reed et al., 1996). Third, given the multimodal response characteristics and functional complexity of IPL region, it is not surprising that the IPL is involved in both tactile perception and movement intention/recognition. Specifically, in this bi-directional mapping study, the dorsal part of IPL (near IPS) is involved in both movement-related and tactile perceptions, whereas the ventral part of IPL (near S2) is almost exclusively related to the tactile perception. This result indicates that although the neurons

in IPL often show multimodal responses, the relative proportion of preferred modality might be different depending on the locations within IPL.

7.4.3. Functional Role of ventral PM

The present findings suggest that vPM is critically involved in the somatosensory perceptual processing for both tactile and proprioceptive information. Consistent with the current findings, a previous HG cortical mapping study reported the significant HG activation in vPM during median nerve stimulation, although its perceptual relevance was unclear (Avanzini et al., 2016). In monkey, the vPM is involved in the transformation of somatosensory information into action, and in the tactile perceptual decision (Romo et al., 2004). In addition, several human studies have suggested that vPM is involved in the movement perception without somatosensory feedback by modulating S1, and is activated during illusory somatosensory perceptions, 'the cutaneous rabbit' (Blankenburg et al., 2006; Christensen et al., 2007). In this study, I showed that DCS on vPM induces artificial somatosensory perception and this area is activated by various types of somatosensory stimuli. Given the present and previous findings, the vPM may be a cortical hub that performs both bottom-up and top-down somatosensory perceptual processing including tactile and proprioceptive sensations to prepare and control the near future action.

7.4.4. Limitation and Perspective

The present study does not assess the hemisphere difference in somatosensory perceptual processing. Additionally, I was unable to construct bi-directional functional maps of unexposed cortical regions such as medial part of S2, insula and cingulum due to the limited spatial coverage of ECoG electrodes. Previous studies have suggested that DCS on these areas elicit various type of sensory-related experiences and that the medial S2 and insula are critically involved in tactile perception (Caruana et al., 2018; Preusser et al., 2015). Although there were only few samples, I also observed transient HG activities in the medial part of S2 and adjacent insula areas from depth electrodes. Further investigation is needed to broaden the current bi-directional map of somatosensory functions.

In this study, movement-related somatosensations elicited by DCS was determined by subjective patients' reports and visual inspection without objective measurements such as EMG recording. Accordingly, it is possible that some movement-related sensations were not elicited by intervention of somatosensory system itself, but by actual motor responses. Indeed, DCS on posterior parietal cortex (PPC) can induce motor responses, because the PPC and M1 are densely interconnected (Gharbawie et al., 2011). Additionally, although I showed in Chapter 6 that the movement-related HG activity in

somatosensory regions mainly represents feedback information from periphery (Ryun et al., 2017a), the activity is possibly inflated by motor-related neural processing. Even considering these possibilities, however, their impacts on the present results would be limited because these issues are unrelated to the difference in HG activity of S2 and IPL regions between movement-related and tactile conditions.

The current findings provide some important insights into the bi-directional brain-machine interface (BMI) researches incorporating somatosensory feedback by cortical stimulation. So far, studies on the cortical stimulation for eliciting somatosensation have mainly focused on the S1 area because the stimulation on this area trustfully induces somatosensory experiences of the specific body part. In the current study, I showed that DCS on the high order cortical regions can induce somatosensory function-specific perceptual experiences depending on the location of stimulation. This result may provide a cortical functional map for multi-regional electrical stimulation to finely control the elicited sensation.

Some degree of spatial difference in alpha-beta band neural activity was observed between movement and tactile conditions, although the spatial distribution of alpha-beta and HG activity was not completely identical. This implies that neural activities of alpha-beta frequency band can be a putative marker for investigating perceptual network in intact human brain by using

non-invasive recording techniques including EEG and MEG. In addition, HG activity was sometimes observed even below 40 Hz because the lower boundary of HG activity exhibits high individual variability. In this case, neural signals representing HG activities can be observed in non-invasive electrophysiological recording, although their response timing and spectrotemporal patterns would be somewhat different.

7.4.5. Conclusion of Chapter 7

In this chapter, I found that somatosensory perception is elicited from widespread somatosensory-related network in the cortex, and the spatial distributions of DCS and HG functional maps showed considerable similarity in spatial distribution between high-gamma and DCS functional maps. In particular, the bi-directional functional maps showed distinct spatial distributions depending on the somatosensory functions, and each area was sequentially activated with distinct temporal dynamics. These results suggest that macroscopic neural processing for somatosensation has distinct hierarchical networks depending on their perceptual functions. Therefore, the results in this chapter provide evidence for the “perception and action” related neural streams of somatosensory system.

PART III. CONCLUSION

Chapter 8: Conclusion and Perspective

In the series of studies, I addressed the macroscopic neural mechanism for perceptual processing of tactile and proprioception in human.

The first study suggested that neural processing for vibrotactile perception involves multi-regional co-operation between the S1 and the downstream regions such as the S2. The results also indicated that neuronal population activities show similarities between artificial vibrotactile stimuli and naturalistic texture stimuli, depending on the spectral compositions of stimuli. These results imply that human vibrotactile sensation involves macroscopic multi-regional hierarchical processing in the somatosensory system, even during the simplified stimulation.

The second study indicated that sensorimotor HG activities are more dominant in S1 than in M1 during actual movement. Specifically, this study showed that movement-related HG activities in S1 mainly represent proprioceptive and tactile feedback from periphery. These results imply that somatosensory feedback processing in parietal region during movement may have more critical roles in movement control than originally expected.

Given the results of previous two studies, the final study aimed to

identify the large-scale cortical networks for perceptual processing in human. This study showed that somatosensory perceptual processing involves neural activation of widespread somatosensory-related network in the cortex. Finally, the present study suggested that macroscopic neural processing for somatosensation has distinct hierarchical networks depending on their perceptual functions – perception for movement and perception for identification. Therefore, these findings provide evidence for the "perception and action" related neural streams of somatosensory system.

8.1. Perspective and Future Work

Practically, one of the major goals of present studies is to develop a cortical stimulation technique for generating specific natural somatosensations, because this technique is directly applied to the bi-directional BMI system, which is attracting attention as a promising future technology. However, the final questions of my present and future studies are how we perceive external world, make a decision for our own purpose, and recognize ourselves as one organized object – I. Somatosensory system has a critical key to unveil the secrets above because this system always informs us about ourselves, whether we are aware of it or not.

In the present study, I showed that somatosensory perception is

elicited by DCS on the downstream cortical areas beyond the S1. Although it is unclear whether the downstream areas also have some degree of somatotopy, given the multimodal and somatotopy-independent activation patterns of the downstream areas, these areas may play a role in actualizing the somatosensory qualities regardless of the represented body parts. In the present study, however, patients could easily report the body parts where the sensation was elicited during DCS on the downstream areas. One possibility for this result is that represented body part for somatosensation induced by DCS on downstream area may depend on our attention to the specific body part. If these hypotheses above are true, we can elicit specific somatosensation at the desired body parts by stimulating downstream areas only, circumventing the DCS on the S1.

The current issue of bi-directional BMI research is to encode somatosensory feedback from the robotic arm by stimulating the somatosensory cortex which represents the corresponding body part. BMI researchers expect that BMI users can control the robotic arm like their own arms through this approach. However, although this approach is very efficient in terms of rehabilitation of some potential BMI users including patients with tetraplegia, it is a limited way to temporarily replace some of the human body parts for receiving somatosensory feedback from other objects. Therefore, conflicts between body schema for specific body parts and information from external object is inevitable. That is, to perceive the somatosensory feedback

from external object as a distinct additional feedback, the body schema should be extended to include the external one. There is ongoing debate as to whether the extension of the body schema is practically possible. However, body schema may not be an innate function but gradually acquired from prenatal period, given that each brain of some Siamese twins independently forms the body schema of the shared body part. Moreover, the representation of body part in the somatosensory area can be changed after amputation. If additional sensory experiences can be induced by brain modulation without intervention of the existing body schema, it is possible that sufficient embodiment for the external object by bi-directional BMI system induces brain plasticity for the extension of body schema. Addressing these issues will be the final goal of my research. Humans can fly without wings now, but still dream about flying with their own wings.

REFERENCES

Adams, R.A., Shipp, S., and Friston, K.J. (2013). Predictions not commands: active inference in the motor system. Brain Struct Funct 218, 611-643.

Aflalo, T., Kellis, S., Klaes, C., Lee, B., Shi, Y., Pejsa, K., Shanfield, K., Hayes-Jackson, S., Aisen, M., and Heck, C. (2015). Decoding motor imagery from the posterior parietal cortex of a tetraplegic human. Science 348, 906-910.

Allison, T., McCarthy, G., and Wood, C.C. (1992). The relationship between human long-latency somatosensory evoked potentials recorded from the cortical surface and from the scalp. Electroencephalography and Clinical Neurophysiology/Evoked Potentials Section 84, 301-314.

Andersen, R.A., and Buneo, C.A. (2002). Intentional maps in posterior parietal cortex. Annu Rev Neurosci 25, 189-220.

Anumanchipalli, G.K., Chartier, J., and Chang, E.F. (2019). Speech synthesis from neural decoding of spoken sentences. Nature 568, 493-498.

Apkarian, A.V., and Shi, T. (1994). Squirrel monkey lateral thalamus. I. Somatic nociresponsive neurons and their relation to spinothalamic terminals. J Neurosci 14, 6779-6795.

Armand, J., Olivier, E., Edgley, S.A., and Lemon, R.N. (1997). Postnatal development of corticospinal projections from motor cortex to the cervical enlargement in the macaque monkey. J Neurosci 17, 251-266.

Armenta Salas, M., Bashford, L., Kellis, S., Jafari, M., Jo, H., Kramer, D., Shanfield, K., Pejsa, K., Lee, B., Liu, C.Y., and Andersen, R.A. (2018). Proprioceptive and cutaneous sensations in humans elicited by intracortical microstimulation. Elife 7.

Avanzini, P., Abdollahi, R.O., Sartori, I., Caruana, F., Pelliccia, V., Casaceli, G., Mai, R., Russo, G.L., Rizzolatti, G., and Orban, G.A. (2016). Four-dimensional maps of the human somatosensory system. Proceedings of the National Academy of Sciences 113, E1936-E1943.

Balestrini, S., Francione, S., Mai, R., Castana, L., Casaceli, G., Marino, D., Provinciali, L., Cardinale, F., and Tassi, L. (2015). Multimodal responses induced by cortical stimulation of the parietal lobe: a stereo-electroencephalography study. Brain 138, 2596-2607.

Bauer, M., Oostenveld, R., Peeters, M., and Fries, P. (2006). Tactile spatial attention enhances gamma-band activity in somatosensory cortex and reduces low-frequency activity in parieto-occipital areas. J Neurosci 26, 490-501.

Bell, J., Bolanowski, S., and Holmes, M.H. (1994). The structure and function of Pacinian corpuscles: a review. Prog Neurobiol 42, 79-128.
Bensmaïa, S., and Hollins, M. (2005). Pacinian representations of fine surface texture. Percept Psychophys 67, 842-854.
Blankenburg, F., Ruff, C.C., Deichmann, R., Rees, G., and Driver, J. (2006). The cutaneous rabbit illusion affects human primary sensory cortex somatotopically. Plos Biol 4, e69.
Bleichner, M.G., Freudenburg, Z.V., Jansma, J.M., Aarnoutse, E.J., Vansteensel, M.J., and Ramsey, N.F. (2016). Give me a sign: decoding four complex hand gestures based on high-density ECoG. Brain Struct Funct 221, 203-216.
Branco, M.P., Freudenburg, Z.V., Aarnoutse, E.J., Bleichner, M.G., Vansteensel, M.J., and Ramsey, N.F. (2017). Decoding hand gestures from primary somatosensory cortex using high-density ECoG. NeuroImage 147, 130-142.
Buneo, C.A., and Andersen, R.A. (2006). The posterior parietal cortex: sensorimotor interface for the planning and online control of visually guided movements. Neuropsychologia 44, 2594-2606.
Burke, D., Gandevia, S.C., and Macefield, G. (1988). Responses to passive movement of receptors in joint, skin and muscle of the human hand. J Physiol 402, 347-361.
Canolty, R.T., Edwards, E., Dalal, S.S., Soltani, M., Nagarajan, S.S., Kirsch, H.E., Berger, M.S., Barbaro, N.M., and Knight, R.T. (2006). High gamma power is phase-locked to theta oscillations in human neocortex. Science 313, 1626-1628.
Carlson, M. (1981). Characteristics of sensory deficits following lesions of Brodmann's areas 1 and 2 in the postcentral gyrus of Macaca mulatta. Brain Res 204, 424-430.
Caruana, F., Gerbella, M., Avanzini, P., Gozzo, F., Pelliccia, V., Mai, R., Abdollahi, R.O., Cardinale, F., Sartori, I., Lo Russo, G., and Rizzolatti, G. (2018). Motor and emotional behaviours elicited by electrical stimulation of the human cingulate cortex. Brain 141, 3035-3051.
Caselli, R.J. (1991). Rediscovering tactile agnosia. Mayo Clin Proc 66, 129-142.
Chandran, K.S.S., Mishra, A., Shirhatti, V., and Ray, S. (2016). Comparison of Matching Pursuit Algorithm with Other Signal Processing Techniques for Computation of the Time-Frequency Power Spectrum of Brain Signals. J Neurosci 36, 3399-3408.
Cheney, P.D., and Preston, J.B. (1976). Classification and response characteristics of muscle spindle afferents in the primate. J Neurophysiol 39, 1-8.

Chestek, C.A., Gilja, V., Blabe, C.H., Foster, B.L., Shenoy, K.V., Parvizi, J., and Henderson, J.M. (2013). Hand posture classification using electrocorticography signals in the gamma band over human sensorimotor brain areas. J Neural Eng 10, 026002.
Cheyne, D., Bells, S., Ferrari, P., Gaetz, W., and Bostan, A.C. (2008). Self-paced movements induce high-frequency gamma oscillations in primary motor cortex. NeuroImage 42, 332-342.
Christensen, M.S., Lundbye-Jensen, J., Geertsen, S.S., Petersen, T.H., Paulson, O.B., and Nielsen, J.B. (2007). Premotor cortex modulates somatosensory cortex during voluntary movements without proprioceptive feedback. Nat Neurosci 10, 417-419.
Chung, Y.G., Kim, J., Han, S.W., Kim, H.-S., Choi, M.H., Chung, S.-C., Park, J.-Y., and Kim, S.-P. (2013). Frequency-dependent patterns of somatosensory cortical responses to vibrotactile stimulation in humans: A fMRI study. Brain Res 1504, 47-57.
Connor, C.E., and Johnson, K.O. (1992). Neural coding of tactile texture: comparison of spatial and temporal mechanisms for roughness perception. The Journal of Neuroscience 12, 3414-3426.
Crone, N.E., Miglioretti, D.L., Gordon, B., and Lesser, R.P. (1998). Functional mapping of human sensorimotor cortex with electrocorticographic spectral analysis - II. Event-related synchronization in the gamma band. Brain 121, 2301-2315.
Crone, N.E., Sinai, A., and Korzeniewska, A. (2006). High-frequency gamma oscillations and human brain mapping with electrocorticography. Prog Brain Res 159, 275-295.
Cusick, C.G., Steindler, D.A., and Kaas, J.H. (1985). Corticocortical and collateral thalamocortical connections of postcentral somatosensory cortical areas in squirrel monkeys: a double-labeling study with radiolabeled wheatgerm agglutinin and wheatgerm agglutinin conjugated to horseradish peroxidase. Somatosens Res 3, 1-31.
Davis, K.D., Wood, M.L., Crawley, A.P., and Mikulis, D.J. (1995). fMRI of human somatosensory and cingulate cortex during painful electrical nerve stimulation. Neuroreport 7, 321-325.
de Lafuente, V., and Romo, R. (2006). Neural correlate of subjective sensory experience gradually builds up across cortical areas. Proceedings of the National Academy of Sciences 103, 14266-14271.
Delhaye, B.P., Long, K.H., and Bensmaia, S.J. (2018). Neural Basis of Touch and Proprioception in Primate Cortex. Compr Physiol 8, 1575-1602.
Delmas, P., Hao, J., and Rodat-Despoix, L. (2011). Molecular mechanisms of mechanotransduction in mammalian sensory neurons. Nat Rev Neurosci 12, 139-153.
Desmurget, M., Reilly, K.T., Richard, N., Szathmari, A., Mottolese, C., and

Sirigu, A. (2009). Movement intention after parietal cortex stimulation in humans. Science 324, 811-813.
Dijkerman, H.C., and de Haan, E.H. (2007). Somatosensory processes subserving perception and action. Behav Brain Sci 30, 189-201; discussion 201-139.
Dimitriou, M., and Edin, B.B. (2008). Discharges in human muscle receptor afferents during block grasping. J Neurosci 28, 12632-12642.
Disbrow, E., Litinas, E., Recanzone, G.H., Padberg, J., and Krubitzer, L. (2003). Cortical connections of the second somatosensory area and the parietal ventral area in macaque monkeys. J Comp Neurol 462, 382-399.
Disbrow, E., Roberts, T., and Krubitzer, L. (2000). Somatotopic organization of cortical fields in the lateral sulcus of homo sapiens: Evidence for SII and PV. The Journal of Comparative Neurology 418, 1-21.
Duhamel, J.R., Colby, C.L., and Goldberg, M.E. (1998). Ventral intraparietal area of the macaque: congruent visual and somatic response properties. J Neurophysiol 79, 126-136.
Edin, B.B., and Vallbo, A.B. (1990). Muscle afferent responses to isometric contractions and relaxations in humans. J Neurophysiol 63, 1307-1313.
Eickhoff, S.B., Amunts, K., Mohlberg, H., and Zilles, K. (2006). The human parietal operculum. II. Stereotaxic maps and correlation with functional imaging results. Cereb Cortex 16, 268-279.
Eickhoff, S.B., Grefkes, C., Zilles, K., and Fink, G.R. (2007). The somatotopic organization of cytoarchitectonic areas on the human parietal operculum. Cereb Cortex 17, 1800-1811.
Flesher, S.N., Collinger, J.L., Foldes, S.T., Weiss, J.M., Downey, J.E., Tyler-Kabara, E.C., Bensmaia, S.J., Schwartz, A.B., Boninger, M.L., and Gaunt, R.A. (2016). Intracortical microstimulation of human somatosensory cortex. Sci Transl Med 8, 361ra141-361ra141.
Francis, S., Kelly, E., Bowtell, R., Dunseath, W., Folger, S., and McGlone, F. (2000). fMRI of the responses to vibratory stimulation of digit tips. NeuroImage 11, 188-202.
Freund, H.J. (2001). The parietal lobe as a sensorimotor interface: A perspective from clinical and neuroimaging data. NeuroImage 14, S142-S146.
Friedman, D.P., Jones, E.G., and Burton, H. (1980). Representation pattern in the second somatic sensory area of the monkey cerebral cortex. J Comp Neurol 192, 21-41.
Friedman, D.P., and Murray, E.A. (1986). Thalamic connectivity of the second somatosensory area and neighboring somatosensory fields of the lateral sulcus of the macaque. J Comp Neurol 252, 348-373.

Friedman, D.P., Murray, E.A., O'Neill, J.B., and Mishkin, M. (1986). Cortical connections of the somatosensory fields of the lateral sulcus of macaques: evidence for a corticolimbic pathway for touch. J Comp Neurol 252, 323-347.
Fries, P., Nikolic, D., and Singer, W. (2007). The gamma cycle. Trends Neurosci 30, 309-316.
Frot, M., and Mauguière, F. (1999). Timing and spatial distribution of somatosensory responses recorded in the upper bank of the sylvian fissure (SII area) in humans. Cereb Cortex 9, 854-863.
Gallace, A., and Spence, C. (2014). In Touch with the Future, 1 edn (United Kingdom: Oxford University Press).
Gardner, E.P. (1988). Somatosensory cortical mechanisms of feature detection in tactile and kinesthetic discrimination. Can J Physiol Pharmacol 66, 439-454.
Gardner, E.P. (2010). Dorsal and ventral streams in the sense of touch. Senses A Compr Ref 6, 233-258.
Gazzaniga, M.S. (2009). The Cognitive Neurosciences, Fourth edn (MIT Press).
Gharbawie, O.A., Stepniewska, I., and Kaas, J.H. (2011). Cortical connections of functional zones in posterior parietal cortex and frontal cortex motor regions in new world monkeys. Cereb Cortex 21, 1981-2002.
Grigg, P., and Greenspan, B.J. (1977). Response of primate joint afferent neurons to mechanical stimulation of knee joint. J Neurophysiol 40, 1-8.
Harrington, G.S., and Downs III, J.H. (2001). FMRI mapping of the somatosensory cortex with vibratory stimuli: Is there a dependency on stimulus frequency? Brain Res 897, 188-192.
Harvey, M.A., Saal, H.P., Dammann, J.F., and Bensmaia, S.J. (2013). Multiplexing Stimulus Information through Rate and Temporal Codes in Primate Somatosensory Cortex. Plos Biol 11.
Hiremath, S.V., Tyler-Kabara, E.C., Wheeler, J.J., Moran, D.W., Gaunt, R.A., Collinger, J.L., Foldes, S.T., Weber, D.J., Chen, W., Boninger, M.L., and Wang, W. (2017). Human perception of electrical stimulation on the surface of somatosensory cortex. Plos One 12, e0176020.
Hochman, S., Wang, W., Collinger, J.L., Degenhart, A.D., Tyler-Kabara, E.C., Schwartz, A.B., Moran, D.W., Weber, D.J., Wodlinger, B., Vinjamuri, R.K.*, et al.* (2013). An Electrocorticographic Brain Interface in an Individual with Tetraplegia. Plos One 8, e55344.
Hollins, M., and Risner, S.R. (2000). Evidence for the duplex theory of tactile texture perception. Percept Psychophys 62, 695-705.
Hotson, G., McMullen, D.P., Fifer, M.S., Johannes, M.S., Katyal, K.D., Para, M.P., Armiger, R., Anderson, W.S., Thakor, N.V., Wester, B.A., and

Crone, N.E. (2016). Individual finger control of a modular prosthetic limb using high-density electrocorticography in a human subject. J Neural Eng 13, 026017.
Huang, N.E., Shen, Z., Long, S.R., Wu, M.L.C., Shih, H.H., Zheng, Q.N., Yen, N.C., Tung, C.C., and Liu, H.H. (1998). The empirical mode decomposition and the Hilbert spectrum for nonlinear and non-stationary time series analysis. P Roy Soc a-Math Phy 454, 903-995.
Huttunen, J., Wikstrom, H., Korvenoja, A., Seppalainen, A.M., Aronen, H., and Ilmoniemi, R.J. (1996). Significance of the second somatosensory cortex in sensorimotor integration: enhancement of sensory responses during finger movements. Neuroreport 7, 1009-1012.
Inui, K., Wang, X., Tamura, Y., Kaneoke, Y., and Kakigi, R. (2004). Serial processing in the human somatosensory system. Cereb Cortex 14, 851-857.
Jeannerod, M., Michel, F., and Prablanc, C. (1984). The control of hand movements in a case of hemianaesthesia following a parietal lesion. Brain 107 (Pt 3), 899-920.
Jenmalm, P., and Johansson, R.S. (1997). Visual and Somatosensory Information about Object Shape Control Manipulative Fingertip Forces. The Journal of Neuroscience 17, 4486-4499.
Johansson, R.S., and Flanagan, J.R. (2008). The Senses: A Comprehensive Reference (San Diego: Academic Press).
Jones, E.G., and Powell, T.P. (1970). Connexions of the somatic sensory cortex of the rhesus monkey. 3. Thalamic connexions. Brain 93, 37-56.
Jones, E.G., Wise, S.P., and Coulter, J.D. (1979). Differential thalamic relationships of sensory-motor and parietal cortical fields in monkeys. J Comp Neurol 183, 833-881.
Kaas, J.H. (1983). What, if anything, is SI? Organization of first somatosensory area of cortex. Physiol Rev 63, 206-231.
Kaas, J.H. (2012). The Human Nervous System, Third edn (Academic Press).
Kalberlah, C., Villringer, A., and Pleger, B. (2013). Dynamic causal modeling suggests serial processing of tactile vibratory stimuli in the human somatosensory cortex—An fMRI study. NeuroImage 74, 164-171.
Khatri, V., Hartings, J.A., and Simons, D.J. (2004). Adaptation in thalamic barreloid and cortical barrel neurons to periodic whisker deflections varying in frequency and velocity. J Neurophysiol 92, 3244-3254.
Kim, J.H., Greenspan, J.D., Coghill, R.C., Ohara, S., and Lenz, F.A. (2007). Lesions limited to the human thalamic principal somatosensory nucleus (ventral caudal) are associated with loss of cold sensations and central pain. J Neurosci 27, 4995-5004.

Kim, J.S., Singh, V., Lee, J.K., Lerch, J., Ad-Dab'bagh, Y., MacDonald, D., Lee, J.M., Kim, S.I., and Evans, A.C. (2005). Automated 3-D extraction and evaluation of the inner and outer cortical surfaces using a Laplacian map and partial volume effect classification. NeuroImage 27, 210-221.

Knibestol, M. (1973). Stimulus-response functions of rapidly adapting mechanoreceptors in human glabrous skin area. J Physiol 232, 427-452.

Knibestol, M. (1975). Stimulus-response functions of slowly adapting mechanoreceptors in the human glabrous skin area. J Physiol 245, 63-80.

Kurth, R., Villringer, K., Curio, G., Wolf, K.J., Krause, T., Repenthin, J., Schwiemann, J., Deuchert, M., and Villringer, A. (2000). fMRI shows multiple somatotopic digit representations in human primary somatosensoy cortex. Neuroreport 11, 1487-1491.

Lebedev, M.A., and Nelson, R.J. (1996). High-frequency vibratory sensitive neurons in monkey primary somatosensory cortex: entrained and nonentrained responses to vibration during the performance of vibratory-cued hand movements. Exp Brain Res 111, 313-325.

Lemon, R.N. (2008). Descending pathways in motor control. Annu Rev Neurosci 31, 195-218.

Lim, M., Kim, J.S., and Chung, C.K. (2012). Modulation of somatosensory evoked magnetic fields by intensity of interfering stimuli in human somatosensory cortex: An MEG study. NeuroImage 61, 660-669.

Lin, Y.Y., and Forss, N. (2002). Functional characterization of human second somatosensory cortex by magnetoencephalography. Behav Brain Res 135, 141-145.

Luna, R., Hernández, A., Brody, C.D., and Romo, R. (2005). Neural codes for perceptual discrimination in primary somatosensory cortex. Nat Neurosci 8, 1210-1219.

Lyttelton, O.C., Karama, S., Ad-Dab'bagh, Y., Zatorre, R.J., Carbonell, F., Worsley, K., and Evans, A.C. (2009). Positional and surface area asymmetry of the human cerebral cortex. NeuroImage 46, 895-903.

Mackevicius, E.L., Best, M.D., Saal, H.P., and Bensmaia, S.J. (2012). Millisecond precision spike timing shapes tactile perception. The Journal of Neuroscience 32, 15309-15317.

Manfredi, L.R., Saal, H.P., Brown, K.J., Zielinski, M.C., Dammann, J.F., Polashock, V.S., and Bensmaia, S.J. (2014). Natural scenes in tactile texture. J Neurophysiol 111, 1792-1802.

Merzenich, M.M., and Harrington, T. (1969). The sense of flutter-vibration evoked by stimulation of the hairy skin of primates: comparison of human sensory capacity with the responses of mechanoreceptive

afferents innervating the hairy skin of monkeys. Exp Brain Res 9, 236-260.
Merzenich, M.M., Kaas, J.H., Sur, M., and Lin, C.S. (1978). Double representation of the body surface within cytoarchitectonic areas 3b and 1 in "SI" in the owl monkey (Aotus trivirgatus). J Comp Neurol 181, 41-73.
Miller, K.J., Leuthardt, E.C., Schalk, G., Rao, R.P.N., Anderson, N.R., Moran, D.W., Miller, J.W., and Ojemann, J.G. (2007). Spectral changes in cortical surface potentials during motor movement. J Neurosci 27, 2424-2432.
Mountcastle, V.B., Steinmetz, M., and Romo, R. (1990). Frequency discrimination in the sense of flutter: psychophysical measurements correlated with postcentral events in behaving monkeys. The Journal of Neuroscience 10, 3032-3044.
Mountcastle, V.B., Talbot, W.H., Sakata, H., and Hyvarinen, J. (1969). Cortical neuronal mechanisms in flutter-vibration studied in unanesthetized monkeys: Neuronal periodicity and frequency discrimination. J Neurophysiol.
Murray, E.A., and Mishkin, M. (1984). Relative contributions of SII and area 5 to tactile discrimination in monkeys. Behav Brain Res 11, 67-83.
Musall, S., von der Behrens, W., Mayrhofer, J.M., Weber, B., Helmchen, F., and Haiss, F. (2014). Tactile frequency discrimination is enhanced by circumventing neocortical adaptation. Nat Neurosci 17, 1567-1573.
Niu, J., Ding, L., Li, J.J., Kim, H., Liu, J., Li, H., Moberly, A., Badea, T.C., Duncan, I.D., Son, Y.J.*, et al.* (2013). Modality-based organization of ascending somatosensory axons in the direct dorsal column pathway. J Neurosci 33, 17691-17709.
Overduin, S.A., and Servos, P. (2004). Distributed digit somatotopy in primary somatosensory cortex. NeuroImage 23, 462-472.
Padberg, J., Recanzone, G., Engle, J., Cooke, D., Goldring, A., and Krubitzer, L. (2010). Lesions in posterior parietal area 5 in monkeys result in rapid behavioral and cortical plasticity. J Neurosci 30, 12918-12935.
Papademetris, X., Jackowski, M.P., Rajeevan, N., DiStasio, M., Okuda, H., Constable, R.T., and Staib, L.H. (2006). BioImage Suite: An integrated medical image analysis suite: An update. Insight J, 209.
Pause, M., Kunesch, E., Binkofski, F., and Freund, H.J. (1989). Sensorimotor disturbances in patients with lesions of the parietal cortex. Brain 112 (Pt 6), 1599-1625.
Pearson, R.C., and Powell, T.P. (1985). The projection of the primary somatic sensory cortex upon area 5 in the monkey. Brain Res 356, 89-107.
Pei, Y.C., Denchev, P.V., Hsiao, S.S., Craig, J.C., and Bensmaia, S.J. (2009). Convergence of submodality-specific input onto neurons in primary

somatosensory cortex. J Neurophysiol 102, 1843-1853.
Phillips, C.G., Powell, T.P., and Wiesendanger, M. (1971). Projection from low-threshold muscle afferents of hand and forearm to area 3a of baboon's cortex. J Physiol 217, 419-446.
Pistohl, T., Schulze-Bonhage, A., Aertsen, A., Mehring, C., and Ball, T. (2012). Decoding natural grasp types from human ECoG. NeuroImage 59, 248-260.
Pons, T., Garraghty, P., Friedman, D., and Mishkin, M. (1987). Physiological evidence for serial processing in somatosensory cortex. Science 237, 417-420.
Pons, T.P., and Kaas, J.H. (1986). Corticocortical connections of area 2 of somatosensory cortex in macaque monkeys: a correlative anatomical and electrophysiological study. J Comp Neurol 248, 313-335.
Preusser, S., Thiel, S.D., Rook, C., Roggenhofer, E., Kosatschek, A., Draganski, B., Blankenburg, F., Driver, J., Villringer, A., and Pleger, B. (2015). The perception of touch and the ventral somatosensory pathway. Brain 138, 540-548.
Pruett, J.R., Sinclair, R.J., and Burton, H. (2000). Response patterns in second somatosensory sortex (SII) of awake
monkeys to passively applied tactile gratings. J Neurophysiol 84, 780-797.
Qian, T., Zhou, W., Ling, Z., Gao, S., Liu, H., and Hong, B. (2013). Fast presurgical functional mapping using task-related intracranial high gamma activity. J Neurosurg 119, 26-36.
Randolph, M., and Semmes, J. (1974). Behavioral consequences of selective subtotal ablations in the postcentral gyrus of Macaca mulatta. Brain Res 70, 55-70.
Ray, S., Crone, N.E., Niebur, E., Franaszczuk, P.J., and Hsiao, S.S. (2008a). Neural correlates of high-gamma oscillations (60–200 Hz) in macaque local field potentials and their potential implications in electrocorticography. The Journal of Neuroscience 28, 11526-11536.
Ray, S., Hsiao, S.S., Crone, N.E., Franaszczuk, P.J., and Niebur, E. (2008b). Effect of stimulus intensity on the spike–local field potential relationship in the secondary somatosensory cortex. The Journal of Neuroscience 28, 7334-7343.
Ray, S., Niebur, E., Hsiao, S.S., Sinai, A., and Crone, N.E. (2008c). High-frequency gamma activity (80-150 Hz) is increased in human cortex during selective attention. Clin Neurophysiol 119, 116-133.
Reed, C.L., and Caselli, R.J. (1994). The nature of tactile agnosia: a case study. Neuropsychologia 32, 527-539.
Reed, C.L., Caselli, R.J., and Farah, M.J. (1996). Tactile agnosia. Underlying impairment and implications for normal tactile object recognition. Brain 119 (Pt 3), 875-888.

Reed, C.L., Klatzky, R.L., and Halgren, E. (2005). What vs. where in touch: an fMRI study. NeuroImage 25, 718-726.
Rizzolatti, G., Scandolara, C., Matelli, M., and Gentilucci, M. (1981). Afferent properties of periarcuate neurons in macaque monkeys. I. Somatosensory responses. Behav Brain Res 2, 125-146.
Romo, R., Hernandez, A., and Zainos, A. (2004). Neuronal correlates of a perceptual decision in ventral premotor cortex. Neuron 41, 165-173.
Romo, R., Hernandez, A., Zainos, A., Lemus, L., and Brody, C.D. (2002). Neuronal correlates of decision-making in secondary somatosensory cortex. Nat Neurosci 5, 1217-1225.
Romo, R., and Salinas, E. (2003). Flutter discrimination: neural codes, perception, memory and decision making. Nat Rev Neurosci 4, 203-218.
Rossiter, H.E., Worthen, S.F., Witton, C., Hall, S.D., and Furlong, P.L. (2013). Gamma oscillatory amplitude encodes stimulus intensity in primary somatosensory cortex. Front Hum Neurosci 7.
Rothwell, J.C., Traub, M.M., Day, B.L., Obeso, J.A., Thomas, P.K., and Marsden, C.D. (1982). Manual motor performance in a deafferented man.pdf. Brain 105, 515-542.
Rozzi, S., Ferrari, P.F., Bonini, L., Rizzolatti, G., and Fogassi, L. (2008). Functional organization of inferior parietal lobule convexity in the macaque monkey: electrophysiological characterization of motor, sensory and mirror responses and their correlation with cytoarchitectonic areas. Eur J Neurosci 28, 1569-1588.
Ruben, J., Schwiemann, J., Deuchert, M., Meyer, R., Krause, T., Curio, G., Villringer, K., Kurth, R., and Villringer, A. (2001). Somatotopic organization of human secondary somatosensory cortex. Cereb Cortex 11, 463-473.
Ryun, S., Kim, J.S., Jeon, E., and Chung, C.K. (2017a). Movement-Related Sensorimotor High-Gamma Activity Mainly Represents Somatosensory Feedback. Front Neurosci 11, 408.
Ryun, S., Kim, J.S., Lee, H., and Chung, C.K. (2017b). Tactile Frequency-Specific High-Gamma Activities in Human Primary and Secondary Somatosensory Cortices. Sci Rep 7, 15442.
Ryun, S., Kim, J.S., Lee, S.H., Jeong, S., Kim, S.-P., and Chung, C.K. (2014). Movement Type Prediction before Its Onset Using Signals from Prefrontal Area: An Electrocorticography Study. Biomed Res Int 2014, 1-9.
Salinas, E., Hernandez, A., Zainos, A., and Romo, R. (2000). Periodicity and firing rate as candidate neural codes for the frequency of vibrotactile stimuli. The Journal of Neuroscience 20, 5503-5515.
Sanai, N., Mirzadeh, Z., and Berger, M.S. (2008). Functional outcome after

language mapping for glioma resection. New Engl J Med 358, 18-27.
Sanes, J.N., Mauritz, K.-H., Evarts, E.V., Dalakas, M.C., and Chu, A. (1984). Motor deficits in patients with large-fiber sensory neuropathy. Proceedings of the National Academy of Sciences 81, 979-982.
Sathian, K. (1989). Tactile sensing of surface features. Trends Neurosci 12, 513-519.
Scheffer-Teixeira, R., Belchior, H., Leão, R.N., Ribeiro, S., and Tort, A.B. (2013). On high-frequency field oscillations (> 100 Hz) and the spectral leakage of spiking activity. The Journal of Neuroscience 33, 1535-1539.
Schlack, A., Sterbing-D'Angelo, S.J., Hartung, K., Hoffmann, K.P., and Bremmer, F. (2005). Multisensory space representations in the macaque ventral intraparietal area. J Neurosci 25, 4616-4625.
Siegel, A., and Sapru, H.N. (2005). Essential Neuroscience (Philadelphia: Wolters Kluwer Health/Lippincott Williams & Wilkins).
Sinclair, R.J., and Burton, H. (1993). Neuronal activity in the second somatosensory cortex of monkeys (Macaca mulatta) during active touch of gratings. J Neurophysiol 70, 331-350.
Smith, M.C., and Deacon, P. (1984). Topographical anatomy of the posterior columns of the spinal cord in man. The long ascending fibres. Brain 107 (Pt 3), 671-698.
Steinmetz, P.N., Roy, A., Fitzgerald, P., Hsiao, S., Johnson, K., and Niebur, E. (2000). Attention modulates synchronized neuronal firing in primate somatosensory cortex. Nature 404, 187-190.
Stoeckel, M.C., Weder, B., Binkofski, F., Choi, H.J., Amunts, K., Pieperhoff, P., Shah, N.J., and Seitz, R.J. (2004). Left and right superior parietal lobule in tactile object discrimination. Eur J Neurosci 19, 1067-1072.
Sun, H., Blakely, T.M., Darvas, F., Wander, J.D., Johnson, L.A., Su, D.K., Miller, K.J., Fetz, E.E., and Ojemann, J.G. (2015). Sequential activation of premotor, primary somatosensory and primary motor areas in humans during cued finger movements. Clin Neurophysiol 126, 2150-2161.
Tanji, J., and Wise, S.P. (1981). Submodality distribution in sensorimotor cortex of the unanesthetized monkey. J Neurophysiol 45, 467-481.
Tomassini, V., Jbabdi, S., Klein, J.C., Behrens, T.E., Pozzilli, C., Matthews, P.M., Rushworth, M.F., and Johansen-Berg, H. (2007). Diffusion-weighted imaging tractography-based parcellation of the human lateral premotor cortex identifies dorsal and ventral subregions with anatomical and functional specializations. J Neurosci 27, 10259-10269.
Tommerdahl, M., Delemos, K., Whitsel, B., Favorov, O., and Metz, C. (1999a). Response of anterior parietal cortex to cutaneous flutter

versus vibration. J Neurophysiol 82, 16-33.
Tommerdahl, M., Whitsel, B., Favorov, O., Metz, C., and O'Quinn, B. (1999b). Responses of contralateral SI and SII in cat to same-site cutaneous flutter versus vibration. J Neurophysiol 82, 1982-1992.
Verrillo, R.T., Fraioli, A.J., and Smith, R.L. (1969). Sensation magnitude of vibrotactile stimuli. Percept Psychophys 6, 366-372.
von der Behrens, W., Bäuerle, P., Kössl, M., and Gaese, B.H. (2009). Correlating stimulus-specific adaptation of cortical neurons and local field potentials in the awake rat. The Journal of Neuroscience 29, 13837-13849.
Wang, W., Collinger, J.L., Degenhart, A.D., Tyler-Kabara, E.C., Schwartz, A.B., Moran, D.W., Weber, D.J., Wodlinger, B., Vinjamuri, R.K., Ashmore, R.C.*, et al.* (2013). An electrocorticographic brain interface in an individual with tetraplegia. Plos One 8, e55344.
Weber, A.I., Saal, H.P., Lieber, J.D., Cheng, J.-W., Manfredi, L.R., Dammann, J.F., and Bensmaia, S.J. (2013). Spatial and temporal codes mediate the tactile perception of natural textures. Proceedings of the National Academy of Sciences 110, 17107-17112.
Westwood, D.A., and Goodale, M.A. (2003). A haptic size-contrast illusion affects size perception but not grasping. Exp Brain Res 153, 253-259.
Whitsel, B.L., Dreyer, D.A., and Roppolo, J.R. (1971). Determinants of body representation in postcentral gyrus of macaques. J Neurophysiol 34, 1018-1034.
Whitsel, B.L., Rustioni, A., Dreyer, D.A., Loe, P.R., Allen, E.E., and Metz, C.B. (1978). Thalamic projections to S-I in macaque monkey. J Comp Neurol 178, 385-409.
Wiest, M.C., and Nicolelis, M.A. (2003). Behavioral detection of tactile stimuli during 7-12 Hz cortical oscillations in awake rats. Nat Neurosci 6, 913-914.
Wolpert, D.M., Goodbody, S.J., and Husain, M. (1998). Maintaining internal representations: the role of the human superior parietal lobe. Nat Neurosci 1, 529-533.
Womelsdorf, T., Fries, P., Mitra, P.P., and Desimone, R. (2006). Gamma-band synchronization in visual cortex predicts speed of change detection. Nature 439, 733-736.
Xia, M., Wang, J., and He, Y. (2013). BrainNet Viewer: A Network Visualization Tool for Human Brain Connectomics. Plos One 8, e68910.
Xiang, J., Hoshiyama, M., Koyama, S., Kaneoke, Y., Suzuki, H., Watanabe, S., Naka, D., and Kakigi, R. (1997). Somatosensory evoked magnetic fields following passive finger movement. Brain Res Cogn Brain Res 6, 73-82.

Yanagisawa, T., Hirata, M., Saitoh, Y., Kato, A., Shibuya, D., Kamitani, Y., and Yoshimine, T. (2009). Neural decoding using gyral and intrasulcal electrocorticograms. NeuroImage 45, 1099-1106.
Yanagisawa, T., Hirata, M., Saitoh, Y., Kishima, H., Matsushita, K., Goto, T., Fukuma, R., Yokoi, H., Kamitani, Y., and Yoshimine, T. (2012a). Electrocorticographic control of a prosthetic arm in paralyzed patients. Ann Neurol 71, 353-361.
Yanagisawa, T., Hirata, M., Saitoh, Y., Kishima, H., Matsushita, K., Goto, T., Fukuma, R., Yokoi, H., Kamitani, Y., and Yoshimine, T. (2012b). Electrocorticographic Control of a Prosthetic Arm in Paralyzed Patients. Ann Neurol 71, 353-361.
Yeom, H.G., Kim, J.S., and Chung, C.K. (2013). Estimation of the velocity and trajectory of three-dimensional reaching movements from non-invasive magnetoencephalography signals. J Neural Eng 10, 026006.
Zhang, H.Q., Murray, G.M., Coleman, G.T., Turman, A.B., Zhang, S.P., and Rowe, M.J. (2001). Functional Characteristics of the Parallel SI- and SII-Projecting
Neurons of the Thalamic Ventral Posterior Nucleus in the Marmoset. J Neurophysiol 85, 1805-1822.
Zhang, Z.G., Hu, L., Hung, Y.S., Mouraux, A., and Iannetti, G.D. (2012). Gamma-band oscillations in the primary somatosensory cortex--a direct and obligatory correlate of subjective pain intensity. J Neurosci 32, 7429-7438.

국문초록

지각과 행동에 대한 내재적 신경 정보처리: 목적과 기능에 대한 대뇌 지각 네트워크

윤 석 윤

서울대학교 대학원

협동과정 뇌과학 전공

촉각과 자기수용감각은 우리의 생존 및 일상생활에 절대적인 영향을 미치는 중요한 감각 기능이다. 말초신경계에서 이 두 가지 기능들에 필요한 정보를 수집하고 전달하는 기계적 수용기 및 그 구심성 신경들에 대한 신호 전달 메커니즘 및 그 특징들은 상대적으로 잘 알려져 있는 편이다. 그러나, 촉각과 자기수용감각을 형성하기 위한 인간 뇌의 피질에서의 정보 처리 메커니즘에 대하여 우리가 현재 알고 있는 바는 극히 일부분이다. 이 논문에서

제시하는 일련의 연구들은 인간 뇌 피질 단계에서 촉각과 자기수용감각의 지각적 처리과정에 대한 거시적 신경계 정보처리 메커니즘을 다룬다.

첫 번째 연구에서는 뇌피질뇌파를 이용하여 인간 일차 및 이차 체성감각 피질에서 인공적인 자극과 일상생활에서 접할 수 있는 자극을 포함하는 다양한 진동촉감각 및 질감 자극에 대한 거시적 신경계 정보처리 특성을 밝혔다. 이 연구에서는 일차 및 이차 체성감각 피질의 촉감각 주파수 특이적인 하이-감마 영역 신경활동이 자극 주파수에 따라 각각 상이한 시간적 다이나믹스를 가지고 변화하는 것을 확인하였다. 또한, 이러한 하이-감마 활동은 성긴 질감과 미세한 입자감을 가진 자연스러운 질감 자극에 대해서도 진동촉감각의 경우와 유사한 패턴을 보였다. 이러한 결과들은 인간의 진동촉감각이 매우 단순한 형태에 자극일지라도 대뇌 체성감각 시스템에 있어 거시적인 다중 영역에서의 계층적 정보처리를 동반한다는 점을 시사한다.

두 번째 연구에서는 인간의 움직임과 관련된 두정엽 영역에서의 하이-감마 뇌활성이 자기수용감각과 같은 말초신경계로부터의 체성감각 피드백을 주로 반영하는지, 아니면 움직임 준비 및 제어를 위한 피질 간 신경 프로세스에 대한 활동을 반영하는지를 조사하였다. 연구 결과, 자발적 운동 중 대뇌 운동감각령에서의 하이-감마 활동은 일차 체성감각피질이 일차 운동피질보다 더 지배적인 것으로 나타났다. 또한 이 연구에서는,

움직임과 관련된 일차 체성감각피질에서의 하이-감마 뇌활동은 말초신경계로부터의 자기수용감각과 촉각에 대한 신경계 정보처리를 주로 반영하는 것을 밝혔다.

이러한 연구들을 바탕으로, 마지막 연구에서는 인간 대뇌에서의 체성감각 지각 프로세스에 대한 거시적 피질 간 네트워크를 규명하고자 하였다. 이를 위해, 51명의 뇌전증 환자에게서 체성감각을 유발했던 뇌피질전기자극 데이터와 46명의 환자에게서 촉감각 자극 및 운동 수행 중에 측정한 뇌피질뇌파 하이-감마 매핑 데이터를 종합적으로 분석하였다. 그 결과, 체성감각 지각 프로세스는 대뇌에서 넓은 영역에 걸쳐 분포하는 체성감각 관련 네트워크의 신경 활성을 수반한다는 것을 알아냈다. 또한, 뇌피질전기자극을 통한 대뇌 지도와 하이-감마 매핑을 통한 대뇌 지도는 서로 상당한 유사성을 보였다. 흥미롭게도, 뇌피질전기자극과 하이-감마 활동을 종합한 뇌지도들로부터 체성감각 관련 뇌 영역의 공간적 분포가 체성감각 기능에 따라 서로 달랐고, 그에 해당하는 각 영역들은 서로 뚜렷하게 다른 시간적 다이나믹스를 가지고 순차적으로 활성화되었다. 이러한 결과들은 체성감각에 대한 거시적 신경계 프로세스가 그 지각적 기능에 따라 뚜렷이 다른 계층적 네트워크를 가진다는 점을 시사한다. 더 나아가, 본 연구에서의 결과들은 체성감각 시스템의 지각-행동 관련 신경활동 흐름에 관한 이론적인 가설에 대하여 설득력 있는 증거를 제시하고 있다.

주요어: 체성감각, 촉각, 뇌피질뇌파, 뇌피질전기자극, 하이-감마, 자기수용감각

학번: 2013-20398